UNIVERSIDADE DO ALGARVE

Faculdade de Ciências e Tecnologia

"Transport in the blood of an anti-tumor water-soluble ruthenium cyclopentadienyl complex: a Fluorescence study on albumin binding"

BY

ANA MARIA MEDINA MARTÍNEZ

Mestrado em Qualidade em Análises
(European Master in Quality of Analytical Laboratories)

2014

“Transport in the blood of an anti-tumor water-soluble ruthenium cyclopentadienyl complex: a Fluorescence study on albumin binding”

Thesis for the degree of European Master in Quality of Analytical Laboratories

ANA MARIA MEDINA MARTÍNEZ

SEPTEMBER 2014

Supervised by:

Prof. Ana Isabel Tomaz, Universidade de Lisboa, Lisbon

And

Prof. Isabel Cavaco, Universidade do Algarve, Faro

UNIVERSIDADE DO ALGARVE
Faculdade de Ciências e Tecnologia
Faro, Portugal

ACKNOWLEDGEMENT

I would like to start this piece of work expressing my gratitude to the Erasmus Mundus project of the European Commission for sponsoring my work and for awarding me with the opportunity of taking this master.

This work was performed in the Centro de Quimica e Bioquimica, FCUL, Universidade do Lisboa in Lisbon under the supervision of Prof. Ana Isabel Tomaz and Prof. Isabel Cavaco. I am profoundly grateful to Prof. Ana Isabel Tomaz for all the dedicated support, motivation and guidance provided to my person throughout my thesis. It was a pleasure for me to have one great professor and great person as her as a supervisor.

The unconditional support received from Dr. Andreia Valente was incredible, I am deeply thankful to her as she helped me every time I needed.

I am also sincerely grateful to Prof. Miguel Palma for his dedication, time and support throughout the whole master, from the enrolment until the end.

I would like to also express my totally gratitude to Prof. Isabel Cavaco from the University of Algarve for supervising my work and for her role in the development of the whole Master program.

I would like to deeply thank Prof. Rodrigo F. M. de Almeida and his entire research group from Centro de Quimica e Bioquimica for providing all the necessary help, resources and facilities for the fluorescence measurements.

I am also greatly thankful to Dr. Fernanda Marques from C2TN-IST in Lisbon for providing me with the MTT assay results for the cytotoxicity of the complex studied.

I am truly thankful to Prof. Maria Helena Garcia for the support and motivation provided to my person, as well as to the entire Quimica Organometálica e Biorganometálica group that has made me feel very welcome: Leonor, you are a truly inspiration, thank you for all the nice chats, positives thoughts and love. Thanks to the entire group in general for making me feel very welcome from the first moment I arrived, providing your help at any time for anything I needed.

Finally, I would love to thank the most important people in my life, for all the love provided and support in all my ups and downs, for believing in me always in every decision I have made. My mother, father and family thank you for being there always and my boyfriend's parents and rest of family for giving me all their love. I want to thank my boyfriend for being next to me since the moment I decided I wanted to enrol in this adventure, supporting me, loving me and caring for me every single second, I love you and thank you for motivating me every moment since we have been together.

Faro, September 2014
Ana María Medina Martínez

TABLE OF CONTENTS

LIST OF FIGURES

LIST OF TABLES

LIST OF ABBREVIATIONS

Abs	Absorbance
β	Global formation constant
Bipy	2,2'-Bipyridine
CDDP	cis-dichlorodiammineplatinum(II)
CisPt	Cisplatin
Cp	η^5-cyclopentadienyl
C_q	Total concentration of quencher
CO	Carbon monoxide
Conc.	Concentration
DG	Dansylglycine
DMSO	Dimethyl sulfoxide
F or IF	Steady-state intensity or fluorescence
faf	Fatty acid free
FP	Fitting parameter
g	Grams
h	hours
H_2O	Water
HEPES	4-(2-hydroxyethyl)-1-piperazineethane Sulfonic acid
HSA	Human Serum Albumin
IC_{50}	Half maximal inhibitory concentration
IFE	Inner Filter effect
Im	Imidazol
LED	Light-emitting diode
mL	Millilitres

mM	milliMolar
MLC	Metal-ligand complex
MLCT	Metal-to-Ligand Charge Transfer
MW	Molecular weight
nm	nanometres
pmc44 or RuC	$[Ru^{II}Cp(bipy)CO][PF_6]$
PPh3	triphenylphosphane
ps/ch	picosecond/channel
SD	Standard deviation
ϕ_F	Fluorescence quantum yield
Q	Quencher
ref	reference
Ru	Ruthenium
T	Temperature
Tf	Transferrin
TM34	$[Ru^{II}(\eta^5\text{-}C_5H_5)(bipy)(PPh_3)]^+$
Trp	Tryptophan
UV-Vis	Ultraviolet-Visible
v/v	Concentration in volume/volume
WF	Warfarin
WHO	World Health Organisation
α_i	Pre-exponential factors in a multi-exponential intensity decay
γ	inverse of the decay time, $\gamma = 1/\tau$
Γ	Radiative decay rate

λ	Wavelength
λ_{em}	Emission wavelength
λ_{em}^{max}	Maximum emission wavelength
λ_{ex}	Excitation wavelength
τ	Lifetime of the excited state
$<\tau>$	Average decay time or lifetime

ABSTRACT

Ruthenium (Ru) complexes have captivated an increasing interest in recent years; they are a promising alternative to platinum-based complexes due to the fact that some of them have been repeatedly described for showing higher selectivity and lower cytotoxicity regarding their effects on cancer cells.

The interactions studied between the Ru-complexes and serum proteins such as fatty acid free Human Serum Albumin (^{faf}HSA) are of very high importance considering that their bioavailability and effects depend on their binding to albumin to reach the targeted cells. In addition, the Food and Drug Administration (FDA) has set the report on plasma protein binding for prodrugs as a requirement in order to do the screening for potential therapeutic agents.

The interactions and several aspects related to the binding between the ruthenium (II) complex [Ru^{II}(Cp)(bipy)(CO)][PF_6] (or RuC, also named pmc44) and HSA are addressed using fluorescence spectroscopy, steady-state and time-resolved measurements, and UV-Visible absorption in 10 mM HEPES buffered medium pH 7,4. Additionally, in order to obtain a deeper insight into the HSA binding properties of the complex at the specific drug binding sites, displacement experiments with the site markers Warfarin and Dansylglycine (for which the binding site is well known) were performed.

The results show that the complex strongly quenches the intrinsic fluorescence of albumin and that the interaction is quite fast, indicating that the complex successfully binds the protein. The outcome from the Stern-volmer linearizations (both time-resolved and steady-state measurements) displayed more than one type of quenching mechanism; albumin fluorescence is quenched by a combination of dynamic and static quenching mechanisms. The most representative values obtained for K_D and K_S from the averages were $(4,8 \pm 0,3)_x10^4$ M^{-1} and $(2,3 \pm 0,7)x10^4$ M^{-1} respectively, calculated with the Stern-Volmer linearization at λ_{em}=338 nm by a Minimum Square Fit procedure with variance analysis (ANOVA) with a 95% confidence level.

A speciation model with two protein-RuC adducts is proposed with global conditional binding constants of log β'_1= (4,78 ± 0,01) (for the 1:1 adduct {HSA-RuC}) and log β'_2= (9,52 ± 0,01) (for the 1:2 adduct {HSA-$(RuC)_2$} with a fitting parameter of $1,16_x10^5$ using the computer program PSEQUAD.

The conclusions achieved with the site markers´ experiments revealed that the complex binds to both sites I and II of the protein.

Altogether, the results from this work indicated that the complex studied can bind human serum albumin in a moderate way and thus it be efficiently transported in the blood by HSA.

KEYWORDS: Cancer therapy, human serum albumin, fluorescence spectroscopy, ruthenium complexes, ruthenium, UV-Vis absorbance, binding site.

RESUMO

O Cancro é a segunda maior causa de morte em países desenvolvidos. Estima-se que o número global de mortes por cancro aumente em 50% até 2030, criando a necessidade urgente de encontrar soluções para este problema de saúde global. A cisplatina, carboplatina e oxaliplatina são os únicos metalofármacos aprovados para uso clínico em todo o mundo mas, apesar da sua eficácia, apresentam efeitos secundários que limitam muito a sua utilização.

Os compostos de ruténio são já reconhecidos como uma alternativa promissora aos fármacos de platina usados em quimioterapia, dada a sua menor citotoxidade e maior selectividade. Além disso, oferecem diferentes mecanismos de acção e um espectro de atividade diferente, mais alargado, que os metalofármacos de Pt. O seu mecanismo de acção é intensamente estudado actualmente e a ligação a proteínas séricas parece ter um papel importante na sua resposta biológica.

O estudo da interacção com proteínas séricas e com a albumina do plasma humano (HSA) em particular reveste-se de uma grande importância no contexto do desenvolvimento de metalofármacos. Por um lado, a interacção com a albumina tem um impacto importante na biodisponibilidade do complexo em estudo. Por outro lado, a HSA desempenha um papel fulcral no transporte de compostos endógenos e exógenos, sendo também crucial como veiculo transportador de compostos terapêuticos para lhe permitir atingir as células e tecidos-alvo onde exercem a sua acção. Além disso, é um requisito da FDA (*Food and Drug Administration*) que resultados da interacção com proteínas séricas sejam incluídos no processo de pre-selecção de potenciais fármacos e metalofármacos.

Neste trabalho estudou-se a interacção de um complexo organometálico de ruténio(II) de estrutura em banco de piano com a albumina de plasma humano (sem ácidos gordos, ^{faf}HSA). O complexo $[Ru^{II}(Cp)(bipy)(CO)][PF_6]$ (designado neste trabalho por RuC), com uma actividade moderada para o adenocarcinoma de ovário humano, é solúvel em água o que o torna muito interessante no contexto de desenvolvimento de novos agentes terapêuticos. A sua ligação à HSA foi estudada em meio aquoso a pH 7.4 (tamponizado com HEPES) e à temperatura de 37ºC por espectroscopia de UV-Vis e espectroscopia de Fluorescência (em estado estacionário e resolvida no tempo) usando a emissão do resíduo Trp214 da proteína como sonda de fluorescência intrínseca.

A interacção do complexo com a HSA ocorre rapidamente e resulta na extinção da fluorescência do Trp214 por um processo misto estático e dinâmico, para o qual se obtiveram as constantes de Stern-Volmer $K_D = (4{,}8 \pm 0{,}3)_x10^4\ M^{-1}$ e $K_S = (2{,}3 \pm 0{,}7)x10^4\ M^{-1}$ (calculadas a λ_{em}=338 nm pelo método dos mínimos quadráticos para um nível de confiança de 95%).

O modelo proposto para a interacção RuC–HSA engloba a formação de dois aductos complexo-proteína de estequiometrias 1:1 e 1:2 para os quais são calculadas constantes de formação condicionais $\log \beta'_1 = (4{,}78 \pm 0{,}01)$ (para o aducto 1:1 {HSA-RuC}) e $\log \beta'_2 = (9{,}52 \pm 0{,}01)$ (para o aducto 1:2 {HSA-$(RuC)_2$}.

Reacções de competição com "marcadores" conhecidos como a varfarina e a dansilglicina, para os quais a ligação à HSA é específica e está bem estudada, são utilizadas para obter informação sobre os locais de ligação do RuC à proteína.

Os resultados obtidos neste trabalho permitem concluir que o complexo organometálico estudado interactua com a HSA de forma moderada, podendo ser eficientemente transportado pelo sangue através da ligação a esta proteína.

PALAVRAS-CHAVE: Cancro, albumina do plasma humano, Ruténio(II), complexos de Ru(Cp), espectroscopia de fluorescência, locais de ligação, biodisponibilidade.

1.0. INTRODUCTION

1.1.0. Cancer conditions

According to the World Health Organisation (WHO) Cancer is one of the most important causes of death worldwide. The figures show 8.2 million of deaths in 2012, numbers that are expected to rise from 14 to 22 million annual cases within the next two decades [1].

Cancer is characterised by the rapid and uncontrolled growth of cells (abnormal cells) that invade nearby tissues, and eventually spread to vital organs. This later process is known as metastasis and it is started by genetic alterations and mutations in cells. **Figure 1** represents the main stages involved in the progression of a malignant tumour to an invasive cancer (condition) [2].

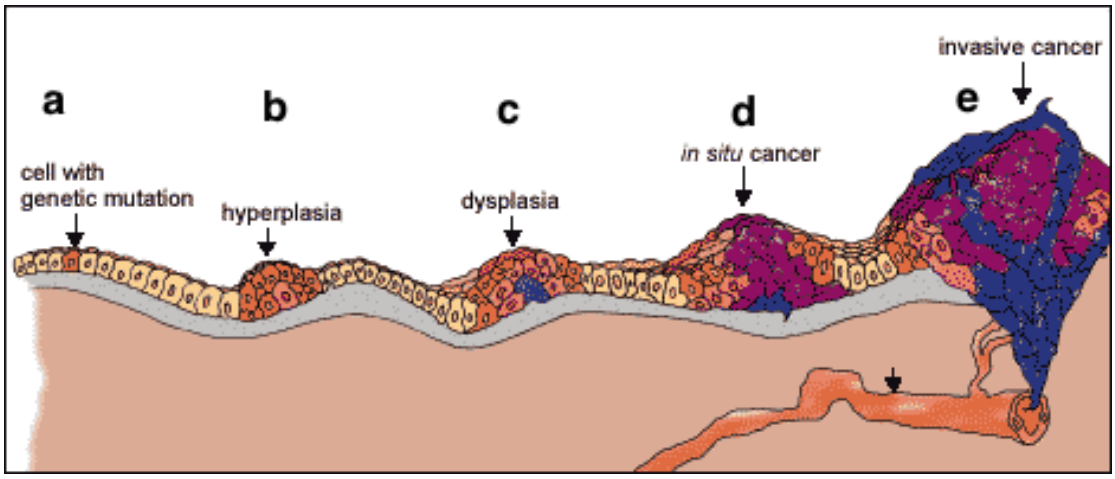

Figure 1. Metastasis development: A malignant tumour expands across time as shown above as a consequence of four mutations. **a.** A cell undergoes a genetic mutation leading to abnormal growth. **b.** Hyperplasia is the rapid division and growth of the mutated cell and its descendants. **c.** Dysplasia is when the cell's descendants look abnormal and divide at a fast rate. **d.** In situ cancer: the tumour that has been assembled with these cells remains in the original tissue. **e.** If the cells suffer further mutations and the tumour infest nearby tissues depositing cells into the lymph or blood the tumour is said to be malignant. The escaped cells are very likely to form new tumours in other parts of the body (metastasis) (modified from ref [3]).

Currently cancer treatment is limited to radiotherapy, surgery and use of cytotoxic agents, which are known for their problems associated with the development of resistance and side effects [4]. The treatment for metastasis is yet to be found because it is the most important target to defeat regarding cancer. Cisplatin became in 2001 the gold standard treatment in combination with radiotherapy against cervical cancer. It still plays nowadays a central role in cancer chemotherapy despite its toxicity and, it is used as first line chemotherapy against several epithelial malignancies. In addition to this, it is used as second and third line treatment against few metastatic malignancies including cancers such as breast, prostate and melanoma to name a few. The response rate for chemotherapy in most advanced cancers is approximately 15% in second and third line treatments and about 50% in first line treatments. There are examples of some other treatments that use a combination of cisplatin or

carboplatin with radiotherapy and other drugs such as gemcitabine or taxanes that increase the response rate up to 80% [5].
Cisplatin (cis-dichlorodiammineplatinum(II)) or CDDP (**Figure 2**) was the first platinum-containing complex used to treat cancer and Rosenberg described its inhibitory activity on the division of Escherichia coli 120 years after its synthesis [6]. In 1968, cisplatin was successfully tested in mice, three years later, phase I trials (first patients) began and was FDA approved for use in 1978. The discovery of severe safety issues derived from the treatment with cisplatin (nephrotoxicity) led to the biological evaluation and synthesis of many cisplatin analogues and other elements. Subsequently, the effort was made aiming at making cisplatin-based drugs safer to patients [7].

Although metal ions were used in medicine already, cisplatin was a very important discovery because prior to this date all cancer treatments where focused on organic molecules. From this achievement, cancer research focused on metallodrugs.

Cisplatin's mode of action has been well studied since its discovery. It was suggested that more than 90% of platinum in the blood after its intravenous administration was covalently bound to the plasma proteins. Thus, the study of the binding cisplatin-protein was of a greater interest than the binding regarding cisplatin-DNA. It is known that once the drug has entered the cell, it was found to bind HSA at C-N and S-H groups. These drugs bind to the Cys-34 as well as to the Met-298 of the protein, causing important conformational changes, which result in considerable perturbations of the amide I and amide II vibrational frequencies [8].

This discovery provoked a high interest in platinum (II) compounds as potential anticancer drugs and many patients with different types of cancer have been successfully treated with CDDP. Due to the success in the clinical use, patients with cancers including: sarcoma, bones, muscles, soft tissue and blood vessels receive a better prognostication and a higher hope for recovery nowadays. These achievements stimulated the search for new platinum derivatives [9,10].

Apart from cisplatin, there are other complexes currently approved for clinical use worldwide: Carboplatin, Oxaliplatin and Nedaplatin (**Figure 2**). Carboplatin and cisplatin are less toxic than cisplatin. Oxaliplatin is highly efficient against colorectal cancer. Nedaplatin is exclusively used in Japan head, neck, testicular, lung, oesophageal, ovarian and cervical cancer. Despite the improvements, these complexes still have to overcome the acquired tumour resistance that they present [10,11].

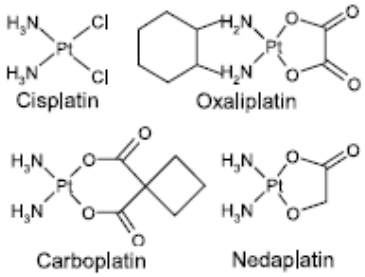

Figure 2. Structure of four platinum derivatives clinically in use (modified from ref [10]).

Concerning the advantages and disadvantages of using platinum drugs, has to be said that: they are highly effective but only on a limited number of cancer conditions, their side effects are highly debilitating due to their high toxicity which are the major drawbacks (nephrotoxicity), these drawbacks may be overcome with alternative treatments, alternative agents with different modes of action that bypass the resistance mechanisms activated in Pt-based treatment.

The greatest challenge in designing anti-cancer drugs is the improvement of the selectivity because even though these anti-cancer drugs are generally cytotoxic, they are also a threat to healthy or normal cells, which is why side effects are repeatedly serious.

Due to the fact that cisplatin is highly toxic, the principal objective during many years has been to accomplish new chemotherapeutic compounds with less toxicity and greater efficacy, metallodrugs with other mechanisms of action [10]. Consequently, the pursuit for alternative therapies has led to the synthesis of new anticancer drugs with metals such as Ruthenium.

1.2.0. Ruthenium complexes

Research on ruthenium-containing compounds as anticancer agents has had the goal to overcome the limitations of platinum compounds against cancer cell lines. The fact that they show fewer side effects and that they can be found in different oxidation states biologically accessible (II, III and IV) under suited conditions, places them in a very well position as potential substitutes. Apart from these, other benefits have demonstrated their potential: (i) the low energy barriers for the transformation between these oxidation states permit ready oxidation state changes within the cell; (ii) octahedral coordinated complexes in contrast to the square-planar geometry of platinum(II), involving two extra ligands in its structure to operate on a different manner from cisplatin compounds; (iii) the possibility of slow ligand exchange rates in water (**Figure 3**), which kinetics are on the cellular reproduction timescale (mitosis). This implicated that if a ruthenium ion establishes any interaction with any component present in the cell, it is possible to continue bound to it for the rest of the cell's lifetime; (iv) ruthenium's ability of performing alike iron in binding establishing to biomolecules, such as Albumin or Transferrin is a very important advantage to become less toxic than platinum drugs.[12, 13]

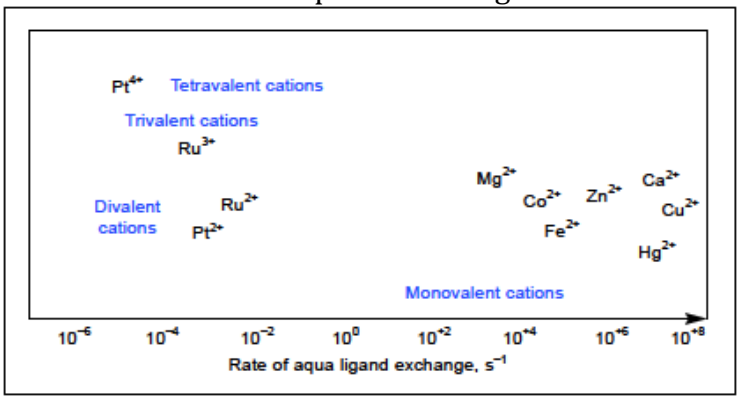

Figure 3. Logarithmic presentation of relative kinetics of aqua ligand exchange for different metal ions, ruthenium shows a relative low rate (modified from ref [14]).

In order to explain the lower toxicity of Ruthenium complexes in comparison with Platinum compounds the "activation by reduction" mechanism is to be mentioned. This mechanism works selectively in solid tumours with low oxygen level (hypoxia), which generates a reducing environment enabling the reduction of Ru (III) to the more reactive Ru (II) species. Tumours grow at a rapid rate due to the deficient formation of new blood vessels and blood supply. The low pH outside the cell, the low oxygen level and the existence of cellular reducing agents contribute to the conditions for the selective reduction of drugs with Ru^{III}/Ru^{II} redox potential. This reducing ability of ruthenium (III) compounds relies on the ligands in the structure. Knowing the net electron donation from ligands to metals helps to predict metal-centred redox potentials and therefore drugs with the desired redox parameters can be obtained. Nonetheless, Ru (III) complexes can undergo hydrolysis or bind to proteins prior to reduction and alter their redox properties [14-17]. Despite the existing wide range of information the mechanism of action of Ru-based anti-tumour agents is still under study.

The first ruthenium complexes that have successfully undergone clinical trials are **KP1019**, indazolium [trans-tetrachlorobis(1 H-indazole)ruthenate(III)] and **NAMI-A**, imidazolium [trans-tetrachloro(dimethylsulfoxide)-imidazoleruthenate(III)] (**Figure 4**) [18].

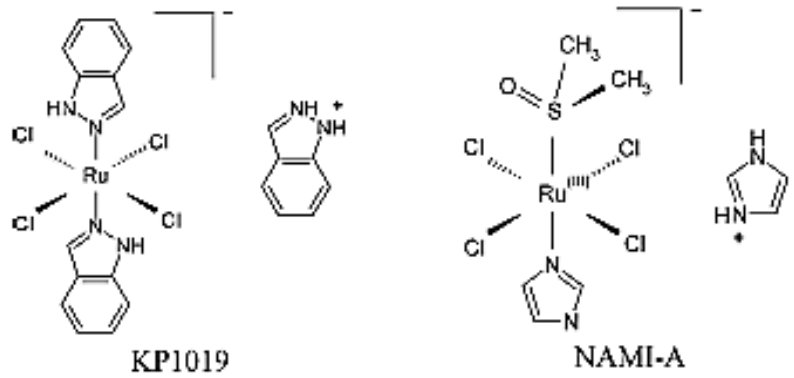

Figure 4. Chemical structure of two ruthenium complexes that have successfully completed phase I clinical trials (modified from ref[16]).

The complex NAMI-A is not very active against solid primary tumours, however, it shows metastasis inhibition in all the experimental models of solid tumours under test. This characteristic is noticeably important because despite the progression in the treatment of primary tumours, metastasis still represents a big challenge in cancer treatment for being the main cause of the death. The cytotoxic activity of NAMI-A against metastasis seems to be related primarily with its antiangiogenic (reducing the growth of new blood vessels) potential. Nonetheless, its capacity to remodel at cytosqueleton level and its ability to alter the cellular adherence are also important [15-17, 19].

The second complex above-mentioned, KP1019, is substantially active against cisplatin resistant colon carcinoma and some primary explanted tumours. It is believed that the protein Transferrin transports the compound until it reaches the targeted cells, after this, the complex is released in the endosomes at acid pH

causing apoptosis through the mitochondrial pathway. In addition, this complex has shown a much moderated toxicity, which is practically non-existent in the clinical trials that it has undergone [14-17].

The complexes mentioned above are Ru(III) compounds with monodentate ligands and it is thought that their mechanism of action entails the reduction to Ru(II), which are more active compounds. Because of this, the interest for the anticancer abilities of Ru(II) complexes has increased [20].

The fact that some Ru-agents are anti-metastatic is one of their most interesting, promising and unique features. Their mechanism of action is proposed to involve serum proteins, therefore, albumin binding is determinant in the bioavailability of the compound and it is also a requirement of the FDA in the drug development process [21].

Possibily the major group of Ru(II) compounds reported as potential metallodrugs are 'Ru(arene)' organometallic mononuclear piano-stool complexes.

RAPTA (Ruthenium-Arene-PTA) complexes comprise a promising family of organometallic compounds in this context (PTA is 1,3,5-triaza-7-phosphaadamantane). There are some RAPTA complexes with anti-metastatic properties such as RAPTA-T [Ru(phenanthroline)(κ-C,N-(2-(2-phenyl-pyridine)$(NCMe)_2$][PF_6] (with a piano-stool geometry), that alike the other derivatives of this family has weak cytotoxicity. However, its cytotoxicity is better expressed on tumour cells than in healthy cells. At the same time that shows an important ability to modify the behaviour of cells concerning metastasis and invasion. In some occasions RAPTA-T acted like RAPTA-C ([Ru(η_6-$C_{10}H_{14}$)(PTA)Cl_2]) showing some activity in vivo in a model of solid metastasizing tumours [15]. Even though the metastases reduction is moderate and it is only evident at certain doses, these effects of the family of RAPTAs on metastasizing tumorous that appear spontaneously are very important as it is the first evidence for another ruthenium-based complex to show some selectivity of anti-tumour activity against metastases [15].

Not many studies in the literature have addressed complexes with the Ru(II)-cyclopentadienyl moiety (Ru(η^5-C_5H_5) or Ru(Cp), isoelectronic with Ru(arene)). The potential of these derivatives in the field of metallodrugs were first reported for [Ru(η^5-C_5H_5)CO'pyridocarbazole'] compounds that exposed strong and selective inhibitors of protein kinases GSK-3 and Pim-1 [22, 23]. Exceptional results have been consistently found for a few other families of Ru(Cp) compounds developed at Faculdade de Ciências, Universidade de Lisboa by the research group of Quimica Organometálica e Biorganometálica.

1.2.1 Ruthenium cyclopentadienyl complexes

Several Ru(Cp) complexes presented potent cytotoxicity against a wide range of human tumour cell lines [24-26]. The first members of this {Ru^{II}(Cp)} family had general formulas of [Ru(Cp)$(PPh_3)_2$L]$^+$ or [Ru(Cp)(PP)L]+ (L being a

monodentate N-heterocycle ligand, PPh_3 being a monodentate thiphenylphosphane and PP a bidentate phosphane ligand) [21]. These complexes exhibited high cytotoxicity against LoVo human colon adenocarcinoma, Mia Paca pancreatic cells and human promyelocytic leukemia HL-60 cells [24, 21]. These complexes reported by M. Helena Garcia workgroup have no labile Cl^- co-ligand, which is distinctive feature from most of the organometallic Ru complexes reported. This family of compounds revealed strong cytotoxicity against several human tumour cell lines with IC_{50} values in the sub-micromolar range, much lower than those found for cisplatin [21, 24-28].

Aiming at accomplishing enhanced chemical stability, a different family was synthesized with the general formula $[Ru(Cp)(LL)(PPh_3)]^+$, where LL is a bidentate ligand. Very promising antitumour features were identified for some complexes, especially for the complex $[Ru^{II}(\eta^5\text{-}C_5H_5)(bipy)(PPh_3)]^+$ (**Figure 5**) (or **TM34**, PPh_3 is the monodentate triphenylphosphane). TM34 is composed by a bidentate quelated ligand (2,2´ bipyridyl binding Ru(II) through its two $N_{pyridine}$ atoms) and the cyclopentadienyl ligand. This compound was found to be chemically very stable in aqueous media and in strong coordinating solvents. A very low amount of a co-solvent (DMSO, 2%) was needed to attain full solubility in pH 7,4 buffered aqueous media and overcome its lack of solubility in water [21].

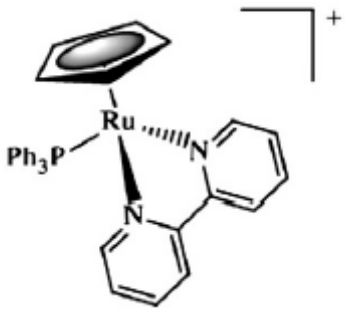

Figure 5. Structure of the Ru(II) complex TM34 (modified from ref[21]).

TM34 exhibited exceptionally high activity against cisplatin resistant tumour cell lines such as e.g. resistant ovarian adenocarcinoma, breast cancer and grade IV prostate cancer. It was also very active against cisplatin sensitive cells: this complex was found to be approximately 15 times more active against A2780 than cisplatin. Its mechanism of action is not yet fully known. It might involve the inhibition of key enzymes in the cell such as poly(ADP-ribose) polymerase 1 (PARP-1) as it has been also proposed for other non-platinum complexes (e.g. some gold complexes) [21] . In fact, TM34 is the strongest inhibitor agent disclosed for PARP-1, with IC_{50} values surpassing those described for cisplatin (CisPt), NAMI-A and RAPTA-T. This complex is also expected to be transported by albumin (HSA) in the blood stream with no loss of activity since the HSA adduct formed kept the complex cytotoxicity fairly unchanged [21].

Electrospray ionization mass spectrometry was useful to understand how tightly the different co-ligands were bound to Ru(II) in these Ru(Cp) complexes [29]. These results indicated that the {Ru(Cp)} moiety was rather robust and very stable, while the complexes lost their less tightly bound ligands with some ease.

In TM34 bearing the bidentate bipy, the co-ligand less tightly bound to Ru(II) was PPh_3 followed by bipy, with the {Ru(Cp)} remaining intact.

The effect that changes in the bipyridyl ligand would have on the biological activity of TM34 was also reported. Excellent results were obtained for the complex $[Ru^{II}(\eta^5\text{-}C_5H_5)(PPh_3)\ (Me_2bpy)][CF_3SO_3]$ (**Figure 6**) (Me_2bpy being 4,4'-dimethyl-2,2'-bipyridine)[28]. This complex showed remarkable cytotoxic activity displaying IC_{50} values in the nanomolar and sub-micromolar range, again largely surpassing the activity of CisPt in several tumour cell lines studied, including quite aggressive CisPt resistant cells such as the grade IV prostate cancer cells (androgen independent) and highly invasive breast cancer cells (estrogen independent). As observed with TM34, the activity of this complex was not affected by its binding to human serum albumin[28].

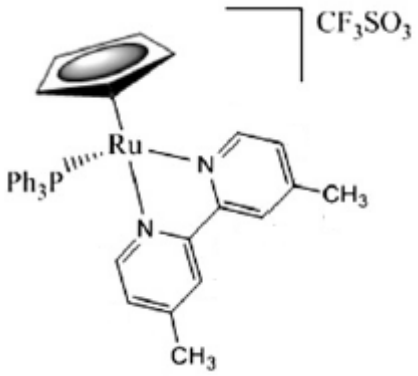

Figure 6. Structure of the ruthenium complex $[Ru^{II}(\eta^5\text{-}C_5H_5(PPh_3)(Me_2bpy)][CF_3SO_3]$ (modified from ref[28])

Using TM34 as a structural unit, a polymeric controlled drug delivery vehicle was synthesized as an alternative to the conventional drug delivery in cancer therapy. A mononuclear {Ru(Cp)} derivative merged with a polymeric unit was achieved in $[Ru^{II}(Cp)(Ph_3)(bpyPLA)][CF_3SO_3]$ (bpyPLA being 2,2′-bipyridine-4,4′-D-glucose end-capped polylactide, a biocompatible polymer linked to bipy) (**Figure 7**) [30]. This RuPMC (Ruthenium Polymer Metal Complex) compound, although less active than TM34, still exhibited cytotoxicity in the micromolar range against human tumour cell lines with different response to cisplatin, with IC_{50} values surpassing (or in the same range as) those reported for CisPt

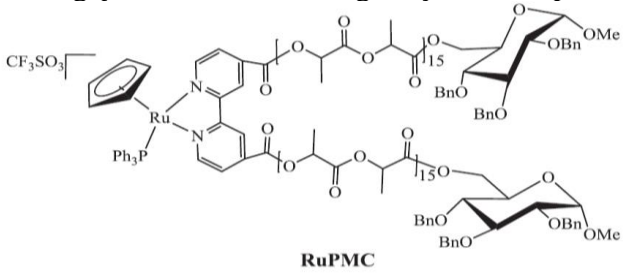

Figure 7. Structure of $[Ru^{II}(Cp)(Ph_3)(bpyPLA)][CF_3SO_3]$, the first RuPMC reported which was inspired on TM34 and is highly active against human ovary and breast adenocarcinomas [30].

Therefore, the complexes of this family are demonstrating to be great potential chemotherapeutic drugs in *in vitro* assays with human tumour cell lines.

1.2.2 The complex [RuII(η^5-C_5H_5)(bipy)(CO)][PF_6]

The group of *Quimica Organometálica e Biorganometálica* from *Faculdade de Ciências, Universidade de Lisboa* coordinated by Prof. M. Helena Garcia has obtained excellent results with the piano-stool ruthenium(II) complexes developed so far.

A new Ru(Cp) complex [Ru^{II}(η^5-C_5H_5)(bipy)(CO)][PF_6] (or pmc44) was recently prepared, and presently being screened for its potential as a chemotherapeutic agent for cancer therapy. This new member of the {Ru(II)Cp} family, which is denominated throughout this work as **RuC**, contains in its structure the bipy ligand and a carbon monoxide (CO) (**Figure 8**). In fact, the only difference between RuC and TM34 is the CO ligand replacing the triphenylphosphane (PPh_3). The rationale for preparing this complex was to combine the therapeutic effect of carbon monoxide with the $[Ru(Cp)(bipy)]^+$ core that has proven to be very cytotoxic for cancer cells.

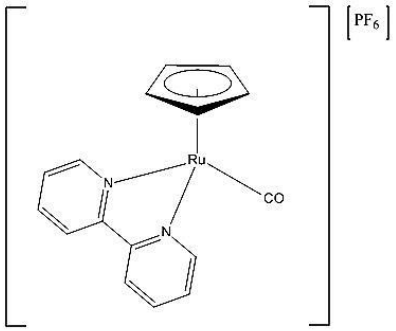

Figure 8. Structure of the complex [Ru^{II}(η^5-C_5H_5)(bipy)(CO)][PF_6] (**RuC**) studied.

Indeed, evidence for the beneficial effects of CO have been consistently building up, with preclinical studies showing the favourable effects of CO in cardiovascular disease, sepsis and shock, cancer, acute and chronic rejection of a transplanted organ, and acute lung, kidney and liver injury [27]. The interest of CO as a ligand is that its unique chemistry reacting exclusively with transition metals is a great advantage for using it as a therapeutic stem. Its chemistry is also varied and highly versatile. The two most-studied CO-based pharmaceuticals are stable and fully water soluble, which are two of the properties expected for the complex studied in this work [27].

Although results for the complex RuC are still being gathered, some were already available when the work in this thesis was executed, and are collected in the following paragraphs.

The structure of RuC and the results previously obtained for TM34 anticipated high chemical stability in solution for this complex. Bipy is well-known as an excellent bidentate chelating ligand that allows electron back-donation due to its low lying energy orbitals (π* empty). It has been extensively used as a building block in supramolecular/macromolecular chemistry and in nanoscience [31]. The two $N_{pyridine}$ donor atoms are very effective in Ru(II) coordination, and form a stable 5-membered chelate ring when coordinated to the metal ion. The Ru(Cp)

core is quite stable too, and carbon monoxide coordinates to the Ru(Cp) moiety quite strongly as was observed when characterizing [32].

RuC is soluble in water with no need for an organic co-solvent, and this is a feature desirable for an easier and effective drug formulation. Its partition coefficient in a water/octanol system (adopted as a rough model for the cell membrane), log $P_{o/w}$ value was -0.66, which means that the complex is hydrophilic (Log $P_{o/w}$ = Log {[complex$_{(org)}$]/[complex$_{(aq)}$]}). Being soluble in water is quite important for drug development.

In what concerns activity, the cytotoxicity of the prospective drug RuC was determined in the human tumour cell line A2780 (ovarian carcinoma, cisplatin sensitive). Cell viability was determined using the well-established MTT assay (MTT = [3-(4,5-dimethylthiazol-2-yl)-2,5-diphenyltetrazolium bromide])[33], after a 72 h exposure and the cytotoxic effect of the compound was quantified by calculating the IC_{50} value (the drug concentration inhibiting tumour cell growth by 50%). A preliminary value of IC_{50}=(49±12) μM was measured which is moderate compared to the results of other ruthenium complexes or CisPt (Dr. Andreia Valente, private communication).

Experiments to evaluate whether the binding of RuC to albumin (^{faf}HSA) would influence the cytotoxic activity of RuC in A2780 cells were also executed. Results indicated that albumin binding does not affect RuC activity in comparison to the compound alone, yielding adducts that maintain the same cytotoxic properties (Dr. Andreia Valente, private communication).

Cell assays are currently being executed on healthy cells to evaluate if the complex has some intrinsic selectivity for cancer cells against healthy cells.

RuC is thus not as highly active as other members of the family, especially TM34. Nevertheless, the water solubility and the lower activity can be important requirements to obtain a metallodrug with a more controlled and selective effect on the target (tumor) tissues.

1.3.0. Blood Serum: Components

Drug delivery is directly dependant on the blood transport. In fact, blood is the most important vehicle for the transport of drugs from the administration site to the targeted spot of action. In addition, serum and its components might modify the compound structure and affect its delivery to the target [34].

Blood consists of cellular and non-cellular parts. The non-cellular part or plasma contains 90% of water; the rest 10% are dissolved substances such as, proteins (C_{HSA} ~ 630 μM), nutrients, hormones, electrolytes and metabolites. Blood serum is distinguished from blood plasma when fibrinogen and other proteins that stimulate coagulation are not present. In order to interpret the speciation of the

metal ions in plasma, it is essential to know the formation constants for the species assembled between them and the metal ions [35].

Countless drugs have demonstrated to be bound to proteins present in plasma when they enter the bloodstream. The extension and strength of this interaction affects the circulation and delivery of the drug into other areas, as well as its toxic and therapeutic responses [35].

The distribution of many drugs and other compounds in the body depend on their affinities for HSA and their binding abilities. Strong binding interactions between this serum protein and drug may decrease the concentration of free drug in plasma while weak binding interactions might lead to a short lifetime or poor distribution. However, if the correct binding is present, albumin can transport the drug bound to it to the targeted location. Therefore, the study of the binding interactions between serum proteins and drugs is essential in pharmacology and pharmacodynamics [36].

1.3.1. Human Serum Albumin

Human serum albumin is a globular protein that has many crucial physiological functions. It is the most abundant protein in plasma (35-50 g/L human serum), accounts for approximately 60% of total plasma protein and its molecular weight is 66.5 kDa. Albumin is synthesised in the liver (as nearly all plasma proteins) and exhibits an average half-life of 19 days. The main function of albumin is to transport fatty acids and apart from acting as the most important nonspecific transporter protein in the circulatory system, HSA is the major protein responsible for the colloid osmotic pressure of the blood [37-39].

This is a very soluble and robust protein, which can be heated at 60 °C for up to 10 h without damaging its structure; it is acidic and stable in pH 4-9 and soluble in 40% ethanol. It is an important agent for the solubilisation of poorly water-soluble drugs and it may also increase their half-life when they are bound to it by decreasing its elimination at the glomerulus. It is an excellent candidate for drug delivery due to the above-mentioned properties as well as for its preferential accumulation in tumour and inflamed tissue, its biodegradability, its ready availability and its lack of immunogenicity and toxicity [37].

Albumin accumulates in inflamed tissue due to the "*enhanced permeability and retention (EPR) effect*" of cancer cells. In the 80´s Y. Matsumura and H. Maeda [40] described that a polymeric protein was more active than the single product, concluding that this effect depends on the special vascular and lymphatic properties of cancer cells [40]. The leaky deficient blood vessels of tumour tissue (with big pores) make it accessible for macromolecules, while in the blood vessels of healthy tissue only small molecules can cross the endothelial barrier. This enhanced retention of macromolecules in tumour tissue is mainly generated by a lack of lymphatic drainage due to a defective lymphatic system. Thus, the responsible for the accumulation of macromolecules in malignant tissue (tumours) is due to the combination of an enhanced permeability and retention [37]. Large molecules would almost selectively be taken and retained by cancer

cells whereas in the case of normal cells the excretion through the healthy lymphatic system would occur [41].

Thus, albumin binding can be a means of effective transport of a metallodrug to its targets, it has an impact of the compound bioavailability and *in vivo* half-life, and can be a route to improve the selectivity of the prospective drug to inflamed and malignant tissue through passive targeting due to the EPR effect.

The strength and reversibility of the binding to the serum protein is an important influence in the different behaviour of Pt- and Ru- metallodrugs. Pt-based compounds are reported to have no important antitumor activity, most likely due to the strong irreversible binding. This is not the case for ruthenium compounds, since HSA plays a big role in the distribution of these compounds throughout the body [35].

HSA is reported to play a big a role in KP1019's mode of action. The initial binding of KP1019 with HSA occurs at the HSA's hydrophobic binding sites in a noncovalent manner, however, the interaction slowly changes to a protein-coordinated form after a longer incubation time. It is known that ruthenium complexes can bind to albumin and transferrin when they are independently incubated with each protein in buffer conditions, however, in the blood serum they show a preference for albumin. The role of protein binding is essential for its bioavailability as it prevents its precipitation and hydrolysis at pH 7,4 [35].

KP1019 is known to bind the protein with moderately strong affinity and in a reversible manner. Several binding constants have been reported for KP1019, ranging from log K'_B=4,02 to log K'_B=5,66, the latter using the same approach (and PSEQUAD program) as the one used in this thesis [35, 42].

1.3.2. Structure and composition of Human Serum Albumin

Albumin is a serum protein consisting of a single polypeptide chain of 585 amino acid residues, which are organized in three structurally similar α-helical domains (I, II and III) resembling a heart shape as shown in **Figure 9(a)**. Each domain is additionally divided into two subdomains, A and B **(Figure 9(b))** that includes six and four α-helices, respectively, connected by long α-helical chains [44].

The stability of the 3D native structure of albumin is maintained by several factors such as inter- and intra-domain forces being hydrophobic interactions, salt bridges and natural boundaries of helical extensions present between three domains [44].

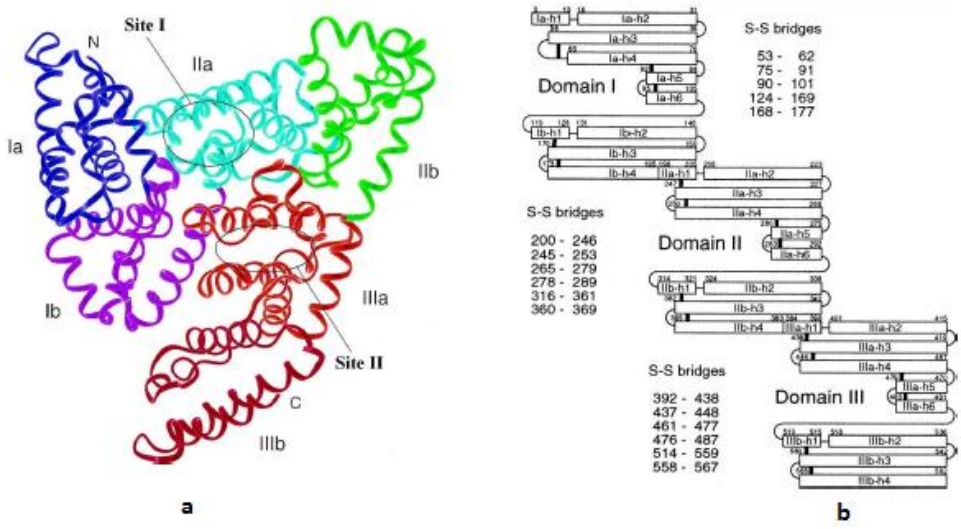

Figure 9. Graphic representation of Human Serum Albumin showing: **a)** tertiary structure (each subdomain is marked with a different colour) and **b)** secondary structure of HSA (disulphide bridges are drawn with thick lines) (modified from ref[43]).

The protein accommodates several amino acid residues that present fluorescence properties, 31 phenylalanine (phen) and 18 tyrosine (tyr) residues and only one tryptophan (Trp214) [45]. For this reason, albumin is the perfect candidate for fluorimetric studies because the tryptophan amino acid can be selectively excited at 295 nm. Tryptophan is located on the 214th position of the sequence and it is spatially oriented towards binding site I (Sudlow´s site I) within the protein. Therefore, any changes in the fluorescence properties of the protein are attributed to modifications in the surroundings of the tryptophan amino acid.

Albumin is a flexible molecule that rapidly assumes different conformations. It could be regarded as an assembly of resilient parts frequently contracting, expanding and flexing through the opening and closing of major crevices under the influence of ligands. As a result of this constant motion of the amino acid chains, the molecule of albumin is well fitted to adapt or discharge the many substances that it transports [46].

This protein is very soluble because it contains a large number of ionized amino acids that contribute to its high total charge. The isoelectric point of the protein, (which is the pH at which the net charge of a molecule is zero) is the pH at which the protein will not move to an electric field, for fatty acid free albumin in 0,15 M NaCl the isoelectric pH is about 4,7. The global charge of the protein at pH 7,4, which was the pH used in the measurements, is negative (-19) [46].

1.3.3. Binding sites on HSA

Specific interactions of drugs and their competition for binding sites on transport proteins might influence their distribution in serum. Therefore, information on the drug-HSA binding will provide a better understanding of the absorption and transportation of a specific drug. Structural examinations have

displayed specific locations of the drug binding sites on HSA affecting some domains or subdomains of the protein [44]. Numerous drugs bind to one of the two primary binding sites on the protein (hydrophobic cavities) in subdomains IIA and IIIA, denominated Sudlow's sites I and II, respectively (**Figure 9(a)**) [47]. These are considered the main ligand binding sites on albumin [47]. According to Sudlow´s classification, site I has been identified for the binding of large ligands with negative charge such as dicarboxylic acids or bulky heterocyclic molecules, whilst site II has been outlined by the binding of aromatic carboxylic acids such as non-steroidal anti-inflammatory drugs [48-50].

Strong binding interactions between drugs and albumin can decrease the free concentration of drug in plasma, while weak binding interactions can lead to a poor distribution or short lifetime. Therefore, too weak or too strong binding between drugs and the serum protein will lead to poor drug distribution. Under the circumstances, it is clear that the investigation of these binding interactions is very important from the pharmacologic and pharmacodynamics point of view [36, 51].

1.4.0. Site markers: Warfarin and Dansylglycine

Warfarin [3-(α-acetonylbenzyl)-4-hydroxycoumarin] (WF) is an anticoagulant drug that has been widely used to treat illnesses such as pulmonary embolism and venous thrombosis [52]. The molecule´s structure is normally drawn like an open chain, however, it is generally thought to exist as a cyclic hemiketal in solution [53] (**Figure 10**). The site I is responsible for the specific binding of warfarin and other drugs such as azapropazone and phenylbutazone, to name a few. Consequently, this site is also called the *warfarin-azapropazone binding site* [54, 55]. Warfarin is used as a marker ligand or competing agent to study the interactions of other drugs for the explicit binding to site I on HSA because under normal therapeutic conditions, warfarin is 99% bound to the serum protein in circulation [56]. Warfarin binds to the site I of HSA with an apparent binding constant log K_b of about 5,71 or 5,79 [42, 57].

Dansylglycine N-[(5-dimethylamino)naphth-1-ylsulfonyl]glycine (DG) belongs to a class of dansylated amino acids, which are largely used as fluorescent probes for the characterization of the binding sites in albumin. This site marker in particular is a probe for the binding site II and its structure is shown in the **Figure 10** [58]. Dansylglycine is used as a marker ligand or competing agent to study the interactions of other drugs for the explicit binding to site II on HSA, it normally binds to the site II of HSA with an apparent binding constant log K_B of about 5,34- 5,36 [35, 57].

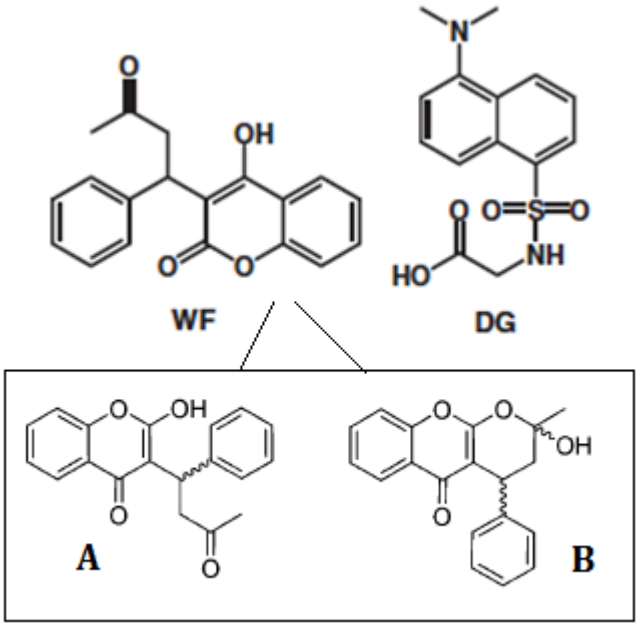

Figure 10. Chemical structures of Warfarin (WF, top left) and Dansylglycine (DG, top right). Bottom: Warfarin displays an open side chain conformation **(A)** and a cyclic hemiketal conformation (**B**), which is how it is normally found in solution (modified from ref [57, 59]).

2.0. OBJECTIVES

The development of new medicines for cancer therapy is a research theme very appealing to me. To be able to work on this topic provides me excitement, motivation, and the feeling that my work will somehow contribute to achieve an important goal with a great impact on society and healthcare.

Ruthenium complexes are a promising option to the toxic platinum-containing compounds available in the Clinic. Ruthenium(II) complexes bearing the {Ru(η^5-C_5H_5)} moiety (or{Ru(Cp)}), in particular compounds with bipyridine (or derivatives) in their coordination sphere have been exhibiting high potential as metallodrugs for cancer treatment.

For new drugs, the evaluation of their binding in the blood to serum proteins is mandatory because it influences the bioavailability of the drug and the efficiency of its distribution through the body. In addition, HSA binding can improve the selectivity of a drug by means of passive targeting to the tumour tissue [21].

The goal of this work was to access the biospeciation in the blood of the complex $[Ru^{II}(\eta^5\text{-}C_5H_5)(bipy)(CO)][PF_6]$ – herein referred to as RuC – by the studying the binding of this complex to human serum albumin. In particular, we were interested in evaluating the interaction of RuC with HSA under physiological conditions, which species may form in the blood and the corresponding binding constants involved.

Spectroscopic techniques were used to achieve this goal, namely UV-Visible absorption and Fluorescence emission. Given the high sensitivity and versatility of the latter, fluorescence was the method chosen to assess the system RuC–HSA and to elucidate the complex binding site(s) on HSA using site-markers.

Conclusions gathered from the study executed in this thesis can be used as model and are expected to be valid for other compounds with the same type of structure and same type of ligands.

The following chapter addresses some details on the techniques used in this work, particularly fluorescence spectroscopy. Chapter 4 describes in detail all the steps followed to execute the experimental work (reactants, equipment, preparation of samples and all the necessary conditions to acquire the results obtained in this thesis). Chapter 5 contains results, graphs and tables obtained from experimental data for the interaction between RuC and ^{faf}HSA, and for the systems ^{faf}HSA–site marker and RuC. Following this chapter, conclusions and future prospects are presented.

3.0. TECHNIQUES USED FOR THE STUDY

The interaction of the metal ion complexes and blood serum components can be monitored by spectroscopic techniques. These techniques provide useful information on the extension and nature of the binding between the metal complex and the blood plasma components, particularly with high molecular components such as albumin.

The quantitative goal of this work is the determination of the binding constants between the protein (HSA) and the complex (RuC). However, before this determination could be performed, the stability of the complex in solution had to be checked so spectroscopic changes in the samples could be traced as an indication of the binding process. In this work, fluorescence and UV-Vis spectroscopies were used to characterize the interaction between RuC and human serum albumin. Both techniques provide experimentally simple and straightforward methods to evaluate the interaction of biomolecules and metal complexes, and in this section some aspects relevant for this work are addressed.

Fluorescence spectroscopy is a highly sensitive technique that has a wide range of applications for biochemical and organic substances. It can be used to identify compounds and it is increasingly applied in biochemistry. This technique was chosen for this work because the serum protein contains natural fluorophores in the near ultraviolet region (amino acids that present aromatic side chains, such as tyrosine, phenylalanine and tryptophan). Fluorescence emission is more sensitive to the environment surrounding the fluorophores than absorption, and this is an effective method to detect and follow the binding of ligands, metal complexes or structural changes in biomacromolecules [60].

UV-Vis spectroscopy is a very common technique, and the basic principles that support it are very well known. As such, this section focuses on the UV-vis spectrum of the Ru(II) metal complex being studied. Fluorescence Spectroscopy was the technique used for the quantitative approach to the systems studied, and for that reason is presented with much more detail.

3.1.0. UV-Vis spectroscopy

UV-Vis absorption spectroscopy was used to assess the stability of the parent complex in aqueous solution and to optimize experimental conditions. It is easy to agree to the use of this technique for optimization studies due to several reasons: it is a method that provides simplicity, results achieved in a rapid manner, precision and low cost.

Apart from the n- π* and π- π* transitional bands that can be observed in any molecule, some specific bands are identified in the electronic spectra of transition metal complexes, such as d-d bands and charge transfer bands.

Charge transfer (CT) bands are often detected in transition metal complexes. When the ligand contains a group of orbitals of low energy, there is a possibility of a new transition that involves the charge transfer between metal and ligand,

Metal-to-Ligand Charge Transfer (MLCT) (**Figure 11**). There is also the possibility of transitions between the d-d orbitals from the metal and the orbitals from the ligands. These charge transitions between the metal and ligand derive into absorption bands in the visible, whereas the transitions in the ultraviolet come from the transitions within the ligand orbitals, which are normally n- π* and π- π* [61].

The compound studied in this work is a ruthenium(II)-cyclopentadienyl complex with a piano-stool structure. In this structure, quite different from the octahedral or tetrahedral geometries typically found in metal complexes, the cyclopentadienyl ligand is considered as the seat of the stool, and the three remaining coordinating positions are considered the three legs. The crystal structure of the complex $[Ru(Cp)(bipy)(PPh_3)]^+$ (also known as TM34) is reported in the literature; this complex is very similar to RuC, with a triphenylphosphine co-ligand (PPh_3, Ph or C_6H_6 is a phenyl substituent) replacing the CO ligand [21].

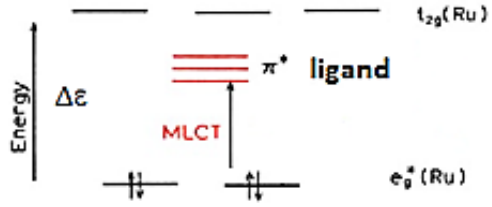

Figure 11. Scheme to elucidate the possibility of charge transfer bands in a tetrahedral geometry for a low spin Ru(II) complex where the two orbitals d of lower energy are complete with four electrons. According to the Cristal Field Theory (CFT), t_{2g} orbitals comprise three d orbitals d_{xy},d_{xz},d_{yz} and e_g refer to the d orbitals d_{x2-y2} and d_{z2}; the relative energy of the two sets of d orbitals is strongly dependent on the metal complex structure (octahedral or tetrahedral). (Δε, energy difference between e_g and t_{2g}, MLCT, metal-to-ligand charge transfer) (modified from ref[60]).

The UV-vis absorption spectrum of RuC in pH 7,4 HEPES buffered medium is shown on **Figure 12**.

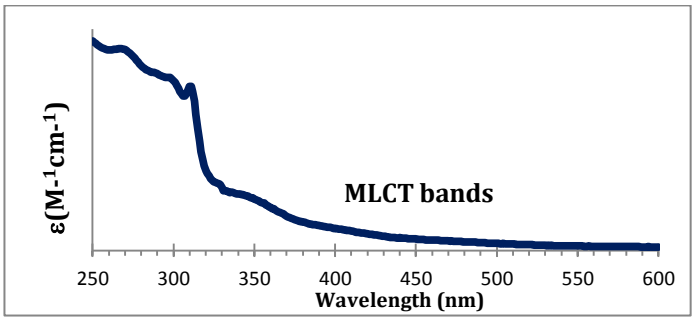

Figure 12. UV-VIS absorption spectrum for RuC, (in 10 mM HEPES pH 7,4)

The intense bands in the UV range (250 nm-320 nm) are assigned to π- π* electronic transitions occurring in the coordinated aromatic rings. In the range 320-380 nm the bands are assigned to electronic transtions occurring in the organometallic moiety $[Ru(Cp)(bipy)]^+$ and in the coordinated bipy chromophore, as was observed for the complex TM34 where the triphenylphosphine ligand replaced the CO [21, 26].

In the visible region (380-500 nm) several undefined bands can be assigned to metal-to-ligand charge transfer bands (MLCT) from the Ru 4d orbitals to π* orbitals of the bipy N-heteroaromatic ring [21, 25].

3.2.0. Fluorescence spectroscopy

Luminescence is described as the light emitted from any substance which occurs from electronically excited states. Depending on the nature of the excited state, luminescence is divided into two categories: phosphorescence (involving excited triplet states) and fluorescence (relating to excited singlet states) [60, 62].

Two processes are thus included in fluorescence spectroscopy, the absorption of light from a beam of electromagnetic radiation (promoting an electron to an excited state) and the emission of light by a chemical compound (the fluorophore).

After a fluorophore is excited to a higher vibrational level (S_1 or S_2), molecules in condensed phases (with few exceptions) rapidly relax to the lowest vibrational level of S_1. This process is called internal conversion and occurs rapidly, within 10^{-12} s or less. The return to the ground state (S_0) can be accompanied by luminescence or by other non-radiative decay (internal conversion or intersystem crossing, to name a few). These processes are typically depicted in a Jablonski diagram (**Figure 13**) and the light energy emitted is always of longer wavelengths [60].

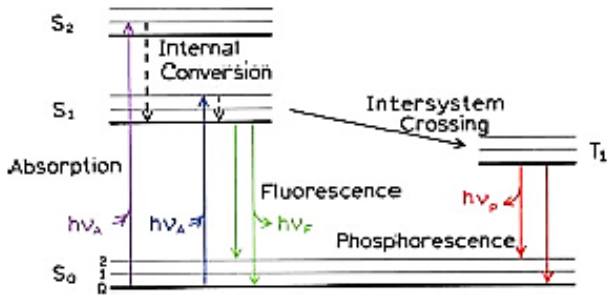

Figure 13. Displays one form of a Jablonski diagram where the luminescence phenomena are represented (ref[60]).

The fluorescence quantum yield (ϕ_F) is defined as the ratio of the number of photons emitted to the number absorbed and depends on the emissive rate of the fluorophore (Γ) and on the non-radiative decay to S_0 (k_{nr}), which depopulate the excited state. One of the approaches to obtain the fluorescence quantum yield is as follows (**Equation 1**):

$$\phi_F = \frac{\Gamma}{\Gamma + knr} \qquad \textbf{Equation 1}$$

The different fluorescence measurements performed in this thesis are described in the next subsections.

3.2.1. Steady-state measurements: emission spectra.

If there is only one species in the fundamental state, the excitation spectrum is identical to the absorption spectrum (i.e. the two spectra overlap). However, if more than one species is present or only one species but in different ionization states, the spectra do not overlap.

Considering all emitted photons, whatever their energy in order to express the steady-state fluorescence intensity per absorbed photon as a function of the wavelength of the emitted photons $F_\lambda(\lambda_F)$ and satisfying the relationship (**equation 2**), where ϕ_F is fluorescence quantum yield defined above.

$$\int_0^\infty F_\lambda(\lambda_F)d\lambda_F = \phi_F \qquad \textbf{Equation 2}$$

$F_\lambda(\lambda_F)$ symbolizes the fluorescence spectrum or emission spectrum, reflecting the distribution of probability of several transitions from the lowest vibrational level (S_1) to the various vibrational levels of S_0. The emission spectrum is characteristic of a given compound [62].

The steady-state fluorescence intensity I_F (λ_F) measured at wavelength λ_F (chosen by a monochromator with a certain wavelength bandpass $\Delta\lambda_F$) is proportional to F_λ (λ_F) and to the number of photons absorbed at the excitation wavelength λ_E (selected by a monochromator) [62].

The Stokes shift is the gap between the maximum of the first absorption band and the maximum of the fluorescence emission spectrum and it is most dramatic for polar fluorophores in polar solvents, due to interactions between the fluorophore and its immediate environment. This important parameter provides information on the excited states. For example, when the dipole moment of a fluorescent molecule is greater in the excited state than in the ground state, the Stokes shift increases with solvent polarity, which means emissions with lower energy or longer wavelengths (red shift). These shifts are very useful in fluorescence spectroscopy in order to predict the polarity of the area where the fluorophore is located [60, 62].

3.2.2. Fluorescence quenching mechanisms

Fluorescence quenching is the process that decreases the fluorescence intensity of any sample. There are a variety of molecular interactions that could result in quenching, including: molecular rearrangements, energy transfer, ground-state complex formation, excited-state reactions and collisional quenching.

In systems where more than one species is present, fluorescence emission intensity can be diminished by a process of self-absorption/Inner filter effect exerted by one of the components. Inner filter effect is the phenomenon arising when the recorded fluorescence intensity is not proportional to the concentration of the fluorophore due to the absorption of a fraction of the incident light before it reaches the point in the sample at which luminescence is observed, and re-absorption of some of the emitted light before it leaves the cell.

As a consequence, the observed fluorescence intensity depends on the optical density of the sample at both excitation and emission wavelengths [63]. These effects are quite important when a species absorbs light in the wavelength range where the emission of the fluorophore is collected. In other words, these effects are undoubtedly observed when the emission spectrum of the fluorophore overlaps with the absorption spectrum of other species that coexist in solution. This results in a "quenching effect" that does not indicate any interaction. Nevertheless the effect can be corrected using **Equation 3**:

$$IF_{corrected} = IF_{measured} x 10^{(Aex+Aem)/2} \qquad \textbf{Equation 3}$$

Where $IF_{corrected}$ and $IF_{measured}$ are the corrected and measured fluorescence intensities, and Aex and Aem are the absorptivities at the excitation and emission wavelengths in the samples, respectively [60]. The inner filter effect was performed for the range of all the absorbances of the spectra obtained.

There are two types of quenching: static and dynamic. Static and dynamic quenching needs molecular contact between the quencher and fluorophore in order to successfully quench the intensity. However, there is also the possibility of a dual mechanism when both occur at the same time.

In the case of collisional or dynamic quenching, the quencher must spread to the fluorophore during the lifetime of the excited state and after the contact, the fluorophore returns to the ground state without emitting a photon. This mechanism happens without any enduring change in the molecules (without a photochemical reaction).

Collisional quenching can be described by the Stern-Volmer equation:

$$\frac{IF0}{IF} = 1 + k_q \, \tau_0 \, Cq = 1 + K_D \, Cq \qquad \textbf{Equation 4}$$

In this equation IF_0 and IF are the fluorescence intensities in the absence and presence of quencher, respectively; k_q is the bimolecular quenching constant; τ_0 is the lifetime of the fluorophore in the absence of quencher, K_D is the Stern-Volmer quenching constant and Cq is the concentration of quencher.

The Stern-Volmer quenching constant indicates the sensitivity of the fluorophore to a quencher: for a fluorophore buried in a macromolecule and inaccessible to water-soluble quenchers the value of K is low, and larger values are observed for a fluorophore that is on the surface of a biomolecule.

Fluorescence quenching can also occur by other processes. In static quenching the ligand is bound to the protein and the fluorescent intensity decreases with an increasing concentration of protein-ligand complexes. The result of the quenching is due to the formation of a non-fluorescent ground-state complex between the fluorophore and the quencher. The equilibrium between a fluorophore plus a quencher and the fluorophore-quencher complex is given in **Equation 5**.

$$F + nQ \underset{k_{-1}}{\overset{k_1}{\rightleftharpoons}} FQ_n \qquad \textbf{Equation 5}$$

In this equation F is the free fluorophore, n is the number of quenching molecules that bind to the fluorophore, Q is the free quencher, k_1 is the association rate, k_{-1} is the dissociation rate and FQ_n is the fluorophore-quencher complex. The association constant K_s can be calculated with the following equation (**Equation 6**).

$$K_S = \frac{[FQ_n]}{[F][Q]^n} = \frac{k_1}{k_{-1}} \qquad \textbf{Equation 6}$$

The total concentration can be calculated with the following equations (the start concentrations of protein and ligand are given by $[F]_0$ and Cq_0, respectively)

$$[F]_0 = [F] + [FQ_n] \qquad \textbf{Equation 7}$$

$$[Q]_0 = [Q] + n[FQ_n] \qquad \textbf{Equation 8}$$

After substituting equation 8 into equation 7 and some other arrangements with equation 6, the following equation is obtained:

$$\frac{IF_0}{IF} = \frac{[F_0]}{[F]} = 1 + K_S[Q]^n \qquad \textbf{Equation 9}$$

where K_s is the association constant and [Q] or C_q the concentration of the unbound fraction of the quencher.

A linear Stern-Volmer plot is generally an indication of the presence of a single class of fluorophores, all equally accessible to the quencher. If two fluorophore populations are present and one is not accessible to the quencher, or if the number of acting quencher molecules is more than one, the Stern-Volmer plots deviate from linearity towards the x-axis.

In many occasions the fluorophore can be quenched by both collisions and by complex formation with the same quencher. The characteristic feature displayed on the Stern-Volmer plots in these circumstances is an upward curvature concave towards the y-axis (see **Figure 15 in 3.2.3**).

As a result, the Stern-Volmer equation is modified and second order in C_q, which accounts for the upward curvature observed (**Equation 10**).

$$\frac{IF_0}{IF} = \left(1 + K_D C_q\right)\left(1 + K_S C_q\right) = 1 + (K_D + K_S)C_q + K_D K_S C_q^2 \qquad \textbf{Equation 10}$$

The dynamic portion of the observed quenching can be resolved with lifetime measurements (see next section).

Quenching measurements can reveal the accessibility of quenchers to fluorophores because if the protein was impermeable to the quencher and the fluorophore was situated inside the macromolecule, neither static nor dynamic

quenching would occur. Therefore, quenching studies are utilised to acknowledge the position of fluorophores in membranes and proteins [60].

Steady-state fluorescence is a very common method to study protein-ligand interactions. (In this context, "Ligand" can be an organic molecule or a metal complex that interacts with the protein and binds to it). In proteins, the three aromatic amino acids – phenylalanine, tyrosine, and tryptophan – are all intrinsic fluorophores, the dominant fluorophore being the indole group of tryptophan.

The emission spectra of tryptophan often changes in response to denaturation, conformational transitions, subunit association or substrate binding. Tryptophan seems to be only sensitive to collisional quenching, due to a tendency of excited-state indole to donate electrons, and can be quenched by nearby groups within the protein or by externally added quenchers.

In fluorescence, proteins are normally excited at 280 nm or longer wavelengths. The absorption of proteins at this wavelength is due to tyrosine and tryptophan residues, but when the protein is excited at longer wavelengths than 295 nm, the absorption is mainly due to tryptophan [60].

Human serum albumin (HSA) exhibits 18 Tyrosine residues and one lone Tryptophan, Trp214 (**see section 1.3.2.**). Thus Trp214 can be used as a structural probe in the protein, using 295 nm as the excitation wavelength, and this very attractive feature combined with the high sensitivity of the Fluorescence spectroscopy makes it a preferred method for studying the binding of small molecules to HSA.

3.2.3. Time-resolved measurements

In time-resolved Fluorescence it is the intensity decay of the fluorescent sample that is measured: the sample is exposed to a pulse of light (such as a LED source), and the emission intensity decay is recorded with a high-speed detection system on the nano-second timescale [60].

The relationship between steady-state and time-resolved measurements can be understood using **Equation 11**. The steady-state intensity (I_{ss}) is related to the decay time by

$$I_{SS} = \int_0^\infty I_0\, e^{-t/\tau} dt \;=\; I_0\, \tau \qquad \textbf{Equation 11}$$

I_0 can be considered a parameter that depends on the fluorophore concentration and on several instrumental parameters. A steady-state measurement is simply an average of the time-resolved phenomena over the intensity decay of the sample.

There are two methods to measure time-resolved fluorescence: frequency-domain and time-domain. Time-domain is the method used in this thesis and it is described below.

In the frequency domain or phase-modulation method, the sample is excited with intensity-modulated light. The intensity of the incident light is varied at a high frequency typically around 100 MHz, therefore, its reciprocal frequency is comparable to the reciprocal of decay time τ. When a fluorescent sample is excited according to this method, the emission is forced to respond at the same modulation frequency. The lifetime of the fluorophore causes the emission to be delayed in time relative to the excitation, represented as a shift [60].

In the time domain or also called pulse fluorometry method, a pulse of light excites the sample, this is the most popular technique to determine lifetime measurements. The width of light is made as short as possible and it is by preference much shorter than the sample´s decay time τ. In order to register the time-dependent intensity the excitation pulse is followed, the decay time τ is then calculated from the slope obtained by plotting log I(t) versus t or from the time at which the intensity decreases to l/e of the intensity at t=0 [60].

Most instruments are based on the time-correlated single-photon counting (TCSPC) method or also called single-photon timing (SPT). The main principles depend on the fact that the likelihood of detecting a single photon at a certain time t after an exciting pulse is proportional to the fluorescence intensity at that time. Recording a single photon involves the timing between the excitation pulse and its emission, the distribution of collected data recorded over time is represented in the form of a histogram [62].

In this work, the excitation pulse is generated by a nanoLED (pulse light-emitting diodes that emits pulses of light with an ideally regular and infinitesimal duration) which is routed through a discriminator (CFD, constant function discriminator), the corresponding electrical pulse is forwarded to the start input of the time-to-amplitude converter (TAC) that generates a ramped voltage that increases gradually with time. Meantime, the sample is excited by the pulse and emits fluorescence. The optics is adjusted so the photomultiplier does not detect more than one photon per exciting pulse. The corresponding electrical pulse is routed through a discriminator to stop the input of the TAC and then this generates a voltage directly proportional to the delay time between excitation of the pulse and the photon detection (Δt) [62].

The analysis of this pulse is achieved by an analogue-to-digital converter (ADC) that converts the voltage into a digital value and a multichannel analyser (MCA) then adapts the numerical information, developing a histogram from the sum of several pulses (countagens versus time, **Figure 14**) [60, 62].

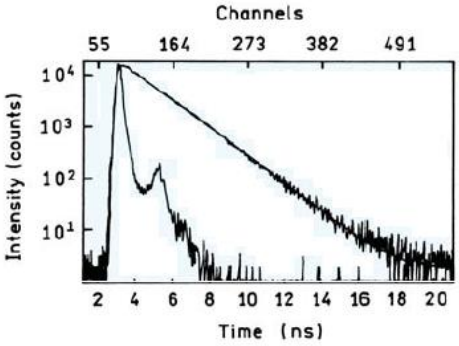

Figure 14. Example of an histogram of a fluorescence species along with the time (modified from ref[60])

Fluorescence intensity decays are achieved after a very short pulse of light with sufficient energy has brought a specific number of molecules to an excited state. Because of the fact that the rate constants for the radiative and non-radiative procedures (k_r and k_{nr}) are first order, the fluorescence intensity $i_{(t)}$ observed at a time *t* after excitation by a very short pulse of light at time 0, is proportional to the instantaneous concentration of molecules still excited [A*], and it is given by the following equation [62]:

$$i_{(t)} = k_r [A^*]_0 \exp(-t/\tau_0) \qquad \textbf{Equation 12}$$

where kr is the radiative rate constant, $[A^*]_0$ is the number of excited molecules per volume unit, t is the time and τ_0 is the lifetime of the excited state (which is at the same time $\tau_0 = 1/(k_r + k_{nr})$). The intensity decreases with time according to an exponential law and the fluorescence decays can be described by a single exponential (simple decay) or by a sum of them (complex decays). The following equation describes a multi-exponential decay with n components, intensity decays are typically fit to this model [60, 62]:

$$i_{(t)} = \sum_{i=1}^{n} \alpha_i \exp(-t/\tau_i) \qquad \textbf{Equation 13}$$

where α_i is a pre-exponential factor which is related to f_i (fractional contribution of each chromophore species to the total fluorescence intensity) and τ_i is the lifetime of the i species. Therefore, according to this equation, after the pulse excites the molecules, the fluorescence intensity decreases exponentially along with time [62].

The natural way of describing an average decay time (or lifetime) when the fluorescence decay of a fluorophore is multi-exponential is [62]:

$$\langle \tau \rangle_f = \frac{\sum_{i=1}^{n} \alpha_i \tau_i^2}{\sum_{i=1}^{n} \alpha_i \tau_i} = \sum_{i=1}^{n} f_i \tau_i \qquad \textbf{Equation 14}$$

Each decay time is weighted by the corresponding fractional intensity. The average is called the intensity-averaged decay time (or lifetime). This corresponds to the lifetime of the excited state that is defined as the average time that a molecule spends in the excited state before returning to the fundamental state [60, 62].

Another possibility is to use the amplitudes or pre-exponential factors as weights:

$$\bar{\tau} = \frac{\sum_{i=1}^{n} \alpha_i \tau_i}{\sum_{i=1}^{n} \alpha_i} = \sum_{i=1}^{n} \alpha_i \tau_i \qquad \textbf{Equation 15}$$

where α_i are the fractional amplitudes

$$a_i = \frac{\alpha_i}{\sum_{i=1}^{n} \alpha_i} \quad \text{being} \quad \sum_{i=1}^{n} a_i = 1$$

The weighted amplitude-average lifetime is proportional to the quantum yield and therefore it is also called *weighted lifetime for quantum yield* [62].

This type of measurement provides information not available from the steady-state data: to distinguish static from dynamic quenching processes lifetime measurements are essential [60]. In fact, the dynamic portion of the observed quenching can be in a mixed static and dynamic quenching process can be determined by lifetime measurements using:

$$\tau_0/\tau = 1 + K_D C_q. \qquad \textbf{Equation 16}$$

which accounts for the linear dashed line (with slope K_D) in **Figure 15**.

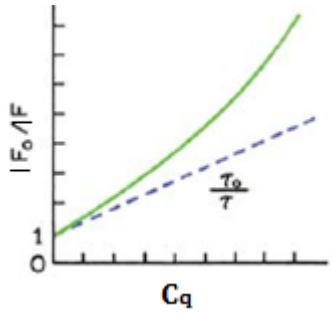

Figure 15. Stern-Volmer plot of a dual mechanism dynamic and static quenching of the same population of fluorophores [60].

3.3.0. PSEQUAD

PSEQUAD is the program used in this work for the estimation of binding constants. In a quantitative approach to any binding process, the major goal is to calculate the binding constant(s) involved in the system and the stoichiometry of the bound species formed.

The equilibrium process can be described by

$$p\,(\text{ligand}) + q\,(\text{HSA}) \rightleftharpoons \{(\text{ligand})_p(\text{HSA})_q\}$$

and the global conditional binding constant β_{pq}' in a buffered medium is defined by

$$\beta'_{pq} = \frac{[(ligand)_p(HSA)_q]}{[ligand]^p[HSA]^q} \qquad \textbf{Equation 17}$$

In this notation "ligand" refers to any small molecule binding to the protein (HSA). In the specific case of the work involved in this thesis, "ligand" is in fact either RuC or a site-marker.

The computer program PSEQUAD evaluates spectroscopic and/or potentiometric equilibrium data using analytical derivatives [64]. The equilibrium system can be defined by the following mass-balance equations such as:

$$C_t = \sum_{j=1}^{n} \alpha_{jt} [S_j] = \sum_{j=1}^{n} \alpha_{jt} \beta_j \prod_{i=1}^{k} [c_i]^{\alpha ji} \quad (t = 1 \dots k) \qquad \textbf{Equation 18}$$

where C_t is the total concentration of the t^{th} component, n corresponds to the number of species present in the system (including the components), S_j is the j^{th} species present in the system, k is the number of components in the system, $[c_i]$ is the equilibrium concentration of the i^{th} component, β_j is the global formation constant of the j^{th} species, and α^{ji} the stoichiometric numbers, giving the number of the i^{th} component in the j^{th} species, α is called composition matrix.

In order to solve this equation, PSEQUAD calculates the unknown free concentrations based on the standard Newton-Raphson procedure and obtains the unknown formation constants and/or molar absorbances by minimizing the F function by an iterative cyclic procedure.

$$F = \sum_{q=1}^{n_d} F_q = \sum_{q=1}^{n_d} \sum_{i=1}^{r_q} \left(w_1 (\Delta X_1^V)^2 + \sum_{l=2}^{m} w_l \left(\Delta X_l^p\right)^2 + w_A \sum_{l=m+1}^{p} (\Delta X_l^A)^2 \right) \qquad \textbf{Equation 19}$$

where w_l is the weighting factor of the titrant´s volume or total concentrations, w_l is the weighting factor for the l^{th} potential measurements, w_A is the weighting factor for the absorbance measurements and F_q is any function correctly composed from the experimental data [64]. As a result, what is is minimized in the calculations is:

$$wA \sum (\Delta A_{experimental} - \Delta A_{calculated})^2 \qquad \textbf{Equation 20}$$

where ΔAcalculated is achieved for each wavelength, from the reagents´ concentrations used, log β values in use and Δε values in use for each emitting component. The meaning of "in use" is that the values are being used for a determined iteration and changing between iterations until the minimization of the function is accomplished.

Steady-state fluorescence results were used to calculate binding constants for adducts formed using PSEQUAD. In these calculations, RuC is simply referred to as C for clarity; so, and adduct formed between albumin and RuC with a 1:1 stoichiometry is {HSA-C}, one with a 1:2 stoichiometry is {HSA-C_2}. The systems analysed also included {HSA-site marker} and {HSa-site marker-Ru^{II}complex} adducts. For the systems evaluated in this work, the mass-balance equations can be written as [64]:

$$C_{ligand} = [ligand] + \sum_{i=l}^{n} p_i \beta'_{pq} [ligand]^{p_i} [HSA]^{q_i} \qquad \textbf{Equation 21}$$

$$C_{HSA} = [HSA] + \sum_{i=1}^{n} q_i \beta'_{pq} [ligand]^{p_i} [HSA]^{q_i} \qquad \textbf{Equation 22}$$

where,

β'_{pq}= overall conditional binding constant of HSA- "ligand" complexes

c_x= analytical (total) concentration of component x (HSA or "ligand")
[x]= equilibrium concentration of component x
Q= 1 (typically for the albumin system)

whereas,

$$I_i=\Phi^i_{ligand} \times [ligand]+\Phi^i_{HSA} \times [HSA]+\Phi^i_{HSA\text{-}ligand} \times [HSA\text{-}ligand] \quad \textbf{Equation 23}$$

with

I_i=fluorescence emission intensity at "I" nm (at each wavelength i)
Φ^i_x=proportional constant for component x at "I" nm (between I^i and equilibrium concentration of x); "molar intensity"

It is important that strictly identical parameters of the instrument are used at each measuring set for results evaluated in the same input file for PSEQUAD.
The program provides the standard deviation of the stability constant(s) calculated. The quality of the calculations achieved with PSEQUAD is reported by the program in the form of a fitting parameter, FP (which includes the error square sum), that represents how good the fit between the measured and calculated values is.

In the case of the fluorimetric titrations, the measured and calculated emission spectra are compared, and PSEQUAD calculates values of β'_{pq} with iterative cycles (Newton-Raphson procedure) by fitting these spectral data till the minimum difference between the data is reached. For fluorescence data, an FP in the range of 2_x10^5-3_x10^5 represents ca. 1-2,5% deviation between the measured and calculated values at the emission maximum.

4.0. EXPERIMENTAL PART

4.1.0. Reagents

Commercially available chemical reagents and albumin were used as delivered from the supplier without any further purification.

Human Serum Albumin fatty acid free (^{faf}HSA or simply HSA) (A3782) was provided by Sigma-Aldrich, lyophilized powder with a molecular mass of ca. 67000 g/mol. Warfarin (WF) (A2250) and Dansylglycine (DG) (D0875) (lyophilized powder) were purchased from Sigma-Aldrich and used without any further purification.

The ruthenium(II) complex studied in this thesis was [Ru^{II}Cp(bipy)(CO)][PF_6] which was synthesised and provided by Dr. Andreia M. Valente from the *Quimica Organometálica e Biorganometálica* group, Faculdade de Ciências, Universidade de Lisboa.

4.2.0. Preparation of solutions

Water: Millipore® water from a Millipore Milli-Q water purification system was used to prepare all aqueous solutions.

Buffer: 4-(2-hydroxyethyl)-1-piperazineethane Sulfonic acid (**HEPES**) was prepared and then used to make the samples. In order to prepare this buffer, typically 1.19 g of HEPES provided by Sigma-Aldrich were weighted, transferred into a 500 mL volumetric flask and then filled up with Milli-Q water yielding a final concentration of 10mM. Concerning the pH adjustment, concentrated solutions of HCl 2 M and KOH 4 M provided by VWR, were required to achieve a final pH of 7,4.

Ruthenium complex (RuC) solutions: the preparation of stock solutions and following dilutions was required in order to achieve more accurate pipetting. To prepare the ruthenium solutions for the experiments with the ruthenium complex, typically 1 mg of the complex was weighted into a 10 mL volumetric flask and dissolved in HEPES 10 mM, pH 7,4, yielding a typical concentration of $1,9\text{-}3,6_x10^{-4}$ M. The solutions were freshly prepared for each experiment immediately before use.

Albumin solutions: Albumin solutions were freshly prepared for every experiment by dissolving ^{faf}HSA in 10 mM HEPES. Albumin stock solutions were allowed to stand for at least 30 minutes at room temperature to allow the protein to hydrate and fully dissolve, being gently swirled from time to time. The concentration of each ^{faf}HSA solution was determined spectrophotometrically by UV-vis absorption using a molar extinction coefficient of ε_{278} nm =36850 M^{-1} cm^{-1} [65, 66].

HSA-RuC samples: These samples were prepared varying conditions such as concentration of the protein and incubation time to optimize measurement

conditions and equipment parameters (eg. bandwidth for the excitation and emission of the fluorescence intensity). Individual protein-complex samples were prepared to ensure in each assay the same incubation time at (37,0 ± 0,5) ºC. All samples were prepared with a total volume of 4 mL in glass vials. The specific volumes of protein and complex solutions were added to each glass vial according the concentration required and then filled up with HEPES to a total volume of 4 mL. Samples were then inserted into the oven and allowed to incubate for (24 ± 1) h.

Samples of the experiments incubated and measured at (37 ± 1) ºC had a final protein concentration that varied from 2,0 μM to 5,2 μM (kept constant), and the complex concentration was varied accordingly to obtain HSA:RuC molar ratios ranging from 1:0,5 to 1:24.

Samples with the same complex concentration but with no protein were prepared for appropriate background correction.

Warfarin (WF) stock solutions: Warfarin stock solutions of approximately 100 μM was prepared and used within a week (maximum). The stock solution concentration was determined on the basis of the UV-vis spectrum using $\varepsilon_{308\ nm}$=14475 M-1 cm-1, Molecular weight (MW) = 308,34 g/mol [57].

Warfarin samples: In order to prepare these samples, adequate dilutions from the stock solution were executed to obtain a final concentration in these samples that varied from 5 to 80 μM. The final volume of these samples was 4 mL.

Warfarin-HSA-samples: These samples were prepared with a final volume of 4mL in HEPES medium, keeping the concentration of HSA constant at 2 μM and varying the concentration of WF from 0 to 40 μM. Samples were incubated at 37 ºC for at least one hour before measuring the fluorescence. A sample of HSA alone was prepared simultaneously with the other samples and measured for background corrections.

WF-HSA-RuC samples: These solutions were prepared in HEPES medium keeping the concentrations of HSA and WF constant at 2 μM (equimolar) and varying the concentration of RuC from 0 to 44 μM, for a final volume of 4 mL. Before adding the complex to the samples, the adduct {HSA-WF} was incubated at 37 ºC for one hour, after which an adequate volume of RuC stock solution was added to each sample. These were then incubated for 24 hours in the oven at 37 ºC. A sample containing complex alone was prepared simultaneously with the other samples and measured for background corrections.

Dansylglycine (DG) stock solutions: Dansylglycine stock solutions were prepared following the same procedure as for Warfarin and the final concentration was assessed by UV-Visible spectroscopy using a molar extinction coefficient of $\varepsilon_{327\ nm}$= 5068 M^{-1} cm^{-1}, MW= 308,4 g/mol [57].

Dansylglycine samples: In order to prepare these samples, simple dilutions from the stock solution were performed. The concentrations of these samples varied from 1 to 40 μM.

Dansylglycine-HSA and Dansylglycine-HSA-RuC samples: These samples were prepared from the dansylglycine stock solutions following the same procedure as for WF-HSA and WF-HSA-RuC solutions.

A comprehensive list of the essays performed with detailed information is included in **Annex A1, table 1.**

4.3.0. Equipment

The pH of samples and buffer solutions was adjusted with a VWR international 1000 pH meter in order to monitor the pH changes equipped with a LE409 combined glass electrode from Mettler Toledo.

To keep the samples at the required temperature a Stuart scientific block heater SBH200D/3 (Staffordshire, United Kingdom) was used. This thermoblock device was used when the required temperatures were room temperature or higher. For low temperature measurements, incubations executed in a LAUDA Ecoline star edition bath.

Balance: All reactants were weighted in a AX205 balance from Mettler Toledo with a 0,01 mg sensitivity.

Micro pipettes were from Eppendorf (2-20 μL (±1,0% accuracy), 20-200 μL (±1,0-5,0% accuracy), 100-1000 μL (±0,6-3,0% accuracy) or VWR International (20-200 μL (±2,5-0,5%), 100-1000 μL (±0,9-0,6%), 1-5 mL (±0,6-0,5%)).

Cell holder bath: temperature control in the sample compartment of the spectrofluorometer was set by a Thermomix BU B. Braun thermobath equipped with a Frigomix U B. Braun as the cryostat controller.

Quartz cells: Suprasil quartz cells used 1 cm x 1 cm and 1 cm x 0,4 cm were from Hellma Analytics (Müllheim, Germany). The cells with the 0,4 cm optical path were used for absorbance and fluorescence measurements and the ones with 1 cm optical path only for the stability studies in the spectrophotometer (volume of the cells 1,4 mL)

An INCU-Line® incubator model IL53 from VWR international was used to incubate all samples (±0,5 ºC).

UV-Vis spectrophotometers: A JASCO V-660 spectrophotometer was used to perform all stability studies. Another spectrophotometer JASCO V-560 was used while performing the steady-state measurements. UV-vis absorption spectra were recorded at room temperature in the range 250-600 nm with 0,4 and 1 cm path Hellma® Analytics quartz suprasil cuvettes. Spectra for the experiments involving warfarin and dansylglycine were also recorded at room temperature in

the range 250-600 nm with the same cuvettes. A scan rate of 400 nm/min was typically used.

Spectrofluorimeter: Fluorescence measurements were performed in a Fluorolog-3 v2.2 Jobin Yvon HORIBA. Emission spectra were recorded in the range of 310-550 nm for HSA-RuC samples with $\lambda_{excitation}$=295 nm, in the range of 320-590 nm with $\lambda_{excitation}$=310 nm for the experiments involving warfarin and in the range of 345-620 nm with $\lambda_{excitation}$=335 nm for the experiments involving dansylglycine, using a 0,2 s integration time. Fluorescence emission intensity was corrected for the absorption and emission inner filter effects [60, 67] using the UV-Vis absorption data recorded for each sample (**Equation 3**, see **section 3.2.2**).

Time-resolved measurements were performed in a Fluorohub v2.0 also from HORIBA Jobin Yvon that was connected to the spectrofluorometer with a time scale of 55517 ps/channel. The maximum number of counts was 10000. The nanoLED light source used (279 nm) for the lifetime measurements was from HORIBA Jobin Yvon. Ludox® was used as the scatterer to obtain the instrumental response function and was provided by Sigma-Aldrich.

Suprasil quartz cells 1 cm x 0,4 cm used for steady-state and time-resolved fluorescence measurements were positioned with the largest optical path towards the excitation direction. Consequently, the excitation was performed along the 1 cm face of the cell and the emission collected from the 0,4 cm face. This procedure allowed to increase the intensity of the signal received.

In each assay blank specimens (samples that do not contain the fluorophore) were included, which were subtracted from the intensity for each sample. The entire procedure was executed for all the samples in the same manner, with the adequate excitation wavelength and slits. In order to be able to compare the experiences, these parameters need to be similar for the same type of sample, and they are listed in **Table 1**.

Table 1. Bandwidth or slits (nm) used in spectra recorded from the different experiments performed (emission spectra and lifetime measurements) and the nanoLED source used for each experiment.

Name of samples	Emission spectra (slits, nm)	Lifetime measurements (nanoLED bandwitdth)
HSA-RuC (37ºC):		(279 nm nanoLED)
HSA(2.25μM)	2	15
HSA(2.5μM)*	2	10, 13 and 14
HSA(2μM)	2	15
HSA(2μM)	4	(279 nm nanoLED) 15
Warfarin experiments (37ºC)		
WF alone samples	2 and 3	NA
WF-HSA samples	2 and 2.5	
WF-HSA-RuC samples	2 and 3	
Dansylglycine experiments (37ºC)		
DG alone samples	2 and 4	NA
DG-HSA samples	2 and 2.5	
DG-HSA-RuC samples	2 and 3	

4.4.0. Spectroscopic measurements: other experimental details

Emission spectra can be distorted by variations in the intensity of the excitation light, being these variations due to the dependence of the wavelength on the intensity of the lamp and the efficiency of transmission of the emission monochromator and for the detector response (photomultiplier tube). Because of this, a correction for the acquired spectra is needed, mainly for quantitative measurements [62]. The variations in the intensity of light were eliminated by the division of a reference signal while the remaining distortions were removed by applying a correction to the measured raw signal using correction files provided by the manufacturer.

For time-resolved fluorescence measurements the Fluorohub v2.0 coupled to the spectrofluorimeter (used for the steady-state measurements) was used. This allowed to measure fluorescence decays with the Single Photon Timing (SPT) technique. In this case, the excitation was performed by a pulsed nanoLED and for the detection a photomultiplier tube TBX-04 with a resolution of 50 ps was used.

The nanoLED used was chosen according to its wavelength. This wavelength had to be as close as possible to the excitation wavelength required of the sample in question and the emission collected, to the wavelength of maximum emission. For these measurements it was only necessary to control the emission slits since the radiation emitted from the nanoLED is essentially monochromatic (**Table 1**). During these experiments, the signal was recorded at emission wavelengths chosen according to the results from the steady-state measurements.

In the time-dependence studies, the time needed for the binding of RuC to HSA to reach thermodynamic equilibrium conditions was evaluated. Measurements were performed for the same samples (protein in the presence and in the absence of the complex, and also complex alone) every certain period of time, and one sample of each type was prepared for the whole session (three samples in total). A concentration of 4 μM was chosen for the protein samples and 40 μM for the complex. These three samples were measured at 37 ºC in the spectrofluorometer and straight after in the UV-Vis at room temperature ~25 ºC. For these studies the 1 cm x 0,4 cm quartz cells were used.

4.5.0. Data processing

The change in the UV-Visible absorption spectra was evaluated in: i) the solution stability study for RuC, and ii) in the time-dependence study of the interaction of RuC and the protein. These measurements were executed in 10 mM HEPES pH 7,4. The change in the different spectra recorded was assessed at a specified wavelength value with **Equation 24.**

$$\% \text{ Variation} = \left| \frac{(Abs_i - Abs_0}{Abs_0} \right| x100 \qquad \textbf{Equation 24}$$

Where Abs_i is the absorbance at time i and Abs_0 the absorbance at the initial time (time zero).

-Time-resolved fluorescence decays

Data processing for results from the lifetime measurements was done using the program Time-resolved fluorescence Anisotropy (TRFA) version 1,3 (Minsk, Belarus). The quality of the adjustment was assessed by a reduced χ^2 value that was not higher than 1,8 and a random distribution of weighted residuals and residuals autocorrelation.

Each fluorescence decay was evaluated fitting a sum of one, two or three exponentials and then values of χ^2 were compared in order to identify the best fit. The value of χ^2 is calculated by TRFA from **Equation 25** using the observed experimental fluorescence decay (R(t)) and the final response function (F(t)) by a least squares analysis method that calculates the expected value of R(t) given, considering values of α_i and τ_i. The calculated value [$R_c(t)$] is then compared to the observed one R(t). The α_i and τ_i values are altered until achieving the best fit. The goodness of the fit is calculated with

$$\chi^2 = \sum_{i=1}^{n} w[R(t) - R_c(t)]^2 \qquad \textbf{Equation 25}$$

where w=1/R(t) is a statistical weighting factor to account for the expected error for each value of R(t).

Values of χ^2 between 1 and 1,2-1,3 indicate an excellent fit. In what concerns the autocorrelation or plot of residuals, a random distribution around zero indicates the best fit.

In the present work, the decay recorded in some cases was slightly affected by the quality of the connection of the fibre optic cable, which resulted in lesser quality data and some χ^2 values higher than 1,8.

4.5.1. Static and Dynamic quenching constants

The calculation of the static and dynamic quenching constants (K_s and K_D) was done by a regression with variance analysis (ANOVA), fitting either a straight line or a second order polynomial to the experimental points. Using **Equations 10 and 16** from **sections 3.2.2.** and **3.2.3.,** respectively, a linear fit to the fluorescence lifetime τ_0/τ plot yielded K_D, and K_S was then calculated from the parameters adjusted by the quadratic fit to IF_0/IF. A confidence level of 95% was used in all fits and the value of R^2 obtained is indicated in all cases.

PSEQUAD – Global conditional binding constants

The emission spectra obtained from the steady-state measurements were used to create input files for the determination of the conditional binding constants with the computer program PSEQUAD [64]. In the input file, the total concentrations of each of the components of the system (RuC, protein, site-

marker) is required and the program reports the best values for the global conditional binding constants (calculated as Log β'_{pq} values) from the data used in each input file. The quality of the fit is evaluated by FP, the fitting parameter- please see **Annex C** (for more details on FP and PSEQUAD).

Speciation diagrams

The program HYSS (Hyperquad Symulation and Speciation- version 4.0.31) was used in this thesis to obtain speciation diagrams for the systems being studied. The program uses the binding constants values obtained with PSEQUAD to plot the equilibrium concentration of each species present in the system according to the total concentration of the protein and RuC complex given (e.g. in the conditions used for the measurements). Speciation diagrams presented in this work were drawn using 101 points.

5.0. RESULTS AND DISCUSSION

All results presented in this chapter are expressed as (value ± SD): the results from the Stern-Volmer studies were obtained with variance analysis (ANOVA) regression fit, with the least squares method. The standard error associated to the value is presented as Standard deviation, with a 95% level of confidence).

Results of conditional binding constants obtained with the program PSEQUAD are presented with a fitting parameter (which includes the error square sum), that represents how good the fit between the measured and calculated values is.

5.1.0. Stability of the studied complex (RuC).

The stability of the Ru(II) complex $[Ru^{II}(\eta^5\text{-}C_5H_5)(bipy)(CO)][PF_6]$ (RuC) in the medium that will be used to study its interaction with HSA has to be checked. In addition, it is necessary to choose the best incubation time in order to achieve consistent results on the following experiments. In this study two different aqueous media were used: water and an aqueous medium buffered with 10 mM HEPES pH 7,4. This stability test was performed at room temperature and in absence of light.

- Water

Figure 16 shows the change observed on the UV-VIS spectra at room temperature with increasing time: after 72 h the % of variation at 370 nm is less than 10% which indicates that the complex is moderately stable in aqueous solution.

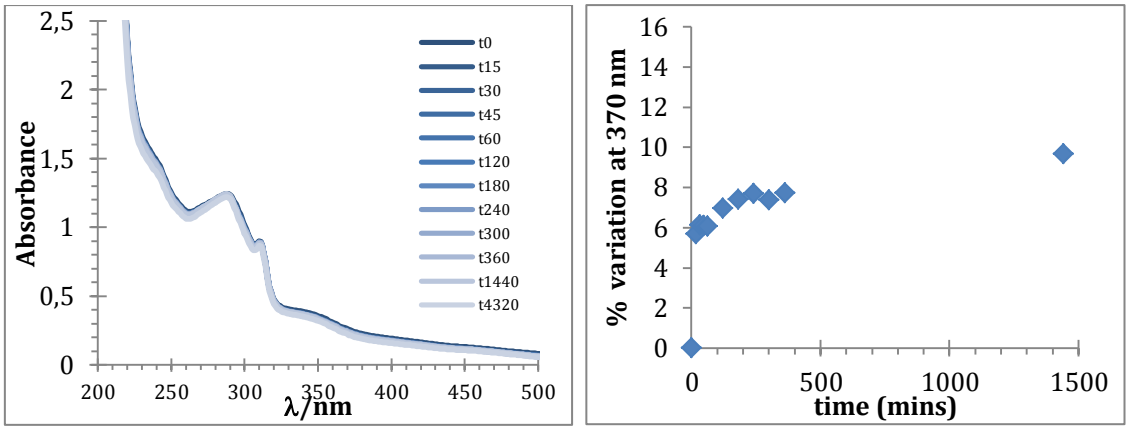

Figure 16. Stability of RuC in water, **Left**. Variation UV-VIS spectra with increasing time (in min, darker shade to lighter shade) for the complex RuC in water during 72 h (room temperature, in the dark),**Right,** change (% of variation (**Equation 24**)) at 370 nm for a period of 25 h: A maximum of 10% of variation is observed after 25 h.

Although water is a good solvent for RuC, the need for a buffered medium for the determination of stability constants percludes its use as the aqueous medium for the essays.

- 10 mM HEPES pH 7.4

Figure 17 shows the change observed on the UV-Vis spectra of RuC in 10 mM HEPES pH 7,4 with increasing time till 44 hours at room temperature. RuC is very stable in this medium: only negligible differences were observed in the spectra up to approximately 30 h (**Figure 17**, inset), confirming that the stability of the complex in HEPES buffer is adequate for the quantitative determination of binding constants as well as for *in vitro* biological studies.

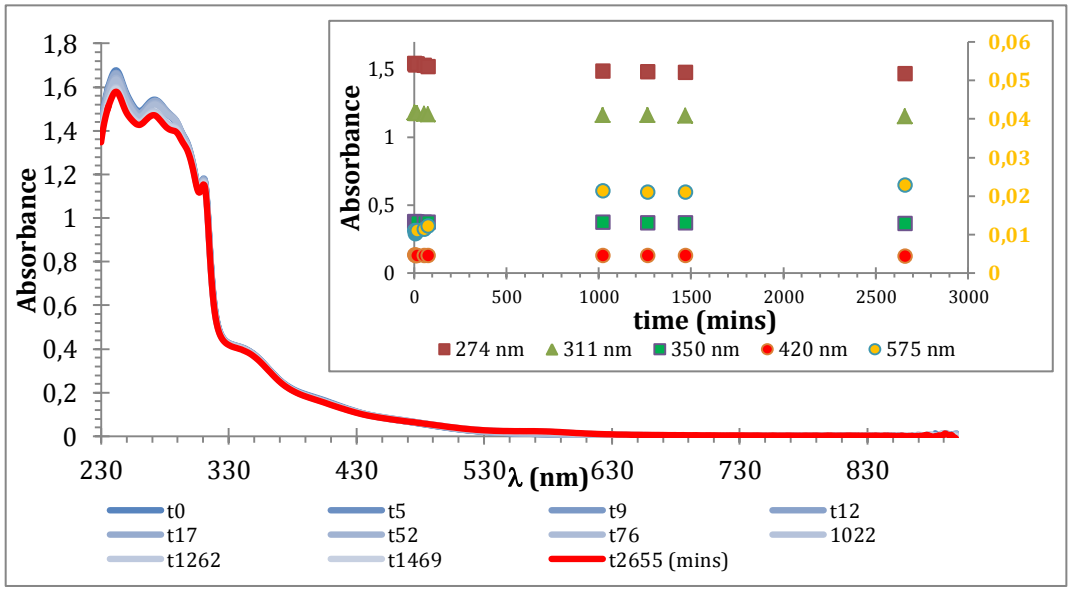

Figure 17. UV-visible spectra recorded over time (44 h) for the complex RuC in the buffer HEPES 10 mM pH 7,4**; inset:** Absorbance versus time at several wavelength values, data for 575 nm are indicated in the secondary axis.

The inset shows minimal variations in the values of Absorbance recorded for the main wavelengths along the 44 hours of the study, indicating that the complex is quite stable in 10 mM HEPES pH 7,4.

The absorbance at 420 nm (a MLCT band, quite representative of changes surrounding the metal ion Ruthenium) shows negligible changes during the 44 hours of the study, which means that HEPES is a suitable buffer to study these systems.

This stability test was performed at room temperature and in absence of light.

5.2.0. Time-dependence of the interaction between RuC and HSA

It is essential that the system under study is in thermodynamic equilibrium conditions for the accurate determination of any binding constants. As such, the time dependance for the interaction at study must be evaluated to establish the incubation time. The most suitable incubation time will combine the requirement of the system being in equilibrium with experimental feasibility. Time dependance for the RuC-HSA system was monitored by UV-VIS absorption and steady-state Fluorescence, and the results are included in **Figure 18** and **Figure 19** respectively.

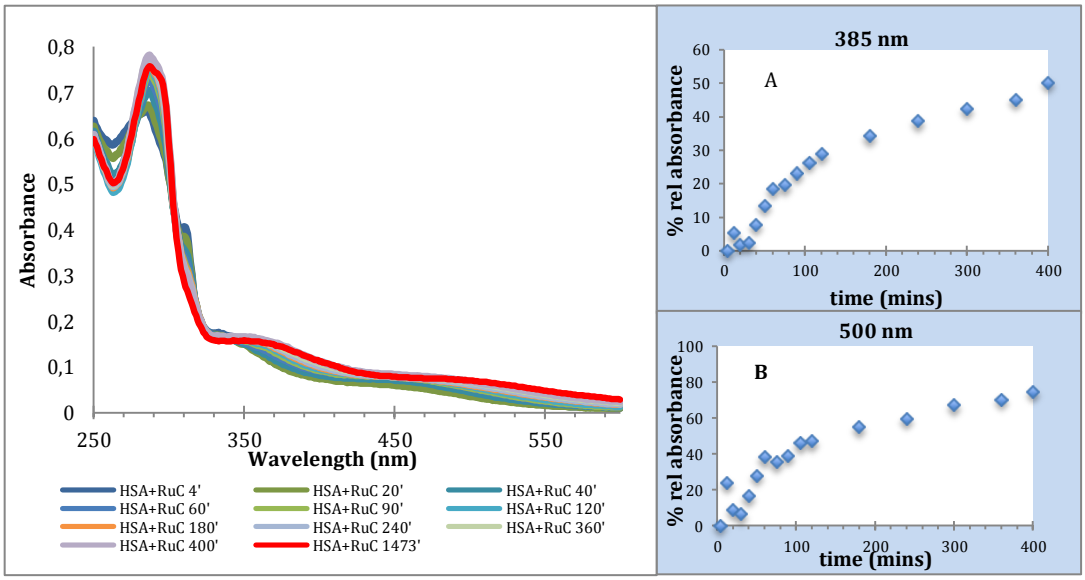

Figure 18. Time dependence for the RuC-HSA system in 10 mM HEPES pH 7,4: evolution of the UV-Vis absorption spectra of the sample HSA+RuC, The incubation time (in minutes) is indicated in different colours (first measurement in the minute 4 and last measurement in the minute 1473), C_{HSA}=4 µM, C_{RuC}=40 µM. Plots A and B show the relative variation of the absorbance at 385 nm and for the MLCT band.

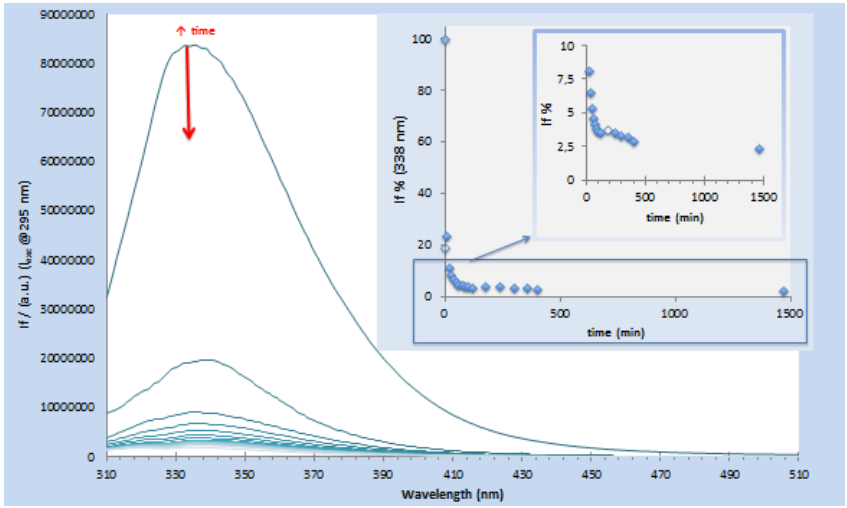

Figure 19. Time dependence evolution of the steady-state fluorescence spectra for the RuC-HSA system in 10 mM HEPES pH 7,4: the main plot displays the fluorescence emission spectra of the sample HSA+RuC until a 24 h contact time, C_{HSA}= 4 µM, C_{RuC}=40 µM. The insets show the relative If for the maximum absorbance at 338 nm.

Fluorescence emission spectra recorded for the system RuC-HSA over a 24h period are included in **Figure 19**. The inset shows the relative variation of the Trp214 emission intensity at 338 nm with time. There is a great decrease in the emission intensity in the first minutes of contact with RuC, indicating that the interaction occurs quite fast: after 10 min I_F decreases to ~20% of the intensity initially recorded for the protein alone (I_{F0}), after 20 min I_F decreases to 10% and after 30 min IF is ~8% of the initially recorded signal. After ~210 min (3,5h) changes in the emission spectrum become less intense until ~400 min when equilibrium is fully reached with %IF ~2,5%.

A 24h-incubation period was chosen to combine the need to assure that the thermodynamic equilibrium was reached and experimental feasibility. The best approach to rationalize the experimental time was to incubate the samples the day before measuring.

5.3.0. The system RuC-HSA

The binding of RuC to albumin (^{faf}HSA) was monitored by fluorescence spectroscopy using Trp214 as the protein intrinsic fluorescence probe.

The quality of experimental data recorded from fluorescence experiments requires much attention to experimental details. It is important to evaluate whether RuC has intrinsic fluorescence at the excitation wavelength chosen for Trp214 (295 nm). It is also important to check whether inner filter / self-absorption effects are operative. The plot **A** shown in **Figure 20** displays the absorption spectrum of the complex studied (RuC) where the excitation wavelength chosen for the emission is indicated (295 nm) and the emission spectrum of the protein is presented. The overlap between RuC absorption spectrum and the protein emission spectrum shown indicates that the reabsorption of emitted light is likely [60]. Therefore, data must be corrected for IFE (**Equation 3**) at both excitation and emission wavelengths to account for these aspects that decrease the steady-state fluorescence intensity and are not the result of a real interaction [60, 62].

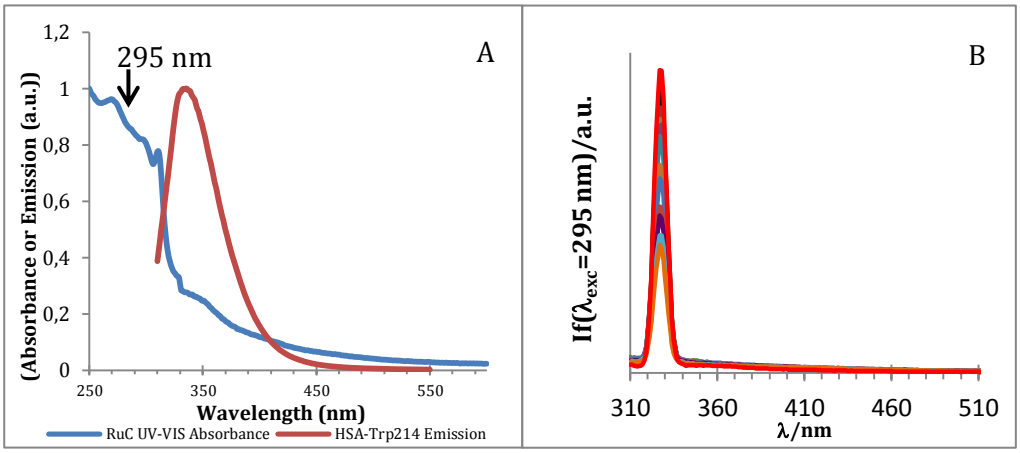

Figure 20. Inner filter effect in 10 mM HEPES pH 7,4: absorption spectrum of the complex RuC (C_{RuC}=40 µM) and the emission spectrum of HSA after its excitation at 295 nm (C_{HSA}= 4 µM) (**A**); Emission intensity RuC in the absence of HSA. A decrease of the intensity of the Raman peak is shown with increasing concentrations of the complex. λ_{exc}=295 nm (**B**).

The Ru(II) complex RuC did not exhibit any intrinsic fluorescence (only the sharp Raman peak due to scattered light was seen in the emission spectra) when it was excited at 295 nm. It is expected that the Raman peak would have the same fluorescence intensity for the different RuC concentrations, which is not the case in **Figure 20-B**: by seeing the different intensities the complex is showing some absorption of light, which confirms that the inner filter effect or self-absorption corrections are needed.

5.3.1. Steady-state fluorescence emission quenching

Fatty-acid-free HSA was used to evaluate the potential of the protein to bind the Ru^{II}-complex. Steady-state fluorescence emission was measured for the HSA-RuC system in several samples prepared from different stock solutions in different assays (see **Annex A**, **table 1**). **Figure 21** and **22** are representative of the results obtained in the different measurements.

In the absence of complex, the emission maximum intensity for Trp214 is observed at 335 nm, showing that in the protein this residue is protected from the aqueous solvent, where Trp would show a maximum emission at *ca.* 350 nm [60]. **Figure 21** presents the effect of increasing concentration of RuC on the protein fluorescence emission (in equilibrium conditions): the complex RuC quenches the fluorescence emission intensity of the protein with no shift (within the experimental error) in the maximum λ_{em} (**Figure 22-Left**). This quenching effect was expected from the time-dependence measurements, and it shows that the environment around the residue Trp214 is being affected by the presence of RuC, indicating that the complex might be binding the protein in the vicinity of Trp214. Further experiments with the site markers will help to reveal more details about the binding between the protein and the complex.

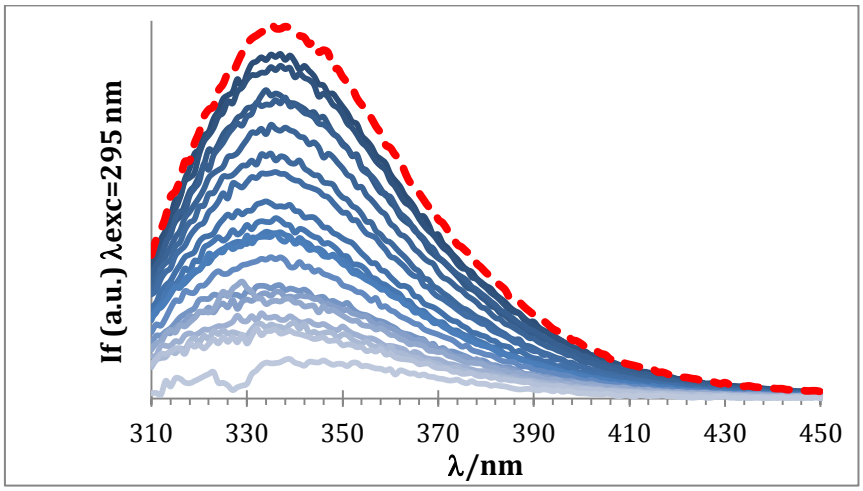

Figure 21. Fluorescence emission spectra for the HSA-RuC system in 10 mM HEPES pH 7,4 (data from experiment #8 samples were incubated and measured at 37 ºC. The concentration of the complex studied varied from 2 µM (darkest shade) to 48 µM (lightest shade), the C_{HSA}= 2 µM was kept constant for each sample during the whole experiment; the red discontinuous line is the protein alone emission.

In this study, fatty-acid-free HSA was used to evaluate the potential of the protein to bind the Ru^{II}-complex. In the absence of complex, the emission maximum intensity for Trp214 is observed at 335 nm, displaying that in the protein this aminoacid residue is protected from the aqueous solvent, where Trp would show a maximum emission at ca. 350 nm [60]. **Figure 21** presents the effect of the increasing concentration of RuC on the fluorescence of the protein: displaying the quenching of the fluorescence emission of the protein with no shift in the maximum λ_{em} (**Figure 22-Left**).

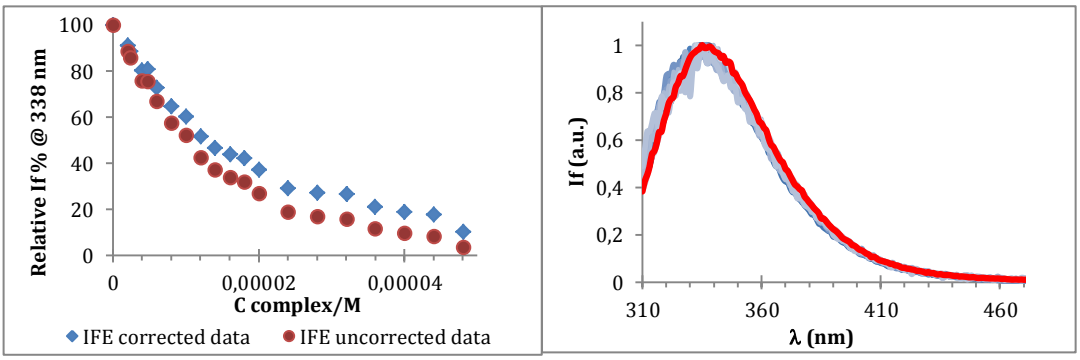

Figure 22. Left, Relative fluorescence intensity for the HSA-RuC system (data from experiment #8) at 338 nm in 10 mM HEPES pH 7,4 before and after the inner filter effect correction**, right** Emission spectra for the HSA-RuC system normalized at 338 nm (data from experiment #8).

From **Figure 22** some conclusions can be highlighted: **22-left** the quenching achieved by the complex at the maximum concentration tested (48 µM) reaches 10% which shows that the complex is binding to the protein quite strongly and changing the environment of Trp214, **22-right** shows the normalized spectra of the experiment #8 without any displacement of the wavelength.

It is important to access the quenching mechanism involved in this interaction, and for that purpose time-resolved fluorescence experiments are needed.

5.3.2. Time-resolved fluorescence measurements.

In a time-resolved or fluorescence lifetime measurements, a fluorescence emission decay is obtained after a very short excitation pulse, and the emission intensity decreases with time according to a sum of exponentials (see **section 3.2.3**.).

The fluorescence intensity decay with time was recorded for all the samples of the binary system HSA–RuC, which were measured and incubated at 37 ºC. Two illustrative decay examples (for HSA in the absence of RuC and for HSA at the highest concentration of RuC tested) are displayed in **Figure 23**. This figure shows that the decay becomes faster (indicating a shorter fluorescence lifetime) in the presence of the complex.

A sum of three exponentials was needed to achieve the best fit shown in **Figure 23**, which is a typical behaviour for Trp214 residues of proteins [60]. The following parameters were used to obtain the best fit in the top plot: (1) For HSA alone: α_1= 0,29; α_2=0,32; α_3=0,39, τ_1=0,79 ns; τ_2=4,05 ns; τ_3=7,37 ns (χ^2=1,305); (2) for HSA plus complex RuC 48 µM: α_1= 0,75; α_2=0,20; α_3=0,05; τ_1=0,39 ns; τ_2=1,87 ns; τ_3=5,64 ns (χ^2=1,200). The randomly distributed residuals of both fits are shown in the bottom plot in **Figure 23**. Further details on the lifetime measurements – such as values obtained for α_i and for τ_i in each sample measured – are included in **Annex D, Table 1**.

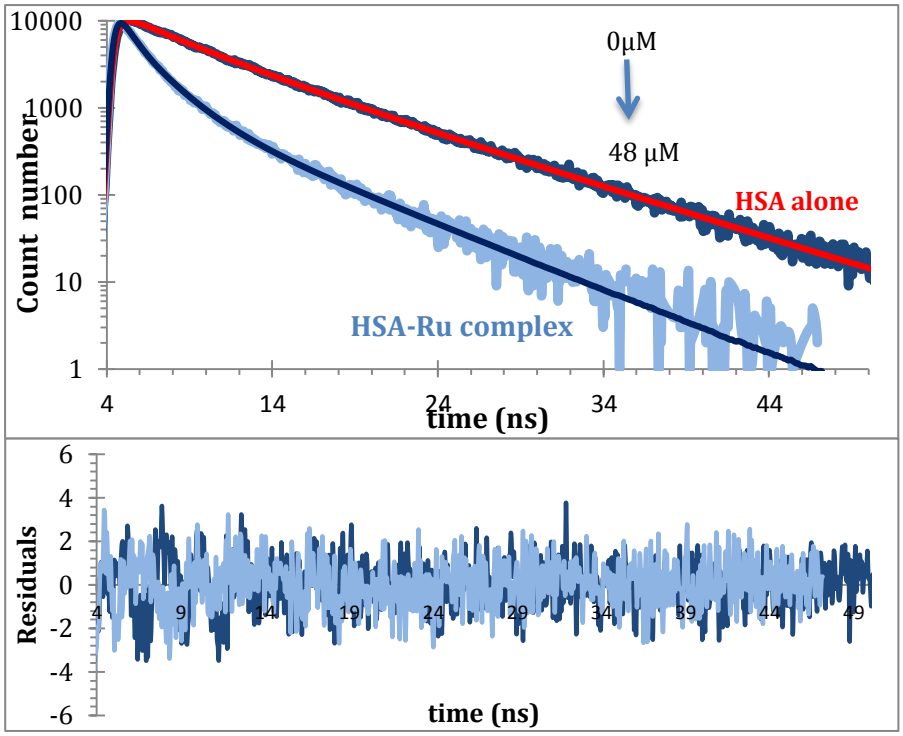

Figure 23. Fluorescence intensity decay of HSA (Trp214) in the absence (dark blue) and in the presence (light blue) of RuC (48 µM) measured by the single photon counting technique (data from **experiment #8**) in 10 mM HEPES pH 7,4. The lines are the best fit of a sum of three exponentials (for further details, see **Annex D**). The bottom plot shows the residuals from the best fits for both samples. The experimental conditions were as follows: C_{HSA}= 2 µM, kept constant; samples prepared in 10 mM HEPES buffer pH 7,4; 23,2 h incubation at (37,0 ± 0,5) ºC; measurements at (37,0 ± 0,5) ºC.

RuC therefore behaves as a quencher of the Trp214 fluorescence of HSA, and a Stern-Volmer plot combining steady-state and time-resolved fluorescence is very useful to evaluate the nature of this quenching process.

5.3.3. Stern-Volmer analysis – the quenching mechanism

The Stern-Volmer analysis was performed for each assay and (whenever possible) for the average of three replicate experiments. The results were organized according to the different concentration of protein used. A higher concentration of protein resulted in a better signal-to-noise ratio and in a more intense fluorescence signal. However, to comply with the requirement of keeping the optical density of the sample low, a higher concentration of protein also limits the maximum concentration of RuC that can be used.

- C_{HSA}= 2,0 µM

Figure 24 summarizes the results obtained for the HSA-RuC system from experiments #7 to #9, and includes the average experimental points thus obtained. In experiments #7 and #8 samples were incubated and measured at 37 ºC; experiment #9 was incubated at 37 ºC but measured at room temperature due to electrical problems; however, the results from experiment #9 are comparable with

those from #7 and #8 and therefore were included in the average executed (**Figure 24**).

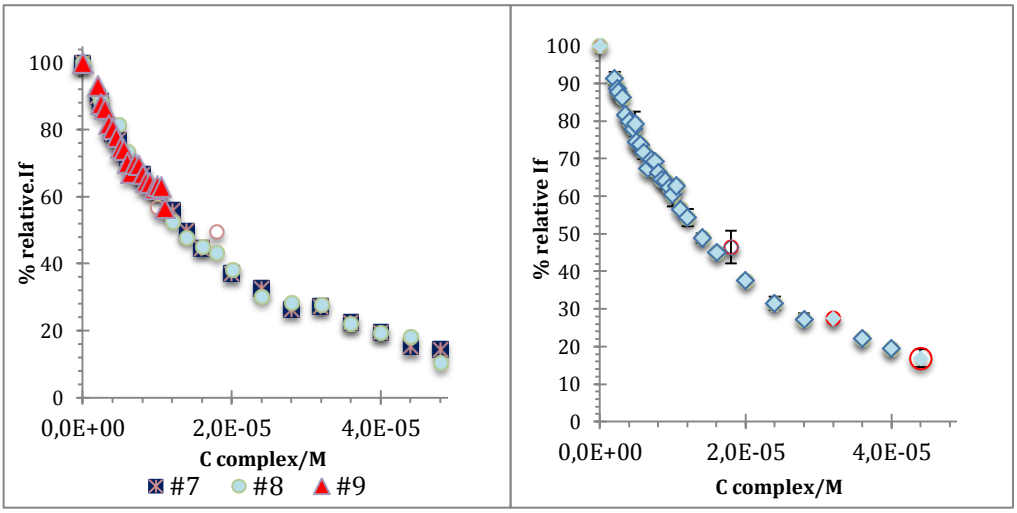

Figure 24. Relative fluorescence intensity for the system HSA-RuC in 10 mM HEPEs pH 7,4 at 338 nm: **Left**-relative fluorescence intensity for each one of the independent experiments #7, #8 and #9,(C_{HSA}= 2 µM). **Right-**relative fluorescence intensity averaged from these three experiments (standard deviation is included as error bars).

It is quite clear from **Figure 24 (left)** that the results from experiments #7, #8 and #9 are mostly very precise and reproducible, which indicates that data measured is of high quality as they were obtained from three different experiments (prepared from three different stock solutions of both ^{faf}HSA and complex). **Figure 24 (right)** shows the average of the experiments presented in **24-left** with their error bars (some points are the average from #7 and #8; and also some other points come from only #9).

In order to determine the quenching mechanism involved in this interaction a Stern-Volmer plot analysis is needed. A typical plot is shown in **Figure 25** for experiments #7, #8 and #9. Stern-Volmer fits (and values of K_D and K_S) obtained for other experiments are included in **Annex B**.

The intensity I_F emitted at 338 nm was used to build the Stern-Volmer plot in **Figure 25**. This wavelength was chosen because it is near the maximum emission wavelength (sensitivity is close to maximum), but it is further to the red from the water Raman scattering peak. Therefore, the signal-to-background ratio is much more favourable than it would be if the real maximum emission wavelength was used.

It can be clearly observed that the Stern-Volmer plot for HSA quenching by RuC is well described by a quadratic equation, which shows that there is more than one quenching mechanism. Since If one of the quenching processes also affects the fluorescence lifetime, then the mechanism will implicate both static and dynamic quenching processes.

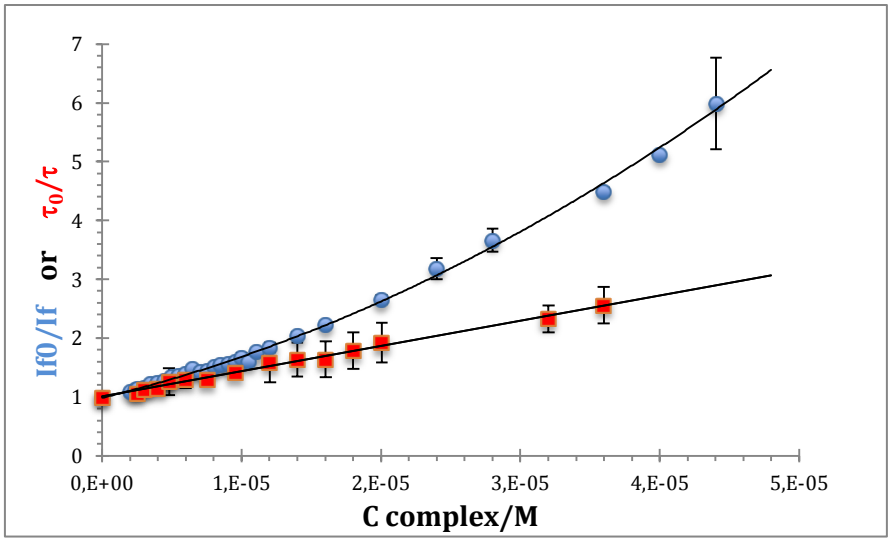

Figure 25. Stern-Volmer plots for the steady-state (blue circles) and time-resolved measurements (red squares) fluorescence data measured at 338 nm for the system HSA-RuC in 10 mM HEPES pH 7,4. (Results are from experiments #7, #8 and #9). Error bars indicate the Standard Deviation from three replicates. For more information on Stern-Volmer analysis, see **Annex B, Table 1**.

Considering that the steady-state data are described by a quadratic equation, it can be assumed that it involves two separate quenching mechanisms, and the relationship shown in **Equation 10** is valid. K_S and K_D from the equation are the constants associated with each quenching process.

If the time-resolved Stern-Volmer plot is well represented by a straight line, one of the constants (K_D, the dynamic quenching constant) can be retrieved from this fit (**Figures 25** and **27** represented by squares) according to the **Equation 16.** In fact, the Stern-Volmer variation of τ with increasing concentrations of RuC is linear (R^2= 0,993 for the average study of #7, #8 and #9).

The intensity emitted at 338 nm was used to build the Stern-Volmer plot represented in **Figure 25 (**and **Figure 27)**. This wavelength was chosen because it is near the maximum emission wavelength (sensitivity is close to maximum), but it is further to the red taking from reference the water Raman scattering peak, therefore, the signal-to-background ratio is much more favourable than it would be if the real maximum emission wavelength was used. It can be clearly observed that the Stern-Volmer plot for HSA quenching by RuC is well described by a quadratic equation, which shows that there is more than one quenching mechanism. If one of the quenching processes also affects the fluorescence lifetime, then the mechanism will implicate both static and dynamic quenching processes.

Considering that the steady-state data are described by a quadratic equation, it can be assumed that it involves two separate quenching mechanisms, and the relationship shown in **Equation 10** is valid. K_S and K_D from the equation are the constants associated with each quenching process.

If the time-resolved Stern-Volmer plot is well represented by a straight line, one of the constants (dynamic quenching constant K_D) can be retrieved from this fit (**Figures 25** and **27** represented by squares) according to the **Equation 16.**

In this study, the Stern-Volmer variation of τ with increasing concentrations of RuC is in fact linear. The fit of #7, #8 and #9 yields $\boldsymbol{\tau_0/\tau = (1{,}01 \pm 0{,}02) + (42{,}88 \pm 0{,}97)_x 10^3\ Cq}$ **(R^2=**0,993**)** and to $\boldsymbol{K_D = (4{,}3 \pm 0{,}1)_x 10^4\ M^{-1}}$**.** This constant ($K_D$), which is associated with the dynamic quenching mechanism, is quite large (some orders of magnitude above the value expected from arbitrary collisions between the fluorophore and the complex, generally 10-100 M^{-1} [60, 62]). This indicates a concentration of quencher in the vicinity of Trp214 higher than the analytical concentration of complex in solution, implying its preferential proximity to the protein, which is consistent with a 'loose' specific interaction of RuC with the HSA. The fact that the quenching mechanism affects the fluorescence lifetime of Trp214 suggests that the complex is still free to move through the protein surface when bound, or that its binding is sufficiently loose to keep a considerable degree of translational and rotational freedom.

The steady-state fluorescence data are best characterized by the quadratic fit (R^2= 0,997) $\boldsymbol{If_0/If = (0{,}98 \pm 0{,}02) + (5{,}8 \pm 0{,}4)_x 10^4\ C_q + (1{,}22 \pm 0{,}09)_x 10^9\ C_q^2}$ (the best linear fit affords R^2= 0,98). Thus, in addition to the dynamic quenching of Trp214 fluorescence identified upon binding of RuC to HSA, the second process detected is static quenching. In order to obtain K_S, the value of K_D was used in the coefficients of **Equation 10**, and it was calculated then from both (K_S+K_D) and K_SK_D relationships. In this case the value obtained for $\boldsymbol{K_S}$ was $\boldsymbol{(2{,}8 \pm 0{,}2)_x 10^4\ M^{-1}}$.

- C_{HSA}= 2.5 μM

To obtain consistent results, experiments with different concentration of protein were performed.

Figure 26 and **Figure 27** show the experimental data obtained from experiments #3, #4, #5 and #6, and their average. All four experiments were incubated at 37 ºC but only #6 was measured at 37 ºC. Experiments #3, #4 and #5 were measured at room temperature (~25º) due to problems with the bath for the cell holder in the fluorometer. However, the results from experiment #6 are comparable with the rest and therefore the average was executed (**Figure 26**). The quenching achieved from the binding between the complex and the protein reaches approximately 35% when the complex is present at a concentration of 25 μM.

Figure 26-left shows that the results from experiments #3, #4, #5 and #6 are of high quality and very reproducible as they are four different experiments prepared from four different stock solutions for ^{faf}HSA and complex that have yielded very similar data. **Figure 26-right,** shows the average from the experiments presented in **26-left** with the error bars (some points are the average from the four experiments, other points are the average from #4, #5 and #6 and also some other points come from only #3).

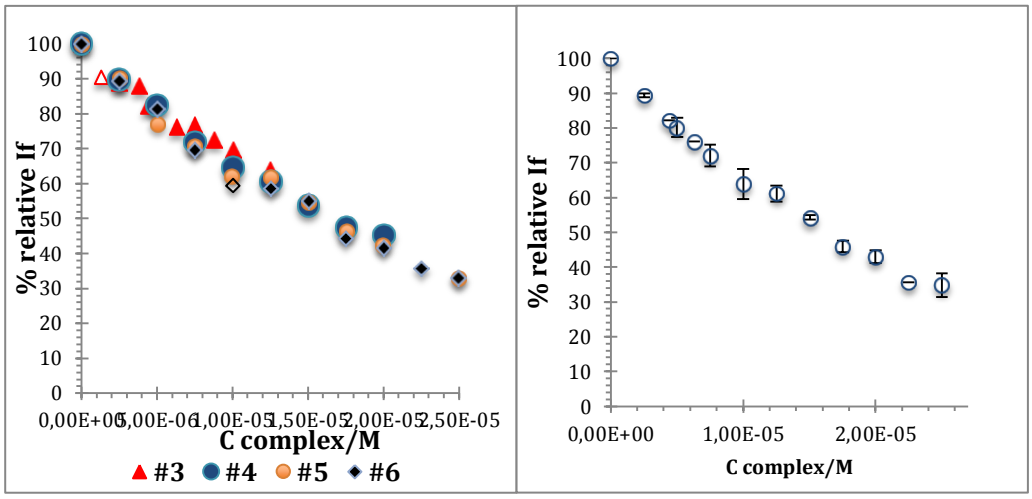

Figure 26. Relative fluorescence intensity at 338 nm for the system HSA-RuC in 10 mM HEPES pH 7,4 at 338 nm: **Left**-relative fluorescence intensity for each one of the independent experiments #3, #4, #5 and #6,(C_{HSA}= 2,5 µM). **Right**-relative fluorescence intensity averaged from these four experiments (standard deviation is included as error bars).

The intensity I_F emitted at 338 nm was used to build the Stern-Volmer plot in **Figure 27**. As explained in sections 3.2.2, 3.2.3, the system HSA-RuC exhibits two quenching processes happening simultaneously: according to Lakowicz [60] there is a dual mechanism when static and dynamic quenching occurs at the same time.

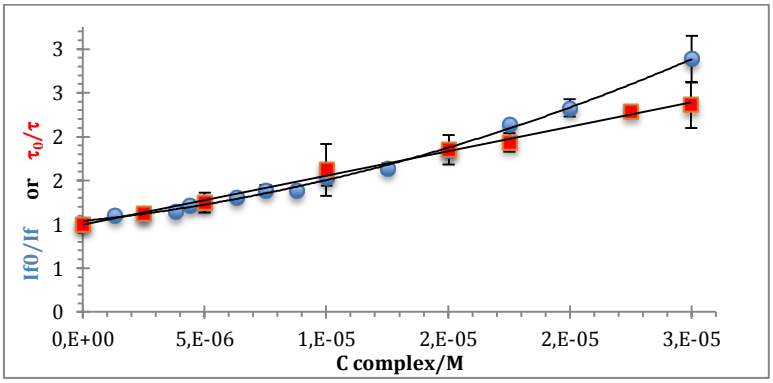

Figure 27. Stern-Volmer plots for steady-state (blue circles) and time-resolved measurements (red squares) fluorescence data measured at 338 nm for the system HSA-RuC in 10 mM HEPES pH 7,4. (Results are from experiments #3, #4, #5 and #6). Error bars indicate the Standard Deviation from four replicates. For more information on Stern-Volmer analysis, see **annex B**, **Table 1.**

If the plot for the steady-state measurements would have showed a linear Stern-Volmer fit, it would have been generally an indication of a single class of fluorophores, all equally accessible to the quencher. Following the same approach if two fluorophore populations are present and one is not accessible to the quencher, the Stern-Volmer plots deviate from linearity towards the x-axis, which is the case presented here.

The average of the lifetime experiments measured from #3, #4, #5 and #6 yields a Stern-Volmer fit equation: $\boldsymbol{\tau_0/\tau = (9,9 \pm 0,3)_x 10^1 + (5,6 \pm 0,2)_x 10^4\ Cq}$ and $\boldsymbol{K_D = (5,6 \pm 0,2)_x 10^4\ M^{-1}}$ (R^2= 0,995)

Steady-state fluorescence data are best described by the quadratic fit (R^2= 0,997) $\mathbf{If_0/If = (1,04 \pm 0,02) + (2,9 \pm 0,4)_x10^4\ C_q + (1,8 \pm 0,2)_x10^9\ C_q^2}$ (the best linear fit only affords R^2=0,97). Following the same procedure as for C_{HSA}= 2 μM, $\mathbf{K_S}$ was calculated as $\mathbf{Ks= (3,2 \pm 0,3)x10^4\ M^{-1}}$.

An average of the values obtained for the Stern-Volmer quenching constants from the different measurements yields: $\mathbf{K_D}$= (4,8 ± 0,3) M^{-1} and $\mathbf{K_S}$= (2,3 ± 0,7) M^{-1} for the system HSA-RuC in 10 mM HEPES pH 7,4 after an incubation period of 24 h at 37 ºC.

A critical point to consider is that the substitution of the equilibrium concentrations by total concentrations (analytical concentrations) in data processing for the Stern-Volmer approach may not provide trustworthy stability constants. This drawback is overcome with calculations using the program PSEQUAD, but the Stern-Volmer constants calculated might not be comparable with PSEQUAD thermodynamic binding constants.

5.3.4. Calculation of the binding constants with PSEQUAD

Conditional binding constants (β' global formation constants) for the system HSA-RuC can be calculated with PSEQUAD. The program affords not only the global formation constants involved but also the stoichiometry of the protein-complex adducts formed by solving the mass-balance equations for the system and calculating the equilibrium concentrations of RuC and protein from their total concentrations in solution.

PSEQUAD was used in all experimental data sets to determine the best binding model for the HSA-RuC system in the experimental conditions used: 10 mM HEPES pH 7,4 at 37ºC after a 24h incubation period. Adducts with a 1:2 protein:RuC stoichiometry typically require higher concentrations of complex to be detected from experimental data, and in fact log β' values can be calculated yielding a good fit from long-titration data with PSEQUAD. Values obtained with PSEQUAD for the conditional stability constants for the different experimental sets are summarized in **Annex C**, **Table 1**. The results obtained with PSEQUAD are robust in the sense that a minimum is always reached and for different initial values for the calculation, the program gives back the same log β' values within the SD or experimental error.

	Adduct stoichiometry	T(ºC)* C_{HSA} (μM)	PSEQUAD log β ± SD	PSEQUAD log K ± SD	Stern-Volmer log K_D; log K_S
#1	HSA-RuC	RT 5,12	log β_1= 4,38 ± 0,01	log K_1=4,38 ± 0,01	4,11 ; 4,42
	HSA-$(RuC)_2$		log β_2= 8,53 ± 0,07	log K_2= 4,15 ± 0,07	
#2	HSA-RuC	36,9 2,24	log β_1= 4,72 ± 0,01	log K_1= 4,72 ± 0,01	N/A
	HSA-$(RuC)_2$		N/A	N/A	
#3	HSA-RuC	RT 2,51	log β_1= 4,67 ± 0,01	log K_1=4,67 ± 0,01	4,41 ; 4,12
	HSA-$(RuC)_2$		N/A	N/A	
#4	HSA-RuC	RT 2,50	log β_1= 4,74 ± 0,01	log K_1=4,74 ± 0,01	4,41 ; 4,35
	HSA-$(RuC)_2$		log β_2= 9,45 ± 0,02	log K_2= 4,71 ± 0,02	
#5	HSA-RuC	RT 2,51	log β_1= 4,71 ± 0,01	log K_1= 4,71 ± 0,01	4,41 ; 4,35
	HSA-$(RuC)_2$		N/A	N/A	
#6	HSA-RuC	36,9 2,50	log β_1= 4,76 ± 0,01	log K_1= 4,76 ± 0,01	4,78 ; 4,30
	HSA-$(RuC)_2$		N/A	N/A	
#7	HSA-RuC	36,9 2,00	log β_1= 4,81 ± 0,01	log K_1=4,81 ± 0,01	4,61 ; 4,38
	HSA-$(RuC)_2$		log β_2= 9,34 ± 0,02	log K_2= 4,53 ± 0,02	
#8	HSA-RuC	36,9 2,00	log β_1= 4,776 ± 0,005	log K_1=4,776 ± 0,005	4,71 ; 4,36
	HSA-$(RuC)_2$		log β_2= 9,402 ± 0,012	log K_2=4,626 ± 0,013	
#9	HSA-RuC	RT 2,00	log β_1= 4,90 ± 0,01	log K_1=4,90 ± 0,01	4,66 ; 4,35
	HSA-$(RuC)_2$		log β_2= 10,24 ± 0,02	log K_2=5,34 ± 0,02	
#12	HSA-RuC	37 2,00	log β_1= 4,93 ± 0,01	log K_1=4,93 ± 0,01	4,93 ; 4,48
	HSA-$(RuC)_2$		log β_2= 9,74 ± 0,02	log K_2=4,81 ± 0,02	
#19	HSA-RuC	37 2,00	log β_1= 4,42 ± 0,01	log K_1=4,42 ± 0,01	4,59 ; 4,39
	HSA-$(RuC)_2$		log β_2= 9,57 ± 0,01	log K_2=5,15 ± 0,01	

Table 2. Conditional stability constants obtained from PSEQUAD and Stern-Volmer analysis for the system HSA-RuC at 37 ºC in 10 mM HEPES pH 7,4 after an incubation period of 24h. *T_m is the sample temperature during the measurement; all samples in the assays indicated were incubated for 24h at 37 ºC before the measurements. Fitting parameters values for all fits are presented in Annex C.

From the experimental data gathered in this work, two models can be proposed with the computer program PSEQUAD: model 1, predicting the formation of a single 1:1 {HSA-RuC} adduct, and model 2 with adducts with 1:1 and 1:2 stoichiometries. These are presented in **Table 3**. The fitting parameter is very similar for both models and low SD values are obtained in both cases which makes it difficult to choose between the two.

From the time-resolved fluorescence measurements two different quenching processes were identified. Although these processes can indicate either the formation of two distinct adducts or the existence of two different types of binding interaction of RuC with albumin, those results offer further support to a model with the formation of two complex-protein adducts. In fact, the log K' values

obtained with PSEQUAD for {HSA-RuC} and {HSA-$(RuC)_2$} adducts, and the Stern-Volmer constants K_s and K_D constants obtained are quite comparable (see **Table 2**).

	log β' (± SD)		log K'$_{binding}$
	Model 1	**Model 2**	**Model 2**
HSA–C	4,72 (± 0.01)	4,78 (± 0.01)	4,78
HSA – C_2	´----	9,40 (± 0.01)	4,62
RuC concentration range **HSA concentration** **slits**	0-10 µM 2,24 µM 2 nm	0-48 µM 2,00 µM 2 nm	-
Fitting parameter	9,7 x 10^4	8,9 x 10^4	-
Number of points	9	16	-
ºC of freedom	1168	2336	-

Table 3. Conditional binding constants (log β') and log K'$_{binding}$ at 37 ºC calculated from the steady-state fluorescence measurements for the system RuC-HSA in 10 mM HEPES for the two binding models proposed. Details on the fit for all measurements are included in Annex C.

5.3.5. Speciation model for the system RuC-HSA

The evaluation of the species that can form in a system and of their stability constants allows plotting equilibrium concentration distribution curves for the system in different conditions.

Figure 28 presents the speciation of HSA and RuC in the experimental conditions used for the fluorescence measurements and blood conditions for the two models presented in **Table 3**:. The formation of two species in 10 mM HEPES pH 7,4 (C_{HSA}= 2,0 µM,) can be confirmed: as it is shown in **Figure 28-B,** {HSA-RuC} is basically formed as soon as the complex makes contact with the protein; however, in the case of {HSA-$(RuC)_2$} the species is seen when it reaches about 20% of the formation relative to HSA and this occurs approximately when the complex in solution reaches a concentration of about 15 µM. Some experiments were performed with a maximum concentration of complex of 10-12,5 µM (#2, #3), and this explains why those models proposed from PSEQUAD do not show the formation of HSA-$(RuC)_2$.

From **Figure 28** it is interesting to note that, although the two adducts may form in some experimental conditions, in blood serum (with an albumin concentration of ~630 µM) the species {HSA-$(RuC)_2$} it is not very relevant since its formation is negligible. Therefore, even though the formation of two complex-protein adducts is possible, only the 1:1 adduct {HSA-(RuC)} is relevant in the context of the distribution of RuC by albumin binding in the blood plasma.

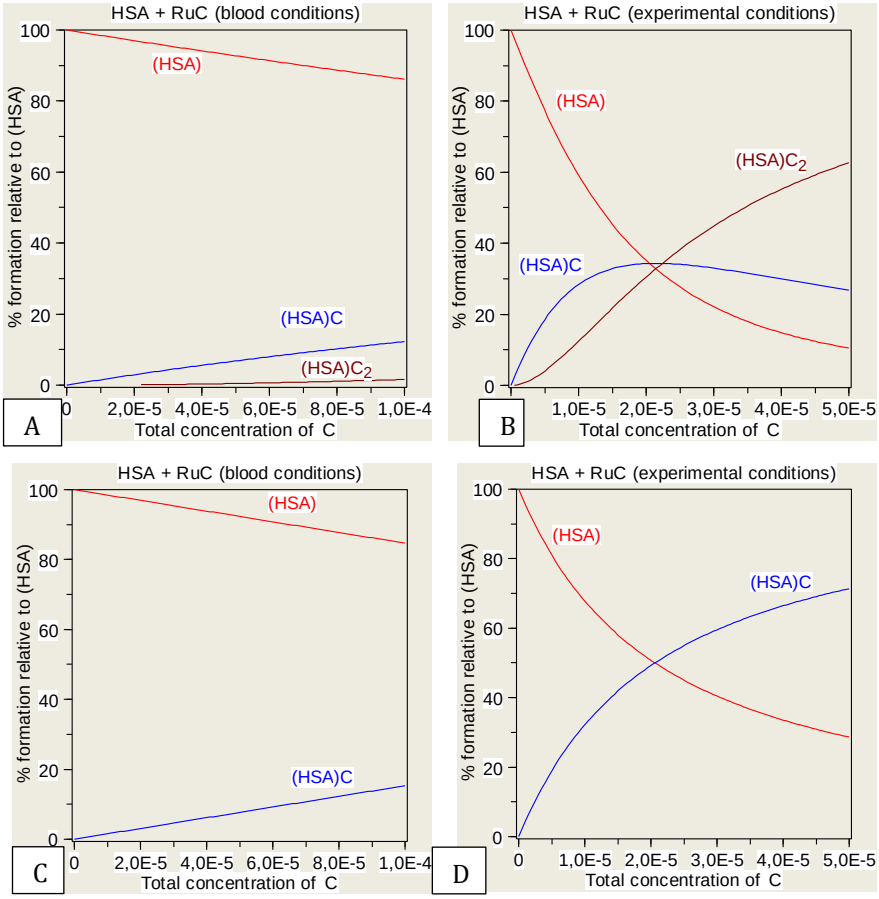

Figure 28. Speciation diagrams for the system HSA–RuC in 10 mM HEPES pH 7,4 at 37ºC. **A, B:** concentration plots obtained with Model 2 for the albumin concentration in the blood and for the fluorescence experimental conditions where HSA-C and HSA-C_2 refer to the two adducts formed with complex RuC (total concentration of C is in Molar). **C, D**: concentration plots obtained with Model 1 for blood conditions and for the experimental conditions; These diagrams were obtained with the HySS computer program using the conditional binding constants in **table 3**.

5.4.0. Characterization of the binding sites of RuC on HSA.

Researchers have shown a remarkable interest in determining the binding sites of metallodrugs on biomolecules in order to improve the design of future drug candidates [42].

For most drugs, the binding sites of HSA are located in hydrophobic cavities in subdomains IIA and IIIA, designated as Sudlow's drug binding site I (in domain IIA) and drug binding site II (in domain IIIA). These interactions are normally quite fast, in contrast with a covalent type of binding, which usually takes a long time to reach equilibrium. Trp214 is located very near to the drug binding site I, and a strong quenching of its fluorescence is usually interpreted as an indication that the compound is binding at site I. Nevertheless Trp214 emission can be sensitive to changes occurring at site II as well [68].

Covalent binding to the side chain residues of the protein is possible and was reported for Ru complexes that have a labile ligand (typically a Cl-) in the coordination sphere. However, RuC is is stable in solution and does not undergo ligand exchange processes easily because RuC has no labile ligands (such as Cl^-, as

in the case of KP1019 or in RAPTA complexes). Thus covalent binding to HSA (which would imply the loss of one of the co-ligands) is not expected to be an important component of the binding process in the HSA–RuC system.

Displacement reactions were done to elucidate RuC binding sites on HSA using the established site markers warfarin (WF) and dansylglycine (DG). WF was used as site marker for site I and DG was used as a site marker for site II. Because self-absorption of RuC is significant, the correction of the emission intensity with the IFE equation (**Equation 3**) was needed.

5.4.1. Warfarin (drug binding site I, domain II)

Fluorescence monitoring of competitive binding to HSA with Warfarin is often used to determine whether a given ligand/metal complex binds to Sudlow´s Site I. Normally, the displacement of warfarin from its HSA complex {HSA-WF} is easily observed by a decrease of the fluorescence intensity, when the adduct formed between the metal complex and the protein is "stronger" than the {WF-HSA} complex.

Steady-state fluorescence data for the system HSA-W-RuC was evaluated using PSEQUAD. The binding process of WF to HSA was assessed in the experimental conditions used for the HSA–RuC system. Warfarin alone emission, titrations of HSA with warfarin, and titrations of the adduct {HSA-W} with RuC were done. **Figure 29** shows the fluorescence emission intensity at 375 nm (λ_{exc}=310 nm) for all these systems.

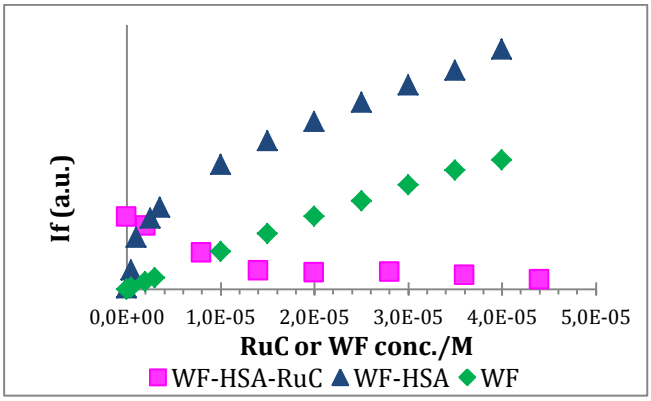

Figure 29. Fluorescence emission intensity (λexc= 310 nm) at the maximum wavelength (375 nm), for the species involved in the ternary system. HSA-WF-RuC in 10 mM HEPES pH 7,4 (Experiments #23, #24 and #25- see **Annex A3, Table 1**)

- **HSA-WF System:**

Figure 30 shows fluorescence emission spectra for the components of the HSA-WF system. Warfarin has weak fluorescence emission when samples are excited at 310 nm. The addition of HSA causes a marked an increase in the emission intensity due to the binding of the site marker to the protein forming the 1:1 adduct {HSA-WF}. In plot B normalized spectra of HSA alone, Warfarin and {HSA-WF} show an evident displacement of 9 nm in the λ_{em} maximum of Warfarin upon binding to HSA.

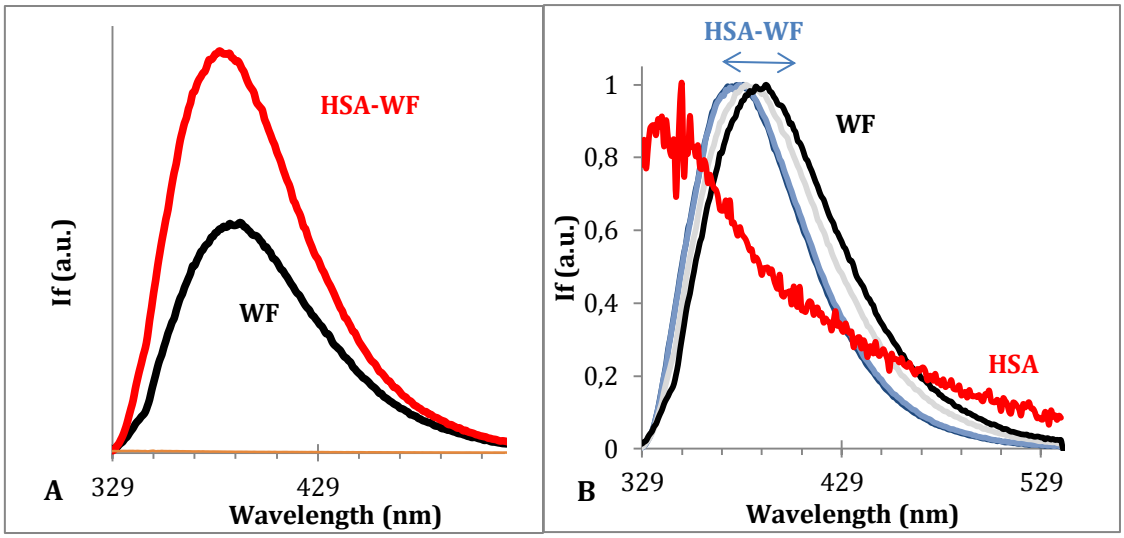

Figure 30. The HSA-WF system. **A**-Fluorescence emission spectra of WF (C_{WF}= 40 µM) and HSA-WF (C_{HSA}= 2 µM, C_{WF}= 40 µM); **B-** Normalized fluorescence emission for HSA, Warfarin, HSA-WF, where the displacement from the bands could be appreciated (10 mM HEPES pH 7,4, 37 ºC, λexc= 310 nm).

- **HSA-WF-RuC System:**

Figure 31 presents the emission spectra recorded for the system HSA-WF-RuC. The intensively emitting 1:1 adduct {HSA-WF} is titrated with RuC and the addition of complex decreases the intensity of the fluorescence emission.

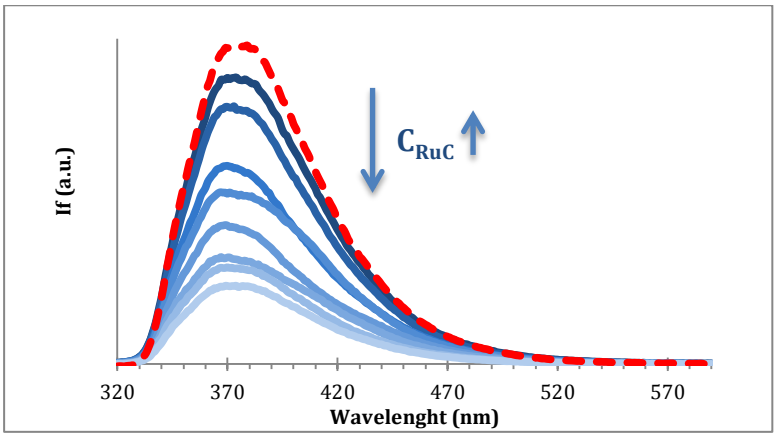

Figure 31. Emission spectra of the system HSA-WF-RuC, experiment #28 (see **Annex A3, Table 1** for further details), the dashed line represents the adduct HSA-WF in equimolar conditions (C= 2 µM), the straight lines represent the system {HSA-WF}-RuC in increasing concentrations (varying from the darkest shade at the lowest concentration of RuC, C_{RuC}= 2 µM to the lightest shade at the highest concentration of complex studied, C_{RuC}= 44 µM).

Figure 32, shows that the initial intensity of the adduct {HSA-WF} decreased by about 20% upon addition of the complex RuC (until a concentration of 44 µM). This decrease of intensity was accompanied by a small shift (**Figure 32-B)** that is normally associated with the increasing free Warfarin due to its displacement from the binding pocket.

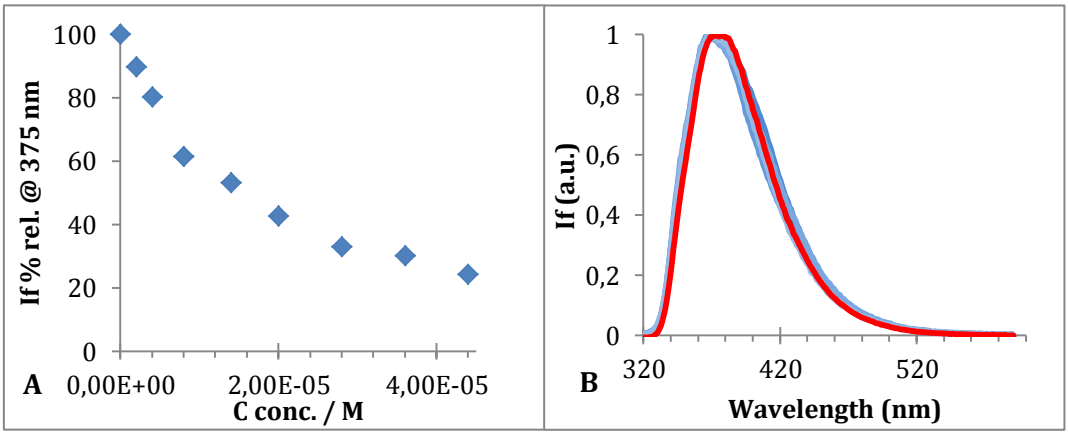

Figure 32. A: relative fluorescence intensity for the ternary system HSA-WF-RuC at its maximum wavelength (375 nm) (data of the experiment #28, corrected for IFE - see **Annex A** for further details); **B:** Normalized spectra from the same experiment as in plot A exhibiting a blue-shift; red line represents emission of the adduct HSA-WF in equimolar conditions, and the blue lines emission of the adduct HSA-WF with increasing concentrations of RuC.

These results are consistent with the displacement of WF from the binding pocket of the protein caused by the complex, which indicates that binding of the complex to Sudlow´s site I is probably occurring. Therefore, the displacement of the site marker at various concentrations of RuC could be followed *via* intensity changes of the emission spectra.

In case of the system shown on **Figure 32-A** (experiment #28), the initial intensity of the adduct {HSA-WF} decreased by about 25% upon addition of the complex RuC with a concentration of 44 µM. This decrease of intensity was not accompanied by a shift in the emission maximum (within the experimental error) (**Figure 32-B**). These results are consistent with a considerable displacement of WF from HSA upon addition of complex, indicating that RuC can bind at drug binding site I in HSA.

It is important to highlight that the displacement of the site marker can be measured when the ligand binds at the binding site of the marker compound. However, if its binding constant is much lower compared to that of the site marker only a high excess of the ligand can result in a detectable effect.

PSEQUAD

Conditional binding constants for the experiments involving the Warfarin ternary system were calculated with PSEQUAD, and the results of the average of the experiments are shown in **Table 4**. Experimental data for WF alone, WF-HSA and HSA-WF-RuC was averaged and evaluated within the same input file. Log β' values for the formation of HSA-WF and HSA-RuC were then calculated, and results are included in **Table 4**.

The conditional binding constant calculated for WF from the HSA-WF binary system was log β'(WF) = log K'(WF)= (6,02 ± 0,01) (**Table 4**). It was found to be in fairly good agreement with values in the literature [42, 57]. The samples for the experiments executed in this thesis did not include salt (to keep the ionic strength of the medium constant) because of the very low solubility of RuC in the presence

of inorganic salts, which cause strong precipitation. Therefore, the differences between the constants obtained in this study and the literature data are likely to be due to these experimental variations.

HSA-WF-RuC System		C_{HSA}/ µM	C_{WF}/ µM	C_{RuC} / µM	Adduct log β' ± SD	FP	Minimum reached?
average file	WF alone	-	0-40	-	-	$2,67x10^5$	Yes
	WF+HSA	2	0-40	-	(HSA-WF) 6,02 ± 0,01		
	WF+HSA+RuC	2	2	0-44	(HSA-WF):6,075 ± 0,003 (HSA-RuC):5,614 ± 0,005		

Table 4. Average values for the conditional binding constants of species involved in the ternary system HSA+WF+RuC calculated with the program PSEQUAD from fluorescence emission data in 10 mM HEPES pH 7,4 at 37 ºC.

It was possible to calculate conditional formation constants for the 1:1 adduct {HSA-RuC} and for the {HSA-WF} adduct (together) from the experimental data with a very low standard deviation and a good fitting parameter. Log β' for the adduct {HSA-WF} calculated from the ternary system (in the presence of RuC) is fairly the same as the value obtained from the binary system. In what concerns the Log β' for the adduct {HSA-RuC} the value calculated from the ternary system is a bit higher than that obtained from the binary system HSA+RuC.

The reason for the overestimation of the {HSA-RuC} formation constant may be that there seems to be an interaction between the two. A fluorimetric titration of warfarin with RuC (see **Annex A3, Figure A**) showed that the intrinsic fluorescence of WF decreases with increasing concentrations of complex. The partial overlap between the absorption spectrum of RuC and the emission spectrum of WF (see **Annex A3, Figure B**) suggests that a mechanism of energy transfer between these two species might be operative. Another possibility is that RuC may be losing one of its co-ligands to bind WF. In fact, the complex is stable enough in aqueous media but the stability in the presence of a competitive ligand was not checked yet and this hypothesis cannot be discarded based on the data collected in this work

Figure 33 and **Figure 34** show the different species present in the HSA-WF-RuC system.

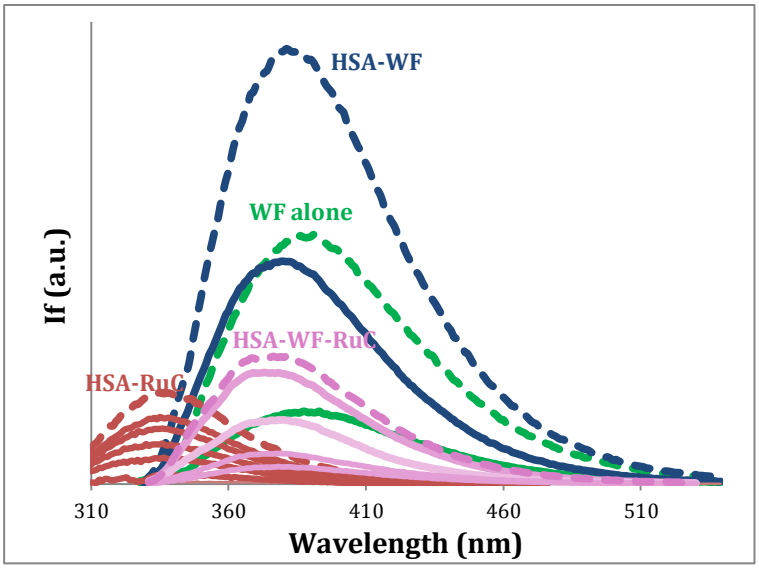

Figure 33. Fluorescence emission spectra of all the species involved in the HSA-WF-RuC system. (Dashed lines represent the maximum intensity for each set, each is represented by a different colour (data from experiments #23, #24 and #25- see **Annex A3, Table 1** for more details).

.

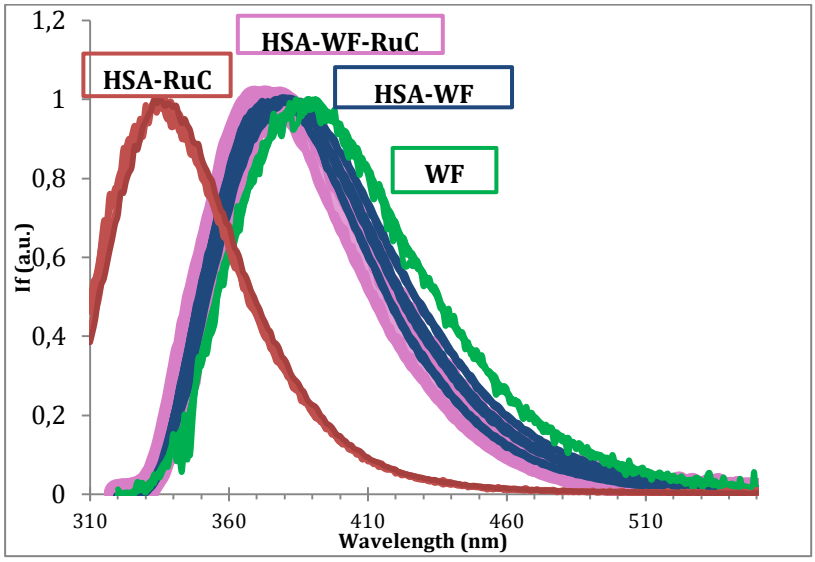

Figure 34. Normalized fluorescence emission spectra of all the species involved in the HSA-WF-RuC system (from Figure 33, from experiments #23, #24 and #25- see Annex A3, Table 1) for more details).

5.4.2. Dansylglycine (drug binding site II, domain III)

In this section, fluorescence monitoring of competitive binding to HSA with DG was used to evaluate the binding at Sudlow´s Site II. As in the case of warfarin, the displacement of DG from its HSA complex {HSA-DG} is observed by a decrease of the sample fluorescence intensity.

Steady-state fluorescence emission for the system HSA-DG-RuC was evaluated using PSEQUAD. The binding process of DG to HSA was assessed in the experimental conditions used for the HSA–RuC system: 10 mM HEPES pH 7,4. Dansylglycine alone measurements, titrations of HSA with DG and titrations of the 1:1 adduct {HSA-DG} with RuC were done. **Figure 35** shows the fluorescence emission intensity at 490 nm (λ_{exc}=335 nm) recorded for all these systems. It is very visible that the increase in DG concentration makes the adduct´s {HSA-DG} fluorescence emission more intense. However, in the case of the ternary system HSA-DG-RuC the emission fluorescence intensity decreases when the concentration of complex is increased.

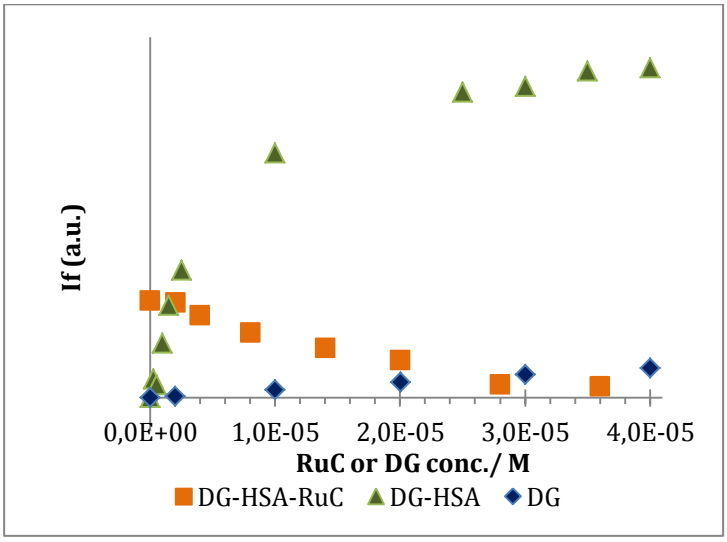

Figure 35. Emission fluorescence intensity (λexc=335 nm) at the maximum wavelength (490 nm), for the species involved in the ternary system HSA-DG-RuC in 10 mM HEPES pH 7,4. (Experiments #33, #34 and #35-**See Annex A4, Table 1**)

- **HSA-DG System:**

Figure 36 shows the fluorescence emission spectra of DG (C_{DG}=40 µM) and HSA-DG (C_{HSA}= 2 µM, C_{DG}=30- 40 µM).

Dansylglycine has negligible fluorescence emission when the sample is excited at 335 nm (see **Figure 35**). The addition of protein causes an increase in the emission intensity and a great shift in the emission maximum of more than 70 nm due to the binding of the site marker to the protein (at Sudlow´s site II).

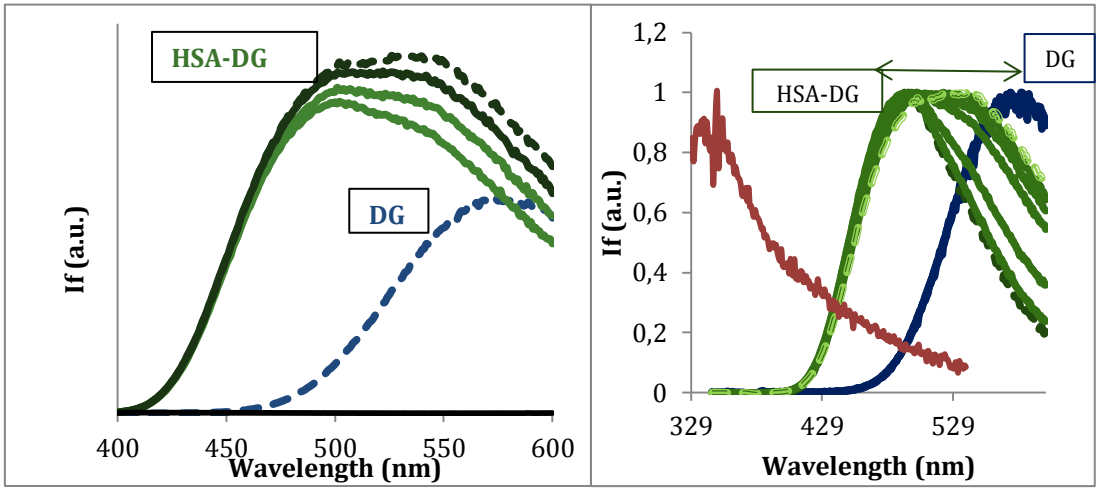

Figure 36. Fluorescence emission spectra of DG (C_{DG}=40 µM) and HSA-DG (C_{HSA}= 2 µM, C_{DG}=(30- 40 µM)) and (right) normalized fluorescence intensity for the different species such as DG, HSA-DG and HSA, where the displacement from the bands could be easily seen. (37 ºC, 10 mM HEPES pH 7,4, λ_{exc}=335 nm)

- **HSA-DG-RuC System:**

Figure 37 shows the emission spectra recorded for the system HSA-DG-RuC. The highly fluorescent 1:1 {HSA-DG} adduct is titrated with RuC, and a marked decrease in the intensity of the fluorescence emission upon the addition of complex is observed.

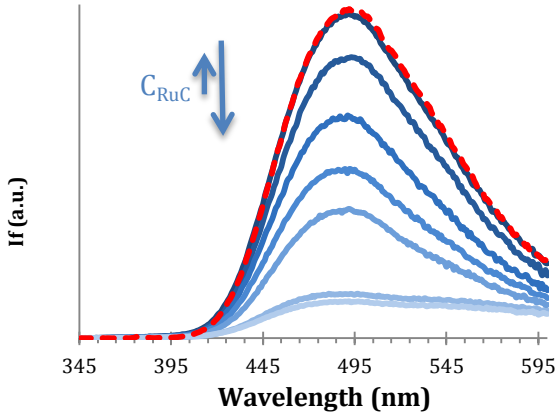

Figure 37. Emission spectra of the system HSA-DG-RuC, experiment #35 (see **Annex A4, Table 1** for further details), the dashed line represents the adduct HSA-DG in equimolar conditions (C_{HSA}=C_{DG}= 2 µM), the straight lines represent the system {HSA-DG}-RuC in increasing concentrations (varying from the darkest shade at the lowest concentration of RuC, C_{RuC}= 2 µM to the lightest shade at the highest concentration of complex studied, C_{RuC}= 36 µM).

Figure 38 shows that the initial intensity of the {HSA-DG} adduct decreases by about 11% upon addition of the complex RuC (until a concentration of 36 µM). This decrease of intensity is accompanied by the development of a band at higher wavelength values, consistent with the presence of a high enough concentration of free DG. The data shows that considerable displacement of DG takes place upon addition of complex, showing that this complex might be binding at the drug binding Site II of HSA.

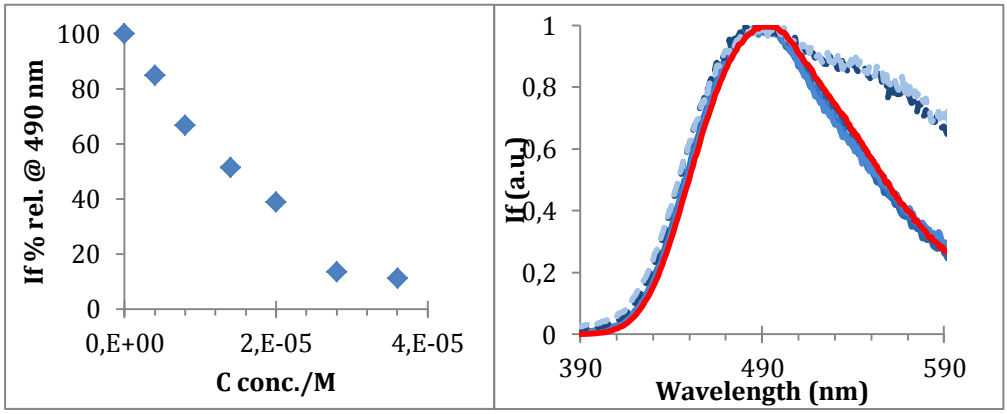

Figure 38. Left, shows the relative fluorescence intensity for the ternary system HSA-DG-RuC of the experiment #35(see **Annex A, Table 1** for further details), at its maximum wavelength (490 nm). Right, Normalized spectra from the same experiment as in the left plot with a clear change in the bands at higher concentrations of complex, red continuous line represents the adduct HSA-DG in equimolar conditions and the blue lines the adduct HSA-DG with increasing concentrations of RuC.

PSEQUAD

As in the case of the warfarin site-marker, conditional formation constants for the experiments in the dansylglycine ternary system were calculated with PSEQUAD, and the results of the average of the experiments are shown in **Table 5**. Experimental data for DG alone, DG-HSA and HSA-DG-RuC was averaged and evaluated within the same input file. The average was made from three independent experiments. Log β' values for the formation of HSA-DG and HSA-RuC were then calculated, and results are included in **Table 5**.

The conditional constant calculated for the binding of DG to HSA using data from the HSA-DG binary system was log β'(DG) = log K'(DG)= (5.47 ± 0,01), which is in fairly good agreement with the values in the literature [42, 57] considering the slight differences in the experimental conditions (absence of the inorganic salt).

HSA-DG-RuC System		C_{HSA}/ µM	C_{DG}/ µM	C_{RuC} / µM	Adduct log β' ± SD	FP	Minimum reached?
average file	DG alone	N/A	0-40	N/A	N/A	$5{,}85_x10^6$	Yes
	DG+HSA	2	0-40	N/A	(HSA-DG): 5,47 ± 0,01		
	DG+HSA+RuC	2	2	0-44	(HSA-RuC):5,04 ± 0,04 (HSA-DG)= 5,64 ± 0,03		

Table 5. Average values for the conditional binding constants of species involved in the ternary system HSA+DG+RuC calculated with the program PSEQUAD from fluorescence emission data in 10 mM HEPES pH 7.4 at 37 ºC.

It was possible to simultaneously calculate conditional formation constants for the 1:1 adduct {HSA-RuC} and for the {HSA-DG} adduct from the experimental data.

Log β' for the adduct {HSA-DG} calculated from the ternary system (in the presence of RuC) is in fairly good agreement with the value obtained from the binary system. In what concerns the Log β' for the adduct {HSA-RuC} the value calculated from the ternary system is quite close to that obtained from the binary system HSA+RuC.

This results further support that the RuC seems to be displacing DG from its binding site on HSA and possibly might be binding at the drug binding Site II of HSA.

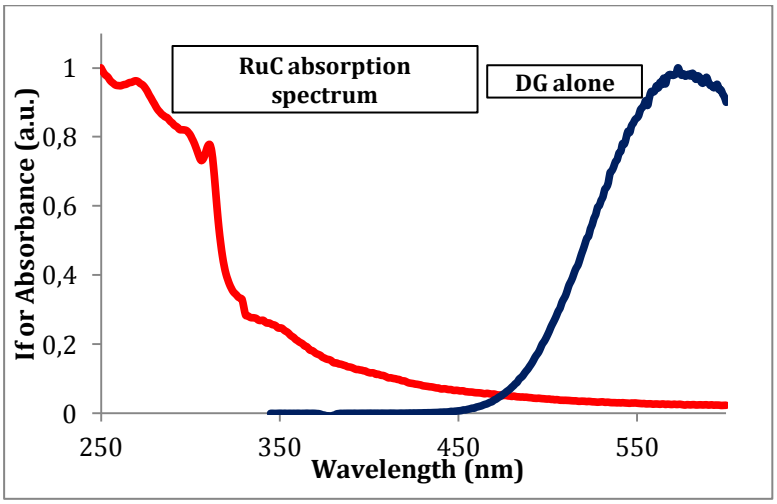

Figure 39. Shows the absorption spectrum of the complex and the emission spectrum of the site marker Dansylglycine.

Figure 40 and **Figure 41** show the different species present in the HSA-DG-RuC system.

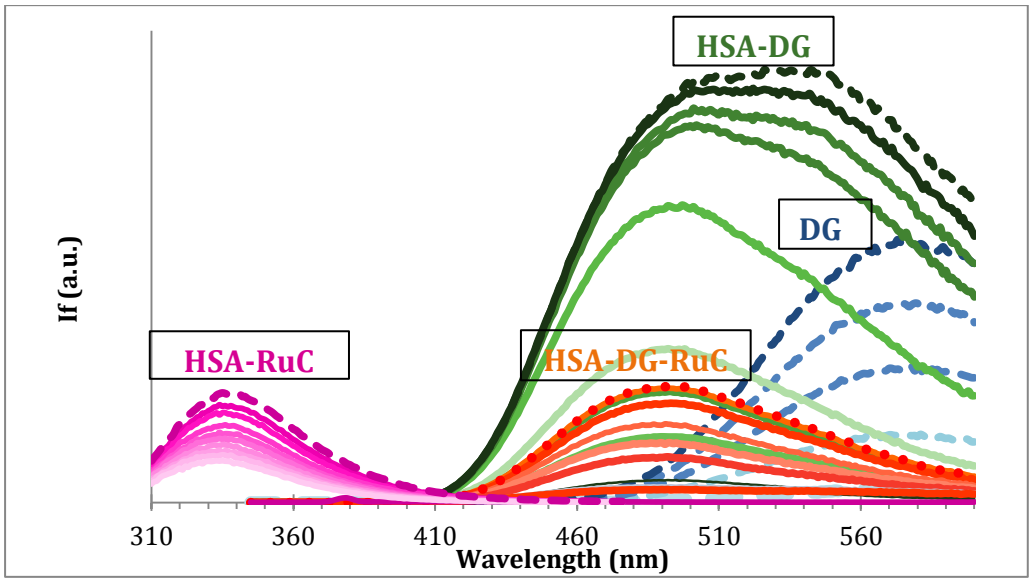

Figure 40. Fluorescence emission spectra of all the species involved in the HSA-DG-RuC system. (Dashed lines represent the maximum intensity for each set of species, each set of species is represented by a different colour, experiments #33, #34and #35).

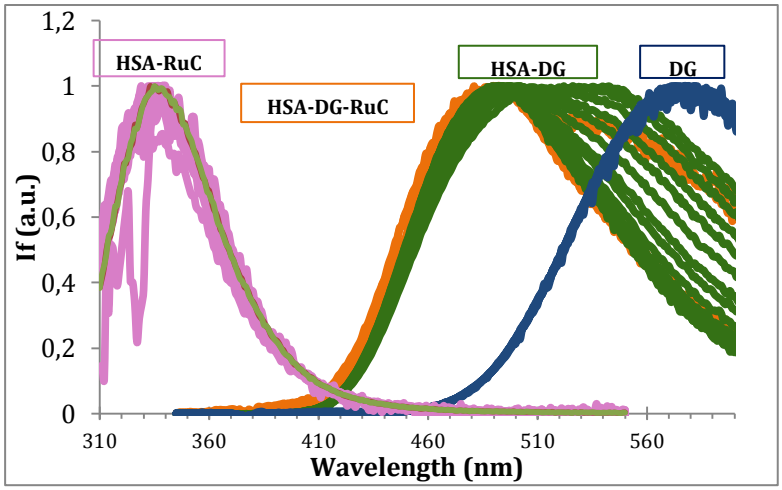

Figure 41. Normalized spectra from Figure 40.

5.5.0. Conclusions

The binding of an organometallic ruthenium(II) complex to human serum albumin was evaluated in this work. The interaction of the piano-stool complex $[Ru^{II}(Cp)(bipy)(CO)][PF_6]$ (or RuC) with fatty acid free human serum albumin at pH 7,4 in 10 mM HEPES at 37ºC was monitored by spectroscopic methods (UV-Vis absorption and Fluorescence spectroscopy). This complex is a water-soluble with a moderate cytotoxic activity against human ovary carcinoma.

The binding process was observed in the changes recorded for UV-Visible spectra for the HSA-RuC system. Steady-state and time-resolved fluorescence spectroscopy were used to get quantitative information on the binding interaction, using Trp214 as a structural fluorescent probe, and selectively exciting this residue. HSA-Trp214 fluorescence was strongly quenched by the complex RuC by a combination of dynamic and static quenching mechanisms with the Stern-Volmer constants K_D = $(4,8 \pm 0,3)_x10^4$ M^{-1} and K_S = $(2,3 \pm 0,7)x10^4$ M^{-1} (obtained for a confidence level of 95%).

Formation of adducts with 1:1 and 1:2 stoichiometries for RuC and HSA were identified and the corresponding conditional global binding constants were calculated using the computer program PSEQUAD: log β_1'({HSA-(RuC)} = (4,78 ± 0,01) and log β_2'({HSA-$(RuC)_2$} = (9,52 ± 0,01) with a fitting parameter of $1,16_x10^5$.

These conditional global binding constants indicate a moderate binding strength of RuC to albumin (in both adducts) and are comparable with those found in the literature for KP1019 which is reported to bind to HSA in a moderate and reversible manner.

Displacement reactions using warfarin and dansylglycine as specific markers for the HSA drug binding Site I and Site II (respectively) were done to obtain more information on the binding of RuC to albumin. Results showed that RuC can displace both site markers from their HSA adducts, indicating that it can bind to both binding sites on HSA.

The conditional global binding constants calculated provide a useful speciation model for the RuC-HSA system: in blood serum conditions the relative importance of the 1:1 and 1:2 adducts is quite different, with the formation of {HSA-$(RuC)_2$ being negligible. This implies that the 1:2 adduct will be of lesser importance in the binding of RuC to HSA, and that the 1:1 adduct will be the prevalent species in the blood.

RuC can thus be efficiently transported in the blood stream through albumin binding, forming an adduct with the protein with a 1:1 stoichiometry.

6.0. CONCLUDING REMARKS

It is essential to explore the interactions between anticancer metallodrugs and serum proteins as these interactions are known to affect in the biodistribution of the drug, possibly its mechanism of action and toxicity.

In fact, this is one of the first steps in evaluating the potential of a new drug: if it binds too tight to albumin the drug does not exert its effect as it is eliminated; if it is not bound tightly enough it cannot be efficiently delivered into the targeted tumour tissue and tumour cells. To have a method that yields good quality data related to the binding between a transport protein with metallodrugs is important.

The complex studied is not commercially available, and the amount of high purity material available was restricted. This implied some limitations in the experimental procedure (e.g. at the time of preparing the samples) to comply with the requirement of using low amounts of material. Regardless of those limitations, very reproducible results were obtained. Fits to the experimental data yielded low SD values and very good fitting parameters, thus indicating high quality experimental data, adequate for quantitative analysis. All the experiments were executed from independent stock solutions that were freshly prepared every day herein, demonstrating the good quality data obtained when achieving similar results for different experiments that were performed in different days. The method accomplished the expected, good fittings, low Standard deviation and consistent results. The approach used in this work is thus reliable, has a good overall consistency and can be safely used on other metal ion compounds that are identified as prospective anti-tumour drugs.

7.0. FUTURE PERSPECTIVES

This work yielded the study of the human albumin binding of a prospective anti-tumour metallodrug, the complex $[Ru^{II}(Cp)(bipy)(CO)][PF_6]$. Stoichiometries and conditional binding constants for the protein-complex adducts were obtained and the interaction was studied with some detail.
Nevertheless some studies would be of value to disclose more information on this system, and/or other techniques would be useful.

From the time dependence studies it is concluded that the equilibrium is achieved fast enough for a non-covalent binding process to be operative. The fact that full equilibrium was reached between 200 and 400 min could indicate that there is some covalent binding component involved in the system studied (because the system takes few hours to reach the equilibrium). To study the covalent binding between the complex and the protein would be interesting as a complement to this work. Experiments with amino acids with the amino-acid binding group blocked could be performed so that a possible interaction with the side chain might be detected.

From PSEQUAD fits it was possible to refine (in some restricted conditions and typically with a lower FP) the formation constant for the ternary species {HSA-site marker-complex}. The formation of this possible species was not clear, and the use of other techniques – such as e.g. circular dichroism – would provide more insight to this topic.

Checking the interaction with amino acids to see if the complex is still stable in their presence or if it binds to the amino acid losing one of the co-ligands of the parent complex would be another interesting project to undertake.

8.0. Bibliography

(1) The World Health Organisation website: entered on the fifth of March 2014, http://www.who.int/mediacentre/factsheets/fs297/en/

(2) J. Massagué, Evolución y metástasis del cáncer, Dossier científico, SEBBM, 160, Junio 2009.

(3) Cell Biology and Cancer NIH Curriculum supplement series-Grades 9-12, teacher's guide: entered on the sixth of March 2014, http://science.education.nih.gov/supplements/nih1/cancer/guide/understanding1.htm

(4) I. Kostova, Ruthenium complexes as Anticancer Agents, Curr. Med. Chem., 13 (2006) 1085-1107

(5) T. Boulikas, M. Vougiouka, Recent clinical trials using cisplatin, carboplatin and their combination chemotherapy drugs (Review), Oncology reports, 11 (2004), 559-595.

(6) B. Rosenberg,, L. Van Camp, T. Krigas, Inhibition of cell division in Escherichia coli by electrolysis products from platinum electrode, Nature, 205 (1965) 698-9.

(7) L. Kelland, The resurgence of platinum-based cancer chemotherapy, Nat. Rev. Cancer, 7 (2007) 573-584.

(8) J.F. Neault, H. A. Tajmir-Riahi, Interaction of cisplatin with human serum albumin. Drug binding mode and protein secondary structure, Biochim. Biophys. Acta, 1384 (1998) 153-159.

(9) B. Rosenberg, Nucleic Acid-Metal Ion Interactions; T. G. Spiro (Ed); John Wiley & Sons, New York, NY, USA, 1 (1980) 1-29.

(10) B. Desoize, C. Madoulet, Particular aspects of platinum compounds used at present in cancer treatment, Crit. Rev. Oncol. Hematol., 42(2002) 317-325.

(11) M. J. Hannon, Metal-based anticancer drugs: From a past anchored in platinum chemistry to a post-genomic future of diverse chemistry and biology, Pure Appl. Chem., 79 (2007) 2243-2261.

(12) S. Page, Ruthenium compounds as anticancer agents, Royal Society of Chemistry- Education in Chemistry (2012) 26-9.

(13) MA Jakupec, M Galanski, V B Arion, C G Hartinger, B K Keppler, Antitumour metal compounds: more than theme and variations, Dalton trans., (2008) 183-94.

(14) J. Reedijk, Metal-Ligand Exchange Kinetics in Platinum and Ruthenium Complexes, Platinum Metals Rev, 52(2008) (1), 2-11.

(15) A Bergamo, C Gaiddon, J H M Schellens, J H Beijnen, G Sava, Approaching tumour therapy beyond platinum drugs: status of the art and perspectives of ruthenium drug candidates, J. Inor. Biochem., 106 (2012) 90-99.

(16) A. Bergamo, G. Sava, Ruthenium complexes can target determinants of tumour malignancy, Dalton Trans., (2007) 1267-72.

(17) A. Bergamo, G. Sava, Ruthenium anticancer compounds: myths and realities of the emerging metal-based drugs, Dalton Trans., 40 (2011) 7817-23.

(18) A Levina, A Mitra, P A Lay, Recent developments in ruthenium anticancer drugs, Royal Society of Chemistry - Metallomics, (2009) 458-68.

(19) G. Sava, S. Zorzet, C. Turrin, F Vita, M Soranzo, G Zabucchi, M Cocchietto, A Bergamo, S DiGiovine, G Pezoni, L Sartor, S Garbisa, Dual Action of NAMI-A in Inhibition of Solid Tumor Metastasis: Selective Targeting of Metastatic Cells and Binding to Collagen, Clin Cancer Res, 9 (2003) 1898-1905.

(20) S H van Rijt, P J Sadler, Current applications and future potential for bioinorganic chemistry in the development of anticancer drugs, Drug Discov. Today, 14 (2009) 1089-97.

(21) A. I. Tomaz, T. Jakusch, T. S. Morais, F. Marques, R.F.M. de Almeida, F. Mendes, É.A. Enyedy, I. Santos, J.C. Pessoa, T. Kiss, M.H. Garcia , $[Ru^{II}(\eta^5\text{-}C_5H_5)(bipy)(PPh_3)]^+$, a promising large spectrum antitumor agent: Cytotoxic activity and interaction with human serum albumin, J. Inorg. Biochem., 117 (2012) 261-269.

(22) H. Bregman, E. Meggers, Ruthenium Half-Sandwich Complexes as Protein Kinase Inhibitors: An N-Succinimidyl Ester for Rapid Derivatizations of the Cyclopentadienyl Moiety, Org. Lett., 24 (2006) 5465-5468.

(23) R. Anand, J. Maksimoska, N. Pagano, E Y Wong, P A Gimotty, S L Diamond, E Meggers, R Marmorstein, Toward the Development of a Potent and Selective Organoruthenium fMammalian Sterile 20 Kinase Inhibitor, J. Med. Chem., 52, 6, (2009) 1602-1611.

(24) M. H. Garcia, T. S. Morais, P. Florindo, M. F. Piedade, V. Moreno, C. Ciudad, V. Noe, Inhibition of cancer cell growth by ruthenium(II) cyclopentadienyl derivative complexes with heteroaromatic ligands, J. Inorg. Biochem. 103 (2009) 354-361.

(25) V. Moreno, J. Lorenzo, F X Aviles, M H Garcia, J P Ribeiro, T S Morais, P Florindo, M P Robalo , Studies of the Antiproliferative Activity of Ruthenium(II) Cyclopentadienyl-Derived Complexes with Nitrogen Coordinated Ligands, Bioinorg. Chem. Appl. (2010) 1-11.

(26) V Moreno, M Font-Bardia, T Calvet, J Lorenzo, F X Avilés, M H Garcia, T S Morais, A Valente, M P Robalo, DNA interaction and cytotoxicity studies of new ruthenium(II) cyclopentadienyl derivative complexes containing heteroaromatic ligands, J. Inorg. Biochem. 105 (2011) 241-249.

(27) R. Motterlini, L.E Otterbein, The therapeutic potential of carbon monoxide, Nat. Rev. Drug Discovery, 9 (2010) 728-743.

(28) T. S. Morais, F. Santos, L. Côrte-Real, F Marques, M P Robalo, P J Madeira, M H Garcia, Biological activity and cellular uptake of $[Ru^{II}(\eta^5\text{-}C_5H_5)\ (PPh_3)(Me_2bpy)][CF_3SO_3]$ complex, J. Inorg. Biochem., 122 (2013) 8-17.

(29) P.J.A. Madeira, T.S. Morais, T.J.L. Silva, P. Floringdo, M.H. Garcia, Gas-phase behaviour of Ru(II) cyclopentadienyl-derived complexes with N-coordinated ligands by electrospray ionization mass spectrometry: fragmentation pathways and energetics, Rapid Commun. Mass Spectrom., 26(2012) 1675-1686

(30) A. Valente, M.H. Garcia, F. Marques, Y. Miao, C. Rousseau, P. Zinck, First polymer "ruthenium-cyclopentadienyl" complex as potential anticancer agent, J. Inorg. Biochem., 127 (2013) 79-81.

(31) G R Newkome, A K Patri, E Holder, U S Schubert, Synthesis of 2,2′-Bipyridines: Versatile Building Blocks for Sexy Architectures and Functional Nanomaterials, Eur. J. Org. Chem., (2004) 235-254.

(32) The strong coordination of carbon monoxide in the complex $[Ru(Cp)(bipy)(CO)]^+$ can be confirmed by the infrared stretching vibration of the CO ligand ($\nu_{C\equiv O}$) occurring at 1970 cm-^{1}, where a shift of ca. -200 cm^{-1} in the $\nu_{C\equiv O}$ ($\nu_{C\equiv O}$, gas=2143 cm^{-1} vs. $\nu_{C\equiv O}$ =1970 cm^{-1} in the complex) indicates a strong π-backdonation effect as expected given the excellent π acceptor character of CO as a coligand. This is confirmed by ^{1}H NMR, where a marked deshielding of the Cp protons was also observed - L. Côrte-Real, M.P. Robalo, F. Marques, G. Nogueira, F. Avecilla, F. C. Santos, A.I. Tomaz, M.H. Garcia, A. Valente, Adapted from the manuscript "The key role of coligands in novel ruthenium(II)-cyclopentadienyl bipyridine derivatives: ranging from non-cytotoxic to highly cytotoxic compounds", submitted to Chemistry - a European Journal .

(33) T. Mosmann, Rapid Colorimetric Assay for Cellular Growth and Survival: Application to Proliferation and Cytotoxicity Assays, J. Immunol. Methods 65, (1983).

(34) D. Sanna, L. Bíró, P Buglyó, G Micera, E Garribba, Transport of the anti-diabetic VO^{2+} complexes formed by pyrone derivatives in the blood serum, J. Inorg. Biochem. , 115 (2012), 87-99.

(35) J. Costa Pessoa, A. I. Tomaz, Transport of Therapeutic Vanadium and Ruthenium Complexes by Blood Plasma Components, Curr. Med. Chem. , 17 (2010) 3701-3738.

(36) D. C. Carter , JX Ho, , Structure of serum albumin, Adv. Protein Chem., 45 (1994), 153-203.

(37) F. Kratz, Albumin as a drug carrier: Design of prodrugs, drug conjugates and nanoparticles, J. control. Release, 132 (2008) 171-183.

(38) T. Peters, Serum albumin, Adv. Protein Che. , 37 (1985) 161-245.

(39) G. Colmenarejo, In silico prediction of drug-binding strengths to human serum albumin. , Med. Res. Rev., 23 (2003) 275-301.

(40) Y. Matsumura, H. Maeda, A New Concept for Macromolecular Therapeutics in Cancer Chemotherapy: Mechanism of Tumoritropic Accumulation of Proteins and the Antitumor Agent Smancs, Cancer. Res. , 46 (1986) 6387.

(41) H. Maeda, The enhanced permeability and retention (EPR) effect in tumor vasculature: the key role of tumor-selective macromolecular drug targeting, Advan. Enzyme Regul., 41 (2001) 189-207.

(42) O, Dömötör, C.G. Hartinger, A.K. Bytzek, T. Kiss, B.K. Keppler, E. Enyedy , Characterization of the binding sites of the anticancer ruthenium(III) complexes KP1019 and KP1339 on human serum albumin via competition studies, J. Biol. Inorg. Chem., 18 (2013) 9-17.

(43) S. Sugio, A. Kashima, S. Mochizuki, M. Noda, K. Kobayashi, Crystal structure of human serum albumin at 2.5 A resolution, Protein Eng., 12 (1999) 439-46.

(44) X. M. HE, D. C Carter, Atomic structure and chemistry of human serum albumin, Nature 358(6383) July (1992), 209-15.

(45) B. Meloun, L. Moravek, V. Kostka, Complete amino acid sequence of human serum albumin, FEBS letters 58(1) (1975) 134-137.

(46) Peters Jr, T., All about albumin: Biochemistry, Genetics and Medical Applications, Academic Press, San Diego, California, 1996.

(47) G. Sudlow, D. J. Birkett, D. N. Wade, The characterization of two specific drug binding sites on human serum albumin, Mol. Pharm. 11(6) (1975), 824-832.

(48) Kragh-Hansen, Relations between high-affinity binding sites for L-tryptophan, diazepam, salicylate and Phenol Red on human serum albumin, Biochem. J., 209 (1983) 135-142.

(49) Kragh-Hansen, Relations between high-affinity binding sites of markers for binding regions on human serum albumin, Biochem. J., 225 (1985) 629-638.

(50) Kragh-Hansen, Evidence for a large and flexible region of human serum albumin possessing high affinity binding sites for salicylate, warfarin, and other ligands, Mol. Pharmacol., 34(2) (1988) 160-71.

(51) F. Zsila, Z. Bikadi, M. Simonyi, Probing the binding of the flavonoid quercetin to human serum albumin by circular dichroism, electronic absorption spectroscopy and molecular modeling methods, Biocherm. Pharmacol., 65 (2003) 447-456.

(52) W.R. Bell, TL Simon, Current status of pulmonary thromboembolic disease pathophysiology, diagnosis, prevention and treatment, Am Heart J., 103 (1982) 239-262.

(53) D. D Giannini, K. Kenneth Chan't nd J. D. Roberts, Carbon-13 Nuclear Magnetic Resonance Spectroscopy. Structure of the Anticoagulant Warfarin and Related Compounds in Solution, Proc. Natl. Acad. Sci. USA, 71-10 (1974), 4221-3.

(54) K. J. Fehske, W. E. Müller, and U. Wollert, , The location of drug binding sites in human serum albumin. (Review), Biochem. Pharmacol. 30 (1981), 687-692.

(55) KJ. Fehske, U. Schläfer,, U. Wollert,, and Müller, W. E., Characterization of an important drug binding area on human serum albumin including the high-affinity binding sites of warfarin and azapropazone, Mol. Pharmacol., 21 (1982), 387-393.

(56) NHG Holford, LZ Benet., Pharmacokinetics & pharmacodynamics: dose selection & the time of course of drug action. In: Katzung BG, ed. Basic & Clinical Pharmacology. (1998), 34-49.

(57) Enyedy, E. a, Horváth, L., Hetényi, A., Tuccinardi, T., Hartinger, C. G., Keppler, B. K., & Kiss, T., Interactions of the carrier ligands of antidiabetic metal complexes with human serum albumin: a combined spectroscopic and separation approach with molecular modeling studies. *Bioorganic & Medicinal Chemistry*, *19*(14) (2011), 4202–10.

(58) FS Graciani, VF Ximenes, Investigation of Human Albumin-Induced Circular Dichroism in Dansylglycine, PLoS ONE, 8-10 (2013), 1-8.

(59) CG Björn, AM Rosengren, P Andersson, IA Nicholls, The Spectrophysics of Warfarin: Implications for Protein Binding, J. Phys. Chem. B., 111 (2007) 10520-10528.

(60) J. R. Lakowicz, Principles of Fluorescence spectroscopy, Springer, New York, 3rd edition, 2006.

(61) C. P. Matos, A. Valente, F. Marques, P. Adão, M. P Robalo, R F M de Almeida, J C Pessoa, I Santos, M H Garcia, A I Tomaz , New Polydentate Ru(III)-Salan complexes: Synthesis, characterization, anti-tumour activity and interaction with human serum proteins, Inorg. Chim. Acta, 394 (2013) 616-26.

(62) B. Valeur, Molecular fluorescence: Principles and applications, Wiley-VCH, NewYork, 2001.

(63) M. Kubista, R. Sjöback, S. E. S. Eriksson, Bo Albinsson, Experimental Correction for the inner-filter Effect in Fluorescence Spectra, Analyst, 119 (1994) 417-419.

(64) I. Nagypál, , L. Zékány, in: Leggett, D. (Ed.), Computational Methods for the Determination of Stability Constants, Plenum Press, New York, (1985), 291.

(65) T. Jakusch, D. Hollender, E.A. Enyedy, CS González, M. Montes-Bavón, A. Sanz-Medel, J. Costa Pessoa, I. Tommaz, T. Kiss, Biospeciation of various antidiabetic $V^{IV}O$ compounds in serum, Dalton Trans. 13 (2009) 2428.

(66) G. H. Beaven, S. H. Chen, A. d'Albis, W. B. Gratzer, A Spectroscopic Study of the Haemin-Human-Serum-Albumin System, Eur. J. Biochem., 41 (1974), 539-546.

(67) I. Bárdos-Nagy, R. ´Galántai, A. D. Kaposi, J. Fidy, Difference in the transport of metal and free-base porphyrins Steady-state and time-resolved fluorescence studies, Int. J. Pharm., 175 (1998) 255-267.

(68) B. Demoro, R. F. M. de Almeida,., Screening organometallic binuclear thiosemicabazone ruthenium complexes as potential anti-tumour agents: cytotoxic activity and human serum albumin binding mechanism., Dalton Trans., 42 (2013) 7131.

9.0. ANNEXES

Annex A1. Binary system

- (A1-HSA-RuC system)

date / experiment	C_{HSA} / M	CComplex/M	ratio	Steady-state measurem.	Time-resolved measurem.	T_{incub} /ºC	T measurem./ºC (bath)	time incub./h	Emission slits/ time-resolved emission slits
8.Oct /#1									
	$5,12_x10^{-06}$	0	0	✓If (λexc=295 nm)	✓	37	RT	19,8	2 nm /8nm
		2,50x10-06	0,5		✓				
		5,01 x10-06	1		✓				
		1,25 x10-05	2,4		✓				
	*	2,51 x10-05	4,9		✓				
	*	5,01 x10-05	9,8		✓				
	*	7,51 x10-05	14,7		✓				
22.Oct / #2									
	2,24 x10-**06**	0	0	✓If (λexc=295 nm)	✓	37	36,9	20,2	2nm/15nm
		1,30 x10-06	0,58		-				
		2,50 x10-06	1,11		✓				
		3,81 x10-06	1,69		-				
		5,00 x10-06	2,22		✓				
		6,29 x10-06	2,79		-				
		7,50 x10-06	3,33		✓				

		8,74 x10-06	3,88		-			
		9,99 x10-06	4,43		✓			
25.Oct / #3								
	2,51 x10-**06**	0,0	0	✓If (λexc=295 nm)	✓	37	RT	23,3	2nm/10nm
		1,30 x10-06	0,52		✓				
		2,50 x10-06	1		✓				
		3,80 x10-06	1,51		✓				
		4,39 x10-06	1,75		✓				
		6,30 x10-06	2,51		✓				
		7,50 x10-06	2,99		✓				
		8,77 x10-06	3,5		✓				
		1,01 x10-05	4,01		✓				
		1,25 x10-05	4,99		✓				
29-Oct / #4								
	2,5 x10-**06**	0,00	0	✓If (λexc=295 nm)	✓	37	RT	24,3	2nm/14nm
		2,51 x10-06	1		✓				
		5,01 x10-12	2,01		✓				
		7,50 x10-06	3		✓				
		1,00 x10-05	4,01		✓				
		1,25 x10-05	5,01		✓				
		1,50 x10-05	6,02		✓				
		1,76 x10-05	7,02		✓				
		2,01 x10-05	8,02		✓				
		2,51 x10-05	10,03		✓				
01.Nov / #5								
	2,51 x10-**06**	0,00	0		✓				
		2,50 x10-06	1		✓				
		5,00 x10-06	1,99		✓				

B

	7,50 x10-06	2,99	✓If (λexc=295 nm)	✓	37	RT	25,8	2nm/13nm
	9,97 x10-06	3,98		✓				
	1,25 x10-05	4,99		✓				
	1,50 x10-05	5,99		✓				
	1,75 x10-05	7		✓				
	1,99 x10-05	7,96		✓				
	2,50 x10-05	9,97		✓				
5.Nov / #6								
2,50 x10-**06**	0,00	0	✓If (λexc=295 nm)	✓	37	36,9	24,2	2nm/14nm
	2,50 x10-06	1,00		✓				
	4,99 x10-06	2,00		✓				
	7,52 x10-06	3,01		✓				
	1,00 x10-05	4,00		✓				
	1,26 x10-05	5,02		✓				
	1,50 x10-05	6,01		✓				
	1,75 x10-05	7,01		✓				
	2,00 x10-05	8,00		✓				
	2,25 x10-05	9,00		✓				
	2,50 x10-05	9,99		✓				
7.Nov / #7								
2,00 x10-**06**	0	0	✓If (λexc=295 nm)	✓	37	36,9	24,0	2nm/15nm
	2,00 x10-06	1,00		✓				
	2,40 x10-06	1,20		✓				
	4,01 x10-06	2,00		✓				
	4,81 x10-06	2,40		-				
	6,00 x10-06	3,00		✓				
	8,00 x10-06	4,00		✓				
	1,00 x10-05	5,00		-				

C

	1,20 x10-05	6,00		✓				
	1,40 x10-05	7,00		✓				
	1,60 x10-05	7,99		✓				
	1,80 x10-05	8,99		-				
	2,00 x10-05	9,99		-				
	2,40 x10-05	11,99		-				
	2,80 x10-05	13,99		✓				
	3,20 x10-05	15,99		✓				
	3,60 x10-05	17,99		✓				
	4,00 x10-05	19,99		-				
	4,41 x10-05	22,03		✓				
	4,80 x10-05	23,98		✓				
12.Nov / #8								
	2,00 x10-**06**	0,00	0,00		✓				
		2,00 x10-06	1,00		✓				
		2,40 x10-06	1,20		✓				
		4,01 x10-06	2,00		✓				
		4,79 x10-06	2,40		✓				
		6,00 x10-06	3,00		✓				
		8,00 x10-06	4,00		✓				
		1,00 x10-05	5,00	✓If (λexc=295 nm)	✓	37	36,9	23,2	2nm/15nm
		1,20 x10-05	6,02		✓				
		1,40 x10-05	6,99		✓				
		1,61 x10-05	8,03		✓				
		1,80 x10-05	8,99		✓				
		2,01 x10-05	10,04		✓				
		2,40 x10-05	12,01		✓				
		2,80 x10-05	14,01		✓				

D

		3,20 x10-05	16,02		✓			
		3,60 x10-05	17,99		✓			
		4,00 x10-05	20,00		✓			
		4,40 x10-05	22,00		✓			
		4,80 x10-05	24,01		✓			
15.Nov / #9								
	2,00 x10-**06**	0,00	0,00		✓			
	*	2,00 x10-06	1,00		✓			
		2,50 x10-06	1,25		✓			
		3,01 x10-06	1,50		✓			
		3,50 x10-06	1,75		✓			
		4,00 x10-06	2,00		✓			
		4,51 x10-06	2,26		✓			
		5,01 x10-06	2,50		✓			
		5,50 x10-06	2,75		✓			
		6,00 x10-06	3,00		✓			
		6,51 x10-06	3,26	✓If (λexc=295 nm)	✓	37	RT	6,5	2nm/15nm
		7,01 x10-06	3,50		✓			
		7,51 x10-06	3,75		✓			
		8,05 x10-06	4,02		✓			
		8,50 x10-06	4,25		✓			
	*	9,02 x10-06	4,51		✓			
	*	9,55 x10-06	4,78		✓			
	*	1,00 x10-05	5,00		✓			
	*	1,05 x10-05	5,26		✓			
	*	1,11 x10-05	5,53		✓			

Table 1: Conditions of the experiments performed for the system HSA + RuC. (RT, room temperature; * λ_{exc}=351 nm + 413 nm + 498 nm, very low emission from the complex at 498; 351/413nm, raman in the middle of the emission band)

- A2- Temperature dependence (HSA + RuC system)

date / experiment	C_{HSA} / M	CComplex/M	ratio	Steady-state measurem.	Time-resolved measurem.	T_{incub} /ºC	Tmeasure/ºC (bath)	time incub/h	Emission slits / time-resolved emission slits
24.Jan / #10									
	2,00 x10-**06**	0,00	0	✓If (λexc=295 nm)	✓	25	25	24,1	2nm/15nm
		2,06 x10-06	1,03		✓				
		4,57 x10-06	2,28		✓				
		6,04 x10-06	3,02		✓				
		8,03 x10-06	4,02		✓				
		1,00 x10-05	5,01		✓				
		1,40 x10-05	7,00		✓				
		1,81 x10-05	9,03		✓				
		2,31 x10-05	11,53		✓				
		2,60 x10-05	13,01		✓				
		3,01 x10-05	15,03		✓				
		3,50 x10-05	17,50		✓				
28.Jan / #11									
	2,00 x10-**06**	0,00	0	✓If (λexc=295 nm)	✓	25	25	23,5	4nm/15nm
		2,00 x10-06	1,00		✓				
		4,54 x10-06	2,27		✓				
		6,00 x10-06	3,00		✓				
		7,99 x10-06	4,00		✓				
		9,99 x10-06	5,00		✓				
		1,40 x10-05	7,00		✓				
		1,80 x10-05	8,99		✓				
		2,30 x10-05	11,51		✓				
		2,60 x10-05	12,99		✓				

		3,00 x10-05	14,99		✓			
		3,50 x10-05	17,50		✓			
31.Jan / #12								
	2,00 x10-**06**	0	0		✓			
		1,99 x10-06	0,99		✓			
		4,52 x10-06	2,26		✓			
		6,05 x10-06	3,03		✓			
		8,04 x10-06	4,02		✓			
		1,00 x10-05	5,01		✓			
		1,40 x10-05	7,00	✓If (λexc=295 nm)	✓	37	36,9	22	4nm/15nm
		1,81 x10-05	9,03		✓			
		2,30 x10-05	11,52		✓			
		2,60 x10-05	13,01		✓			
		3,00 x10-05	15,00		✓			
		3,51 x10-05	17,53		✓			
31.Jan / #13								
	2,00 x10-**06**	0	0		✓			
		1,99 x10-06	0,99		✓			
		4,52 x10-06	2,26		✓			
		6,05 x10-06	3,03		✓			
		8,04 x10-06	4,02		✓			
		1,00 x10-05	5,01		✓			
		1,40 x10-05	7,00	✓If (λexc=295 nm)	✓	20	20	24	4nm/15nm
		1,81 x10-05	9,03		✓			
		2,30 x10-05	11,52		✓			
		2,60 x10-05	13,01		✓			
		3,00 x10-05	15,00		✓			
		3,50 x10-05	17,53		✓			

05.Feb / #14								
	2,00 x10-**06**	0	0	✓If (λexc=295 nm)	✓	30	30	23	4nm/15nm
		2,05 x10-06	1,03		✓				
		4,49 x10-06	2,24		✓				
		6,03 x10-06	3,01		✓				
		8,01 x10-06	4,01		✓				
		1,00 x10-05	5,00		✓				
		1,40 x10-05	7,02		✓				
		1,80 x10-05	9,01		✓				
		2,30 x10-05	11,51		✓				
		2,60 x10-05	13,01		✓				
		3,00 x10-05	15,00		✓				
05.Feb / #15								
	2,00 x10-**06**	0	0	✓If (λexc=295 nm)	✓	20	20	26	4nm/15nm
		2,05 x10-06	1,03		✓				
		4,49 x10-06	2,24		✓				
		6,03 x10-06	3,01		✓				
		8,01 x10-06	4,01		✓				
		1,00 x1005	5,00		✓				
		1,40 x10-05	7,02		✓				
		1,80 x10-05	9,01		✓				
		2,30 x10-05	11,51		✓				
		2,60 x10-05	13,01		✓				
		3,00 x10-05	15,00		✓				
28.Feb / #16								
	2,00 x10-**06**	0	0	✓If (λexc=295 nm)	✓	30	30	22	4nm/15nm
		2,02 x10-06	1,01		✓				
		4,53 x10-06	2,27		✓				

H

	6,07 x10-06	3,04		✓				
	8,00 x10-06	4,00		✓				
	1,00 x10-05	5,01		✓				
	1,41 x10-05	7,04		✓				
	1,80 x10-05	9,01		✓				
	2,30 x10-05	11,52		✓				
	2,60 x10-05	13,01		✓				
	3,01 x10-05	15,04		✓				
28.Feb / #17								
2,00 x10-**06**	0	0		✓				
	2,02 x10-06	1,01		✓				
	4,53 x10-06	2,27		✓				
	6,07 x10-06	3,04		✓				
	8,00 x10-06	4,00		✓				
	1,00 x10-05	5,01		✓				
	1,41 x10-05	7,04	✓If (λexc=295 nm)	✓	15	15	24,2	4nm/15nm
	1,80 x10-05	9,01		✓				
	2,30 x10-05	11,52		✓				
	2,60 x10-05	13,01		✓				
04.Mar / #18								
2,00 x10-**06**	0	0		✓				
	6,01 x10-06	3,00		✓				
	8,01 x10-06	4,01		✓				
	1,00 x10-05	5,01		✓				
	1,40 x10-05	7,01	✓If (λexc=295 nm)	✓	15	15	28	4nm/15nm
	1,80 x10-05	9,01		✓				
	2,30 x10-05	11,52		✓				
	2,60 x10-05	13,02		✓				

		3,00 x1005	15,00		✓				
04.Mar / #19								
	2,00 x10-**06**	0	0		✓				
		2,00 x10-06	1,00		✓				
		2,43 x10-06	1,22		✓				
		4,01 x10-06	2,00		✓				
		4,82 x10-06	2,41		✓				
		6,01 x10-06	3,00		✓				
		8,01 x10-06	4,01		✓				
		1,00 x10-05	5,01		✓				
		1,20 x10-05	6,01	✓If (λexc=295 nm)	✓	37	36,9	23,4	4nm/15nm
		1,40 x10-05	7,01		✓				
		1,60 x10-05	8,01		✓				
		1,80 x10-05	9,01		✓				
		2,00 x10-05	10,02		✓				
		2,40 x10-05	12,02		✓				
		2,80 x10-05	14,02		✓				
		3,20 x10-05	16,00		✓				
		3,60 x10-05	18,01		✓				

Table 2. Conditions of the experiments performed for the system HSA + RuC. (at different temperatures);

- Annex A3-Experiments with Warfarin (37 ºC)

date / experiment	C_{HSA} / M	Conc. WF/M	Complex concs./M	ratio	If (λ_{exc}= 310 nm)	T incub /ºC	T measure/ºC (bath)	time incub. /h	Emission slits/ time-resolved emission slits
05.Dec / #20									
WF alone		0,00							
		5,17 x10-07							
		7,50 x10-07							
		1,01 x10-06							
		1,27 x10-06							
		1,53 x10-06			✓	37	37		2 nm / 15 nm
		1,76 x10-06							
		2,02 x10-06							
		2,51 x10-06							
		3,00 x10-06							
		3,52 x10-06							
06.Dec / #21									
WF+HSA		0,00		0,00					
		5,17 x10-07		0,25					
		7,50 x10-07		0,38					
		1,01 x10-06		0,50					
	2,00 x10-06	1,27 x10-06		0,63	✓	37	37	23,16	2 nm / 15 nm
		1,50 x10-06		0,75					
		1,76 x10-06		0,88					
		2,02 x10-06		1,00					
		2,51 x10-06		1,25					
		3,00 x10-06		1,50					

K

		3,52 x10-06		1,75				
13.Ded / #22								
WF+HSA+RuC			0	0,00				
			2,01 x10-06	1,01				
			4,03 x10-06	2,01				
			8,00 x10-06	4,00				
	2,01 x10-06	2,00 x10-06	1,40 x10-05	7,02	✓	37	37	24	2 nm / 15 nm
			2,00 x10-05	10,02				
			2,80 x10-05	14,02				
			3,60 x10-05	18,02				
			4,40 x10-05	22,02				
21.Jan / #23								
WF alone		0						
		4,98 x10-07						
		7,47 x10-07						
		9,96 x10-07						
		1,24 x10-06						
		1,49 x10-06						
		1,74 x10-06						
		1,99 x10-06			✓	37	37		2 nm / 15 nm
		2,49 x10-06						
		3,01 x10-06						
		3,51 x10-06						
		5,00 x10-06						
		1,00 x10-05						
		1,20 x10-05						
		1,50 x10-05						
		1,80 x10-05						

L

		2,00 x10-05					
		2,50 x10-05					
		3,00 x10-05					
		3,50 x10-05					
		3,80 x10-05					
		4,00 x10-05					
22.Jan / #24							
WF+HSA		0,00	0				
		4,98 x10-07	0,25				
		7,47 x10-07	0,37				
		9,96 x10-07	0,50				
		1,24 x10-06	0,62				
		1,49 x10-06	0,75				
		1,74 x10-06	0,87				
		1,99 x10-06	0,99				
		2,49 x10-06	1,24				
		3,01 x10-06	1,50				
	2,00 x10-06	3,51 x10-06	1,75	✓	37	37	23	2 nm / 11 nm
		1,00 x10-05	5,00				
		1,20 x10-05	5,99				
		1,50 x10-05	7,50				
		2,00 x10-05	9,99				
		2,50 x10-05	12,49				
		3,00 x10-05	14,99				
		3,30 x10-05	16,48				
		3,50 x10-05	17,49				
		4,00 x10-05	19,99				
20.Jan / #25							

M

WF+HSA+RuC			0	0,00				
			2,03 x10-06	1,02				
			4,00 x10-06	2,01				
			8,00 x10-06	4,02				
	2,00 x10-06	1,99 x10-06	1,40 x10-05	7,05				
			2,00 x10-05	10,05	✓	37	37	24	2 nm / 15 nm
			2,80 x10-05	14,07				
			3,60 x10-05	18,09				
			4,40 x10-05	22,11				
20.Feb / #26								
WF alone		0,0						
		1,01 x10-06						
		2,00 x10-06						
		3,01 x10-06						
		5,00 x10-06						
		1,00 x10-05						
		1,40 x10-05						
		1,50 x10-05						
		1,80 x10-05			✓	37	37		3 nm / 15 nm
		2,00 x10-05						
		2,30 x10-05						
		2,50 x10-05						
		2,80 x10-05						
		3,00 x10-05						
		3,30 x10-05						
		3,50 x10-05						
		3,80 x10-05						
		4,00 x10-05						

N

		6,00 x10-05						
		8,00 x10-05						
21.Feb / #27								
WF+HSA		0,00 x10-06		0,00				
		5,04 x10-07		0,25				
		1,01 x10-06		0,50				
		1,49 x10-06		0,75				
		1,76 x10-06		0,88				
		2,00 x10-06		1,00				
		2,50 x10-06		1,25				
	2,00 x10-06	5,00 x10-06		2,50	✓	37	37	1	2,5nm/ 11nm
		1,00 x10-05		5,01				
		1,50 x10-05		7,50				
		2,00 x10-05		10,00				
		2,50 x10-05		12,50				
		3,00 x10-05		15,01				
		3,50 x10-05		17,51				
		4,00 x10-05		20,01				
20.Feb / #28								
WF+HSA+RuC			0	0,00				
			2,01 x10-06	1,01				
			4,02 x10-06	2,01				
			7,97 x10-06	3,99				
	2,00 x10-06	2,00 x10-06	1,40 x10-05	7,01	✓	37	37	25	3 nm / 15 nm
			2,00 x10-05	10,02				
			2,80 x10-05	14,01				
			3,60 x10-05	18,03				
			4,40 x10-05	22,03				

25.Feb / #29								
WF+HSA+RuC			0	0,00				
			2,05 x10-06	1,02				
			4,10 x10-06	2,03				
			8,05 x10-06	3,99				
	2,01 x10-06	2,02 x10-06	1,41 x10-05	6,96				
			2,01 x10-05	9,94	✓	37	37	26,5	3 nm / 15 nm
			2,80 x10-05	13,86				
			3,60 x10-05	17,85				
			4,41 x10-05	21,84				

Table 1. Conditions for the experiments involving the site marker Warfarin. There are three systems Warfarin alone solutions, Warfarin-HSA solutions (keeping the protein constant and increasing the concentration of the site marker) and Warfarin-HSA-RuC solutions (keeping the protein and site marker equimolar and increasing the concentration of the complex).

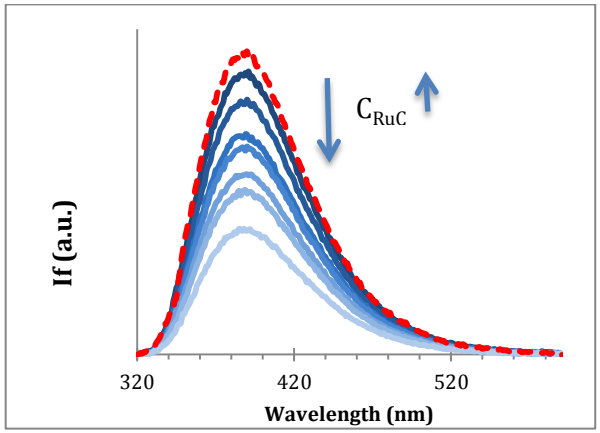

Figure A. Emission spectra of the system WF-RuC recorded from samples of constant concentration of Warfarin with increasing concentrations of RuC (darker shade C_{RuC}=2 µM, lighter shade C_{RuC}= 44 µM) Experiments incubated and measured at 37ºC in 10 mM HEPES (pH 7,4). The red discontinuous line is Warfarin with a concentration of 2 µM.

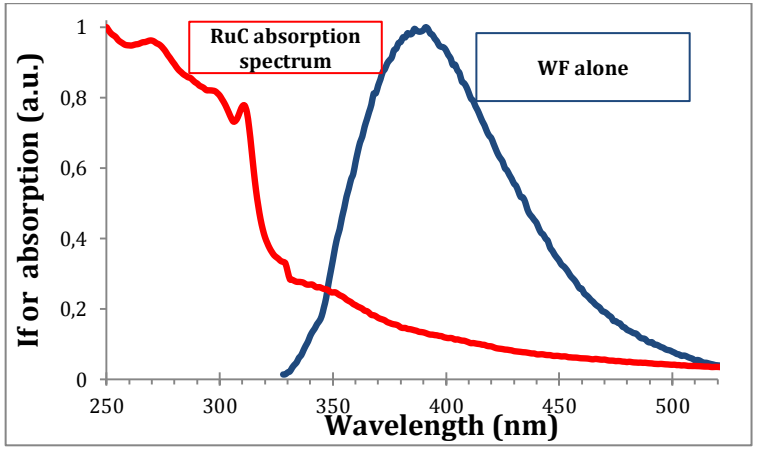

Figure B. Overlapping spectra: absorption spectrum of the complex and the emission spectrum of the site marker Warfarin in 10 mM HEPES pH 7,4.

- A4. Experiments with Dansylglycine (37 ºC)

date / experiment	C_{HSA} / M	Conc. DG/M	Complex concs./M	ratio	If (λ_{exc}= 335 nm)	T incub/ºC	T measure/ºC (bath)	time incub. /h	Emission slits/ time-resolved emission slits
10.Dec / #30									
DG alone		0,00							
		2,00 x10-06							
		5,01 x10-06							
		8,02 x10-06							
		1,00 x10-05			✓	37	36,9	24	2 nm / 15 nm
		1,20 x10-05							
		1,40 x10-05							
		1,50 x10-05							
		1,80 x10-05							
		2,00 x10-05							

Q

		2,30 x10-05						
		2,50 x10-05						
		2,80 x10-05						
		3,00 x10-05						
		3,30 x10-05						
		3,50 x10-05						
		3,80 x10-05						
		4,00 x10-05						
11.Dec / #31								
DG+HSA		0,00		0,00				
		2,00 x10-06		1,00				
		5,01 x10-06		2,51				
		8,02 x10-06		4,01				
		1,00 x10-05		5,01				
	2,00 x10-06	1,50 x10-05		7,51	✓	37	36,9	23,16	2 nm / 15 nm
		2,00 x10-05		10,01				
		2,50 x10-05		12,50				
		3,00 x10-05		15,01				
		3,50 x10-05		17,50				
		4,00 x10-05		20,01				
16.Ded / #32								
DG+HSA+RuC			0	0,00				
			2,05 x10-06	1,03				
			4,04 x10-06	2,02				
	2,00 x10-06	2,00 x10-06	8,02 x10-06	4,02	✓	37	36,9	24	2 nm / 15 nm
			1,41 x10-05	7,03				
			2,00 x10-05	10,02				
			2,80 x10-05	14,04				

R

			3,60 x10-05	18,03				
			4,40 x10-05	22,04				
15.Jan / #33								
DG alone		0						
		2,02 x10-06						
		5,02 x10-06						
		8,01 x10-06						
		1,00 x10-05						
		1,20 x10-05						
		1,40 x10-05						
		1,50 x10-05						
		1,80 x10-05			✓	37	36,9	24	2 nm / 15 nm
		2,00 x10-05						
		2,30 x10-05						
		2,50 x10-05						
		2,80 x10-05						
		3,00 x10-05						
		3,30 x10-05						
		3,50 x10-05						
		3,80 x10-05						
		4,00 x10-05						
16.Jan / #34								
DG+HSA		0,00		0				
		2,55 x10-07		0,13				
	2,01 x10-06	5,10 x10-07		0,25	✓	37	36,9	23	2 nm / 15 nm
		7,44 x10-07		0,37				
		9,99 x10-07		0,50				
		1,51 x10-06		0,75				

S

		1,74 x10-06		0,87					
		2,00 x10-06		0,99					
		2,51 x10-06		1,25					
		4,99 x10-06		2,49					
		7,99 x10-06		3,98					
		1,00 x10-05		4,98					
		1,50 x10-05		7,47					
		2,00 x10-05		9,95					
		2,50 x10-05		12,44					
		3,00 x10-05		14,93					
		3,50 x10-05		17,42					
		4,00 x10-05		19,90					
14.Jan / #35									
DG+HSA+RuC			0	0,00					
			2,04 x10-06	1,02					
			4,02 x10-06	2,01					
			8,03 x10-06	4,02					
	2,00 x10-06	2,00 x10-06	1,40 x10-05	7,02	✓	37	36,9	24	2 nm / 15 nm
			2,00 x10-05	10,02					
			2,80 x10-05	14,02					
			3,60 x10-05	18,04					
20.Feb / #36									
DG alone		0							
		1,00 x10-06							
		2,00 x10-06			✓	37	36,9	23	4 nm / 15 nm
		3,00 x10-06							
		5,00 x10-06							
		1,00 x10-05							

T

		1,20 x10-05					
		1,50 x10-05					
		1,80 x10-05					
		2,00 x10-05					
		2,30 x10-05					
		2,50 x10-05					
		2,80 x10-05					
		3,00 x10-05					
		3,30 x10-05					
		3,50 x10-05					
		3,80 x10-05					
		4,00 x10-05					
21.Feb / #37							
DG+HSA		0	0,00				
		5,00 x10-07	0,25				
		1,00 x10-06	0,50				
		1,50 x10-06	0,75				
		1,74 x10-06	0,87				
		2,00 x10-06	1,00				
		3,00 x10-06	1,50				
	2,00 x10-06	5,00 x10-06	2,50	✓	37	36,9	24	2,5 nm/ 12nm
		1,00 x10-05	5,00				
		1,50 x10-05	7,51				
		2,00 x10-05	10,01				
		2,50 x10-05	12,51				
		3,00 x10-05	15,01				
		3,50 x10-05	17,51				
		4,02 x10-05	20,11				

U

20.Feb / #38								
DG+HSA+RuC	2,00 x10-06	2,00 x10-06	0	0,00	✓	37	37	22	3 nm / 15 nm
			2,02 x10-06	1,01				
			3,99 x10-06	2,00				
			8,03 x10-06	4,02				
			1,40 x10-05	7,00				
			2,00 x10-05	10,01				
			2,80 x10-05	14,03				
			3,60 x10-05	18,03				
			4,40 x10-05	22,05				
25.Feb / #39								
DG+HSA+RuC	2,01 x10-06	2,00 x10-06	0	0,00	✓	37	37	24,5	3 nm / 15 nm
			2,05 x10-06	1,02				
			4,10 x10-06	2,05				
			8,05 x10-06	4,02				
			1,41 x10-05	7,02				
			2,01 x10-05	10,02				
			2,80 x10-05	13,97				
			3,60 x10-05	18,00				
			4,41 x10-05	22,02				

Table 1. Conditions of the experiments involving the site marker Dansylglycine. There are three systems Dansylglycine alone solutions, Dansylglycine-HSA solutions (keeping the protein constant and increasing the concentration of the site marker) and Dansylglycine-HSA-RuC solutions (keeping the protein and site marker equimolar and increasing the concentration of the complex).

ANNEX B. STERN-VOLMER ANALYSIS

The equations and constants obtained from the Stern-Volmer analysis are shown in the following table:

							average data		
	T(ºC)/C_{HSA} (μM)	**Slits**	**(K_D±SD) / M^{-1} x(10^4)**	**(K_S ±SD) / M^{-1} x(10^4)**	**equations**	**R^2**	**(K_D±SD)/M^{-1} x(10^4)**	**(K_S±SD)/M^{-1} x(10^4)**	**R^2 (τ_0 / If_0)**
#1	RT / 5,12	2 nm	(1,30 ± 0,06)	(2,63 ± 0,52)	τ_0/τ=(1,02 ± 0,02) + (1,30 ± 0,06) x 10^4 Cq	0,991	N/A	N/A	N/A
					If_0/If= (1,04 ± 0,06) + (1,10 ± 0,50) x 10^4Cq + (3,42 ± 0,66) x 10^8 Cq^2	0,996			
#2	36,9/2,24	2 nm	N/A	N/A	τ_0/τ= (1,04 ± 0,05) + (5,61 ± 1,11) x 10^4 Cq *	0,927	N/A	N/A	N/A
					If_0/If= (1,01 ± 0,01) + (3,51 ± 0,63) x 10^4 Cq+ (2,45 ± 0,63) x 10^9 Cq^2	0,996			
#3	RT / 2,51	2 nm	(2,59 ± 0,11)	(1,31 ± 0,65)	τ_0/τ= (0,982 ± 0,008) + (2,6 ± 0,1) x 10^4 Cq	0,987	(5,58±0,17)	(3,23±0,32)	0,995/0,997
					If_0/If= (1,01 ± 0,02) + (3,91 ± 0,64) x 10^4 Cq+ (5,64 ± 4,92) x $10^8$$Cq^2$	0,993			
#4	RT / 2,50	2 nm	(2,57 ± 0,14)	(2,24 ± 0,85)	τ_0/τ= (0,99 ± 0,02) + (2,57 ± 0,14) x 10^4Cq	0,985			
					If_0/If= (0,98 ± 0,03) + (5,37 ± 0,55) x 10^4 Cq + (5,74 ± 2,15) x 10^8 Cq^2	0,996			
#5	RT / 2,51	2 nm	(4,89 ± 0,17)	(4,83 ± 0,80)	τ_0/τ= (0,99 ± 0,02) + (4,90 ± 0,17) x 10^4Cq	0,993			
					If_0/If= (1,06 ± 0,05) + (2,33 ± 0,96) x 10^4 Cq + (2,36 ± 0,38) x 10^9 Cq^2	0,994			
#6	36,9 / 2,50	2 nm	(6,08 ± 0,19)	(2,01 ± 0,39)	τ_0/τ= (0,96 ± 0,03) + (6,08 ± 0,19) x 10^4 Cq	0,996			
					If_0/If= (0,98 ± 0,03) + (5,76 ± 0,62) x 10^4 Cq + (1,23± 0,23) x 10^9 Cq^2	0,999			
#7	36,9 / 2,00	2 nm	(4,12 ± 0,14)	(2,41 ± 0,41)	τ_0/τ= (0,98 ± 0,03) + (4,12 ± 0,14) x 10^4Cq	0,995	(4,29±0,10)	(2,84±0,21)	0,993/0,998
					If_0/If= (0,98 ± 0,03) + (6,53 ± 0,39) x 10^4 Cq + (1,04 ± 0,09) x 10^9 Cq^2	0,999			
#8	36,9 / 2,00	2 nm	(5,12 ± 0,18)	(2,28 ± 0,18)	τ_0/τ= (1,11 ± 0,03) + (5,12 ± 0,18) x 10^4 Cq	0,99			
					If_0/If= (0,97 ± 0,02) + (6,20 ± 0,33) x 10^4 Cq + (1,17 ± 0,08) x 10^9 Cq^2	0,999			
#9	RT / 2,00	2 nm	(4,56 ± 0,21)	(2,24 ± 1,30)	τ_0/τ= (1,02 ± 0,01) + (4,56 ± 0,21) x 10^4 Cq	0,981			
					If_0/If= (1,01 ± 0,02) + (5,47 ± 0,70) x 10^4 Cq + (1,02 ± 0,59) x 10^9 Cq^2	0,99			
#10	25 / 2,00	2 nm	(1,5 ± 0,13)	(2,68 ± 0,36)	τ_0/τ= (1,00 ± 0,03) + (1,53 ± 0,13) x 10^4 Cq	0,979	N/A	N/A	N/A

W

					$If_0/If = (1,01 \pm 0,02) + (4,21 \pm 0,33) \times 10^4\ Cq + (0,91 \pm 9,64) \times 10^7\ Cq^2$	0,998			
#11	25 / 2	4 nm	(1,99 ± 0,07)	(1,91 ± 0,51)	$\tau_0/\tau = (1,01 \pm 0,01) + (1,99 \pm 0,07) \times 10^4\ Cq$	0,995			
					$If_0/If = (0,97 \pm 0,04) + (3,91 \pm 0,50) \times 10^4 Cq + (1,86 \pm 1,37) \times 10^8\ Cq^2$	0,994			
#12	36,9 / 2	4 nm	(8,56 ± 0,33)	(3,05 ± 0,26)	$\tau_0/\tau = (0,92 \pm 0,07) + (8,56 \pm 0,33) \times 10^4\ Cq$	0,991	N/A	N/A	N/A
					$If_0/If = (0,95 \pm 0,04) + (9,89 \pm 0,70) \times 10^4 Cq + (2,61 \pm 0,20) \times 10^9\ Cq^2$	0,999			
#19	36,9 / 2	4 nm	(3,90 ± 0,12)	(2,44 ± 0,37)	$\tau_0/\tau = (0,93 \pm 0,02) + (3,90 \pm 0,12) \times 10^4\ Cq$	0,991			
					$If_0/If = (0,99 \pm 0,03) + (4,27 \pm 0,51) \times 10^4\ Cq + (9,51 \pm 1,42) \times 10^8 Cq^2$	0,996			
#13	20 / 2	4 nm	(2,93 ± 0,09)	(3,12 ± 0,43)	$\tau_0/\tau = (1,02 \pm 0,01) + (2,93 \pm 0,09) \times 10^4\ Cq$	0,994	(2,41±0,11)	(1,05±0,44)	0,981/0,995
					$If_0/If = (0,95 \pm 0,03) + (6,05 \pm 0,42) \times 10^4\ Cq + (-1,34 \pm 1,17) \times 10^8\ Cq^2$	0,997			
#15	20 / 2	4 nm	(2,31 ± 0,21)	(1,10 ± 0,69)	$\tau_0/\tau = (1,08 \pm 0,03) + (2,31 \pm 0,21) \times 10^4\ Cq$	0,952			
					$If_0/If = (1,04 \pm 0,03) + (2,99 \pm 0,48) \times 10^4\ Cq + (2,55 \pm 1,56) \times 10^8\ Cq^2$	0,994			
#16	30 / 2	4 nm	(1,31 ± 0,19)	(2,89 ± 0,64)	$\tau_0/\tau = (1,06 \pm 0,03) + (1,31 \pm 0,19) \times 10^4\ Cq$	0,907	(1,57±0,12)	(2,02±0,51)	0,975/0,994
					$If_0/If = (0,99 \pm 0,03) + (4,20 \pm 0,61) \times 10^4\ Cq + (3,20 \pm 1,98) \times 10^8\ Cq^2$	0,996			
#14	30 / 2	4 nm	(1,85 ± 0,14)	(2,79 ± 0,71)	$\tau_0/\tau = (1,03 \pm 0,03) + (1,85 \pm 0,14) \times 10\text{^}4\ Cq$	0,977			
					$If_0/If = (0,99 \pm 0,02) + (2,80 \pm 0,40) \times 10^4\ Cq + (5,17 \pm 1,25) \times 10^8\ Cq^2$	0,997			
#17	15 / 2	4 nm	(1,52 ± 0,09)	*(0,39 ±0,18)	$\tau_0/\tau = (1,01 \pm 0,01) + (1,50 \pm 0,09) \times 10^4\ Cq$	0,989	(1,48±0,11)	(7,65±0,98)	0,978/0,998
					$If_0/If = (1,01 \pm 0,01) + (1,90 \pm 0,16) \times 10^4\ Cq + (1,07 \pm 0,61) \times 10^8\ Cq^2$	0,999			
#18	15 / 2	4 nm	(4,10 ± 0,14)	(2,16 ± 0,52)	$\tau_0/\tau = (1,01 \pm 0,02) + (4,10 \pm 0,14) \times 10^4\ Cq$	0,994			
					$If_0/If = (1,03 \pm 0,05) + (2,29 \pm 0,69) \times 10^4\ Cq + (8,87 \pm 2,12) \times 10^8\ Cq^2$	0,993			

Table 1. Static and dynamic quenching constants and Stern-Volmer equations for each experiment. The average constants are also displayed for the experiments that the calculation was relevant and reliable. (* The results obtained were not good enough for the calculation of reliable constants, N/A: non-applicable because the average could not be made due to difference in the slits or some experimental error, SD: standard deviation).

ANNEX C. PSEQUAD: CALCULATION OF THE BINDING CONSTANTS

								average	
		T(ºC)/C_{HSA} (µM)	**slits**	**log β ± SD**	**FP**	**Minimum reached?**	**log K_D/ log K_S**	**log β ± SD**	**FP**
#1	HSA-RuC HSA-$(RuC)_2$	RT/5,12	2 nm	log β_1= 4,38 ± 0,01 log β_2= 8,53 ± 0,07	201421	Yes	4,11 / 4,42	N/A	N/A
#2	HSA-RuC HSA-$(RuC)_2$	36,9/2,24	2 nm	log β_1= 4,72 ± 0,01 N/A (rejected)	97331	Yes	N/A	N/A	N/A
#3	HSA-RuC HSA-$(RuC)_2$	RT/2,51	2 nm	log β_1= 4,67 ± 0,01 N/A (rejected)	118464	Yes	4,41 / 4,12	log β1= 4,72 ± 0,01 log β2= 9,00 ± 0,07*	129028
#4	HSA-RuC HSA-$(RuC)_2$	RT/2,50	2 nm	log β_1= 4,74 ± 0,01 log β_2= 9,45 ± 0,02	111955	Yes	4,41 / 4,35		
#5	HSA-RuC HSA-$(RuC)_2$	RT/2,51	2 nm	log β_1= 4,71 ± 0,01 N/A (rejected)	159116	Yes	4,41 / 4,35		
#6	HSA-RuC HSA-$(RuC)_2$	36,9/2,50	2 nm	log β_1= 4,76 ± 0,01 N/A (rejected)	179361	Yes	4,78 / 4,30		
#7	HSA-RuC HSA-$(RuC)_2$	36,9/2,00	2 nm	log β_1= 4,81 ± 0,01 log β_2= 9,34 ± 0,02	120189	Yes	4,61 / 4,38	log β1= 4,78 ± 0,01 log β2= 9,52 ± 0,01	116410
#8	HSA-RuC HSA-$(RuC)_2$	36,9/2,00	2 nm	log β_1= 4,776 ± 0,005 log β_2= 9,402 ± 0,012	88796	Yes	4,71 / 4,36		
#9	HSA-RuC HSA-$(RuC)_2$	RT/2,00	2 nm	log β_1= 4,90 ± 0,01 log β_2= 10,24 ± 0,02	116386	Yes	4,66 / 4,35		
#10	HSA-RuC HSA-$(RuC)_2$	25/2,00	2 nm	log β_1= 4,57 ± 0,01 N/A (rejected)	180999	Yes	4,18 / 4,43	N/A	N/A

Y

#11	HSA-RuC HSA-$(RuC)_2$	25/2,00	4 nm	log β_1= 4,52 ± 0,01 log β_2= 9,06 ± 0,09	671146	Yes	4,30 / 4,28		
#12	HSA-RuC HSA-$(RuC)_2$	37/2,00	4 nm	log β_1= 4,93 ± 0,01 log β_2= 9,74 ± 0,02	669517	Yes	4,93 / 4,48	N/A	N/A
#19	HSA-RuC HSA-$(RuC)_2$	37/2,00	4 nm	log β_1= 4,42 ± 0,01 log β_2= 9,57 ± 0,01	436652	Yes	4,59 / 4,39		
#13	HSA-RuC HSA-$(RuC)_2$	20/2,00	4 nm	log β_1= 4,73 ± 0,01 log β_2= 9,31 ± 0,03	659153	Yes	4,47 / 4,49	log β1= 4,70 ± 0,01 log β2= 8,73 ± 0,11	534363
#15	HSA-RuC HSA-$(RuC)_2$	20/2,00	4 nm	log β_1= 4,61 ± 0,01 N/A (rejected)	601801	Yes	4,36 / 4,04		
#14	HSA-RuC HSA-$(RuC)_2$	30/2,00	4 nm	log β_1= 4,53 ± 0,01 log β_2= 8,99 ± 0,05	478050	Yes	4,27 / 4,45	log β1= 4,59 ± 0,01 log β2= 9,32 ± 0,04	519463
#16	HSA-RuC HSA-$(RuC)_2$	30/2,00	4 nm	log β_1= 4,70 ± 0,01 log β_2= 9,27 ± 0,04	609249	Yes	4,12 / 4,46		
#17	HSA-RuC HSA-$(RuC)_2$	15/2,00	4 nm	log β_1= 4,40 ± 0,01 N/A (rejected)	286363	Yes	4,18 / 3,59	log β1= 3,94 ± 0,06 log β2= 9,39 ± 0,03	933484
#18	HSA-RuC HSA-$(RuC)_2$	15/2,00	4 nm	log β_1= 4,51 ± 0,01 N/A (rejected)	528916	Yes	4,61 / 4,33		

Table 1. Global formation constants for the experiments involving the protein HSA and RuC at different concentrations, the temperature shown is the temperaalso varies for the different experiments. (FP stands for Fitting Parameter, * values taken from the average, not every individual experiment showed the formation of the second species HSA-$(RuC)_2$). The experiments performed at 25 ºC were executed with different slits and therefore their average was not determined.

Z

ANNEX D. Time-resolved measurements

date / experiment	C_{HSA} / M	CComplex/M	ratio	$\tau 1$	$\tau 2$	$\tau 3$	α1	α2	α3	χ^2	τ bar	$<\tau>$	time-resolved STV	Slits (nm)
8.Oct /#1														
	$5{,}12_x10^{-6}$	0,00	0,00	0,57	3,58	7,22	0,25	0,32	0,42	1,34	4,36	6,03	1,00	
		$2{,}50_x$10-06	0,49	0,54	3,23	7,12	0,24	0,32	0,44	1,44	4,28	5,99	1,02	
		5,01 **x10**-06	0,98											
		1,25 **x10**-05	2,44	0,40	3,26	7,16	0,37	0,30	0,33	1,34	3,49	5,78	1,25	8
	*	2,51 **x10**-05	4,90	0,50	3,14	7,11	0,41	0,30	0,29	1,29	3,23	5,54	1,35	
	*	5,01 **x10**-05	9,79	0,46	2,73	6,92	0,48	0,29	0,22	1,21	2,58	5,06	1,69	
	*	7,51 **x10**-05	14,68	0,46	2,58	6,77	0,53	0,29	0,18	1,19	2,20	4,64	1,98	
22.Oct / #2														
	2,24 x10-06	0,00	0	0,55	3,05	6,98	0,26	0,29	0,45	1,15	4,15	5,91	1,00	
		1,30 **x10**-06	0,58											
		2,50 **x10**-06	1,11	0,32	2,88	6,93	0,38	0,26	0,36	1,18	3,38	5,79	1,23	
		3,81 **x10**-06	1,69											
		5,00 **x10**-06	2,22	0,29	2,70	6,87	0,43	0,25	0,33	1,29	3,03	5,69	1,37	15
		6,29 **x10**-06	2,79											
		7,50 **x10**-06	3,33	0,26	2,58	6,90	0,43	0,26	0,31	1,34	2,92	5,67	1,42	
		8,74 **x10**-06	3,88											
		9,99 **x10**-06	4,43	0,41	2,77	6,92	0,39	0,29	0,32	1,21	3,18	5,54	1,31	
25.Oct / #3														
	2,51 x10-06	0,00	0,00	0,70	3,81	7,28	0,30	0,28	0,42	1,49	4,31	6,09	1,00	10

AA

		1,30 x**10**-06	0,52											
		2,50 x**10**-06	1,00	0,65	3,51	7,31	0,38	0,29	0,33	1,64	3,66	5,80	1,05	
		3,80 x**10**-06	1,51	0,53	3,26	7,29	0,42	0,28	0,30	1,50	3,30	5,70	1,07	
		4,39 x**10**-06	1,75	0,40	2,79	7,11	0,44	0,27	0,28	1,33	2,97	5,60	1,09	
		6,30 x**10**-06	2,51	0,66	3,05	7,20	0,43	0,31	0,26	1,48	3,09	5,32	1,14	
		7,50 x**10**-06	2,99	0,60	2,84	7,15	0,44	0,31	0,25	1,33	2,92	5,25	1,16	
		8,77 x**10**-06	3,49	0,35	2,41	6,92	0,49	0,30	0,21	1,26	2,33	5,03	1,21	
		1,01 x**10**-05	4,00	0,48	2,58	7,08	0,48	0,33	0,19	1,23	2,43	4,85	1,25	
		1,25 x**10**-05	4,99	0,43	2,40	6,97	0,50	0,34	0,17	1,16	2,18	4,63	1,31	
29-Oct / #4														
	2,50 x10-06	0,00	0,00	0,31	3,25	7,15	0,40	0,22	0,37	1,36	3,53	6,11	1,00	
		2,51 x**10**-06	1,00	0,43	3,55	7,31	0,42	0,26	0,32	1,56	3,43	5,92	1,03	
		5,01 x**10**-12	0,00	0,38	3,05	7,14	0,44	0,24	0,32	1,52	3,17	5,85	1,11	
		7,50 x**10**-06	3,00	0,53	3,35	7,30	0,43	0,28	0,29	1,74	3,27	5,69	1,08	
		1,00 x**10**-05	4,01	0,36	2,94	7,17	0,51	0,25	0,24	1,53	2,65	5,53	1,33	14
		1,25 x**10**-05	5,02	0,34	2,86	7,11	0,54	0,24	0,22	1,42	2,44	5,40	1,45	
		1,50 x**10**-05	6,02	0,44	3,01	7,21	0,52	0,26	0,21	1,33	2,56	5,30	1,38	
		1,76 x**10**-05	7,02	0,46	2,89	7,11	0,53	0,26	0,20	1,46	2,44	5,12	1,45	
		2,01 x**10**-05	8,02	0,45	2,79	7,08	0,56	0,26	0,18	1,34	2,27	4,98	1,56	
		2,51 x**10**-05	10,03	0,51	2,89	7,08	0,57	0,26	0,17	1,60	2,23	4,80	1,59	
01.Nov / #5														
	2,51 x10-06	0,00	0,00	0,44	3,32	7,24	0,31	0,26	0,43	1,17	4,12	6,21	1,00	
		2,50 x**10**-06	1,00	0,48	3,05	7,21	0,35	0,29	0,36	1,18	3,64	5,88	1,13	
		5,00 x**10**-06	1,99	0,53	3,44	7,37	0,40	0,29	0,32	1,14	3,54	5,87	1,17	
		7,50 x**10**-06	2,99	0,23	2,60	7,10	0,53	0,22	0,25	1,31	2,47	5,70	1,67	13
		9,97 x**10**-06	3,97	0,24	2,61	7,10	0,56	0,23	0,22	1,21	2,25	5,52	1,83	
		1,25 x**10**-05	4,98	0,28	2,64	7,11	0,51	0,24	0,24	1,30	2,52	5,58	1,64	
		1,50 x**10**-05	5,98	0,32	2,67	7,08	0,53	0,25	0,22	1,25	2,39	5,37	1,73	

		1,75 x**10**-05	6,99	0,36	2,63	7,05	0,55	0,26	0,19	1,23	2,22	5,10	1,86	
		1,99 x**10**-05	7,94	0,33	2,43	6,93	0,56	0,26	0,18	1,14	2,06	4,98	2,00	
		2,50 x**10**-05	9,96	0,35	2,32	6,82	0,58	0,26	0,16	1,21	1,90	4,71	2,17	
5.Nov / #6														
	2,50 x10-06	0,00	0	0,85	3,89	7,09	0,26	0,32	0,42	1,25	4,43	5,88	1,00	
		2,50 x**10**-06	1,00	0,85	3,74	6,99	0,32	0,32	0,36	1,39	3,99	5,59	1,11	
		4,99 x**10**-06	2,00	0,59	3,22	6,89	0,39	0,30	0,31	1,47	3,34	5,39	1,33	
		7,52 x**10**-06	3,01	0,71	3,28	6,88	0,43	0,29	0,28	1,65	3,18	5,20	1,39	
		1,00 x**10**-05	4,00	0,76	3,21	6,94	0,44	0,30	0,27	1,51	3,13	5,15	1,41	
		1,26 x**10**-05	5,02	0,79	3,28	6,98	0,45	0,30	0,25	1,62	3,08	5,09	1,44	14
		1,50 x**10**-05	6,01	0,32	2,25	6,58	0,49	0,29	0,22	1,42	2,25	4,89	1,97	
		1,75 x**10**-05	7,01	0,40	2,30	6,55	0,50	0,30	0,20	1,39	2,21	4,66	2,01	
		2,00 x**10**-05	8,00	0,85	2,98	6,78	0,53	0,29	0,18	1,48	2,55	4,46	1,74	
		2,25 x**10**-05	9,00	0,47	2,43	6,57	0,56	0,29	0,15	1,26	1,93	4,23	2,29	
		2,50 x**10**-05	9,99	0,39	2,11	6,39	0,56	0,30	0,14	1,33	1,74	4,09	2,55	
7.Nov / #7														
	2,00 x10-06	0,00	0,00	0,67	3,45	6,79	0,28	0,30	0,43	1,24	4,10	5,68	1,00	
		2,00 x**10**-06	1,00	0,53	3,17	6,88	0,31	0,30	0,39	1,60	3,79	5,66	1,08	
		2,40 x**10**-06	1,20	1,39	4,35	7,11	0,31	0,32	0,36	1,79	4,42	5,66	0,93	
		4,01 x**10**-06	2,00	0,99	3,62	6,80	0,35	0,30	0,35	1,40	3,83	5,38	1,07	
		4,81 x**10**-06	2,40											
		6,00 x**10**-06	3,00	0,67	3,32	6,93	0,41	0,29	0,30	1,58	3,33	5,37	1,23	15
		8,00 x**10**-06	4,00	0,26	2,28	6,59	0,44	0,29	0,27	1,41	2,54	5,19	1,61	
		1,00 x**10**-05	5,00											
		1,20 x**10**-05	6,00	0,28	2,25	6,58	0,46	0,29	0,24	1,23	2,38	5,03	1,72	
		1,40 x**10**-05	7,00	0,45	2,53	6,66	0,45	0,31	0,24	1,30	2,58	4,93	1,59	
		1,60 x**10**-05	7,99	1,09	3,71	7,00	0,53	0,28	0,19	1,61	2,96	4,70	1,39	
		1,80 x**10**-05	8,99											

CC

		2,00 x**10**-05	9,99											
		2,40 x**10**-05	11,99											
		2,80 x**10**-05	13,99	0,00	1,37	5,87	0,88	0,09	0,03	2,20	0,32	4,17	12,92	
		3,20 x**10**-05	15,99	0,87	2,95	6,51	0,66	0,23	0,11	1,85	1,96	3,61	2,10	
		3,60 x**10**-05	17,99	0,77	2,78	6,48	0,69	0,23	0,09	1,47	1,72	3,39	2,38	
		4,00 x**10**-05	19,99											
		4,41 x**10**-05	22,03	0,60	2,25	5,99	0,68	0,23	0,09	1,26	1,44	3,12	2,85	
		4,80 x**10**-05	23,98	0,45	1,97	5,79	0,69	0,23	0,08	1,27	1,22	2,98	3,36	
12.Nov / #8														
	2,00 x10-06	0,00	0,00	0,79	4,05	7,37	0,29	0,32	0,39	1,31	4,41	6,06	1,00	
		2,00 x**10**-06	1,00	0,28	2,94	6,91	0,44	0,24	0,32	1,30	3,04	5,72	1,45	
		2,40 x**10**-06	1,20	0,37	3,18	7,03	0,41	0,26	0,33	1,19	3,29	5,75	1,34	
		4,01 x**10**-06	2,00	0,46	2,98	6,91	0,37	0,29	0,34	1,22	3,40	5,60	1,30	
		4,79 x**10**-06	2,40	0,42	2,93	6,89	0,42	0,27	0,31	1,13	3,11	5,50	1,42	
		6,00 x**10**-06	3,00	0,41	2,87	6,89	0,43	0,28	0,29	1,18	2,97	5,40	1,49	
		8,00 x**10**-06	4,00	0,43	2,74	6,82	0,44	0,28	0,28	1,15	2,85	5,30	1,55	
		1,00 x**10**-05	5,00	0,40	2,54	6,71	0,47	0,30	0,24	1,25	2,53	5,00	1,75	
		1,20 x**10**-05	6,02	0,43	2,47	6,73	0,48	0,30	0,22	1,21	2,44	4,91	1,81	
		1,40 x**10**-05	6,99	0,52	2,70	6,76	0,52	0,28	0,20	1,20	2,40	4,79	1,84	15
		1,61 x**10**-05	8,03	0,46	2,40	6,61	0,52	0,29	0,20	1,21	2,23	4,64	1,98	
		1,80 x**10**-05	8,99	0,44	2,41	6,61	0,52	0,29	0,19	1,20	2,20	4,63	2,01	
		2,01 x**10**-05	10,04	0,47	2,48	6,65	0,56	0,28	0,16	1,05	2,04	4,43	2,16	
		2,40 x**10**-05	12,01	0,46	2,29	6,47	0,60	0,27	0,12	1,26	1,71	3,97	2,58	
		2,80 x**10**-05	14,01	0,56	2,44	6,53	0,61	0,27	0,12	1,29	1,77	3,85	2,49	
		3,20 x**10**-05	16,02	0,55	2,36	6,46	0,61	0,27	0,12	1,21	1,72	3,14	2,56	
		3,60 x**10**-05	17,99	0,52	2,29	6,33	0,65	0,25	0,09	1,29	1,51	3,48	2,92	
		4,00 x**10**-05	20,00	0,42	1,94	6,06	0,66	0,26	0,08	1,21	1,25	3,14	3,53	
		4,40 x**10**-05	22,00	0,44	2,11	6,07	0,70	0,23	0,07	1,27	1,24	3,14	3,55	

DD

		4,80 x**10**-05	24,01	0,39	1,87	5,64	0,75	0,20	0,05	1,20	0,95	2,51	4,66	
15.Nov / #9														
	2,00 x10-06	0,00	0,00	0,65	3,77	7,44	0,25	0,30	0,45	1,26	4,63	6,29	1,00	
	*	2,00 x**10**-06	1,00	0,78	3,72	7,47	0,27	0,31	0,42	1,33	4,48	6,18	1,03	
		2,50 x**10**-06	1,25	0,99	4,00	7,63	0,31	0,34	0,35	1,37	4,34	6,01	1,07	
		3,01 x**10**-06	1,50	1,24	3,90	7,45	0,36	0,31	0,33	1,39	4,10	5,72	1,13	
		3,50 x**10**-06	1,75										1,10	
		4,00 x**10**-06	2,00										1,07	
		4,51 x**10**-06	2,26										1,48	
		5,01 x**10**-06	2,50										1,45	
		5,50 x**10**-06	2,75										1,44	
		6,00 x**10**-06	3,00	1,08	3,61	7,50	0,41	0,33	0,26	1,43	3,60	5,43	1,29	15
		6,51 x**10**-06	3,26										1,39	
		7,01 x**10**-06	3,50										1,64	
		7,51 x**10**-06	3,75	1,14	3,55	7,45	0,42	0,32	0,27	1,47	3,58	5,39	1,29	
		8,05 x**10**-06	4,02										1,30	
		8,50 x**10**-06	4,25										1,48	
	*	9,02 x**10**-06	4,51										1,29	
	*	9,55 x**10**-06	4,78	0,97	3,46	7,45	0,45	0,32	0,24	1,32	3,28	5,26	1,41	
	*	1,00 x**10**-05	5,00	0,89	3,07	7,30	0,45	0,32	0,23	1,35	3,06	5,10	1,51	
	*	1,05 x**10**-05	5,26	0,87	2,97	7,17	0,44	0,32	0,24	1,25	3,05	5,07	1,52	
	*	1,11 x**10**-05	5,53	0,89	3,03	7,28	0,48	0,33	0,19	1,42	2,80	4,79	1,65	
31.Jan/ #12														
	2,00 x10-06	0,00 x**10**+00	0,00	0,45	3,25	6,85	0,36	0,29	0,35	1,39	3,48	5,57	1,00	
		1,99 x**10**-06	0,99	0,44	2,89	6,67	0,39	0,29	0,32	1,31	3,13	5,31	1,11	
		4,52 x**10**-06	2,26	0,47	2,66	6,62	0,41	0,32	0,27	1,24	2,82	5,02	1,24	15
		6,05 x**10-06**	3,03	0,52	2,65	6,56	0,43	0,31	0,26	1,53	2,75	4,89	1,27	
		8,04 x**10**-06	4,02	2,43	0,53	6,45	0,33	0,49	0,19	1,52	2,25	4,35	1,55	

		1,00 x**10**-05	5,01	0,34	2,27	6,34	0,59	0,28	0,13	1,75	1,67	4,08	2,09	
		1,40 x**10**-05	7,00	0,38	2,08	6,10	0,62	0,29	0,10	1,62	1,41	3,46	2,47	
		1,81 x**10**-05	9,03	0,37	2,00	5,96	0,63	0,28	0,09	1,56	1,32	3,30	2,64	
		2,30 x**10**-05	11,52	0,50	2,17	6,07	0,67	0,27	0,06	1,45	1,29	2,86	2,70	
		2,60 x**10**-05	13,01	0,35	1,82	5,54	0,72	0,24	0,04	1,46	0,91	2,34	3,83	
		3,00 x**10**-05	15,00	0,39	1,88	5,54	0,71	0,24	0,05	1,59	0,99	2,43	3,51	
		3,51 x**10**-05	17,53	0,39	1,82	5,42	0,74	0,22	0,03	1,44	0,88	2,07	3,97	
04.Mar/ #19														
	2,00 x10-06	0,00	0,00	0,65	3,09	6,52	0,31	0,32	0,37	1,63	3,59	5,24	1,00	
		2,00 x**10**-06	1,00	0,67	2,99	6,41	0,35	0,32	0,33	1,74	3,30	5,01		
		2,43 x**10**-06	1,22	0,70	2,96	6,49	0,34	0,32	0,35	1,69	3,43	5,12	1,05	
		4,01 x**10**-06	2,00	0,81	3,26	6,53	0,39	0,31	0,30	1,47	3,30	4,97	1,09	
		4,82 x**10**-06	2,41	0,82	3,20	6,55	0,39	0,31	0,30	1,74	3,28	4,98	1,09	
		6,01 x**10**-06	3,00	0,72	3,03	6,49	0,39	0,32	0,29	1,42	3,11	4,88	1,15	
		8,01 x**10**-06	4,01	0,74	3,02	6,52	0,42	0,32	0,26	1,32	2,99	4,78	1,20	
		1,00 x**10**-05	5,01	0,70	2,70	6,40	0,43	0,33	0,24	1,42	2,72	4,57	1,32	
		1,20 x**10**-05	6,01	0,69	2,69	6,37	0,45	0,31	0,24	1,33	2,66	4,55	1,35	15
		1,40 x**10**-05	7,01	0,71	2,76	6,47	0,48	0,33	0,20	1,29	2,51	4,37	1,43	
		1,60 x**10**-05	8,01	0,60	2,39	6,25	0,47	0,33	0,20	1,34	2,32	4,25	1,55	
		1,80 x**10**-05	9,01	0,68	2,65	6,31	0,52	0,29	0,19	1,22	2,29	4,21	1,56	
		2,00 x**10**-05	10,02	0,68	2,54	6,26	0,54	0,30	0,16	1,22	2,13	3,97	1,68	
		2,40 x**10**-05	12,02	0,62	2,41	6,12	0,59	0,30	0,11	1,25	1,78	3,51	2,01	
		2,80 x**10**-05	14,02											
		3,20 x**10**-05	16,00	0,59	2,13	5,88	0,61	0,29	0,09	1,21	1,54	3,12	2,33	
		3,60 x**10**-05	18,01	0,54	2,11	5,92	0,61	0,30	0,09	1,22	1,50	3,14	2,38	

Table 1. Parameters obtained from the time-resolved measurements performed at 37 ºC.

FF

Annex E. Example of data treatment.

- Example of the data treatment (difference between raw sample, including Raman peak and its respective blank, to tobtain the sample) (RuC+HSa)

  A: raw sample (HSA-RuC, obtained directly from the fluorometer)
  B: blank samples (RuC, obtained directly from the fluorometer)
  C: data treated (difference between plots A and B)

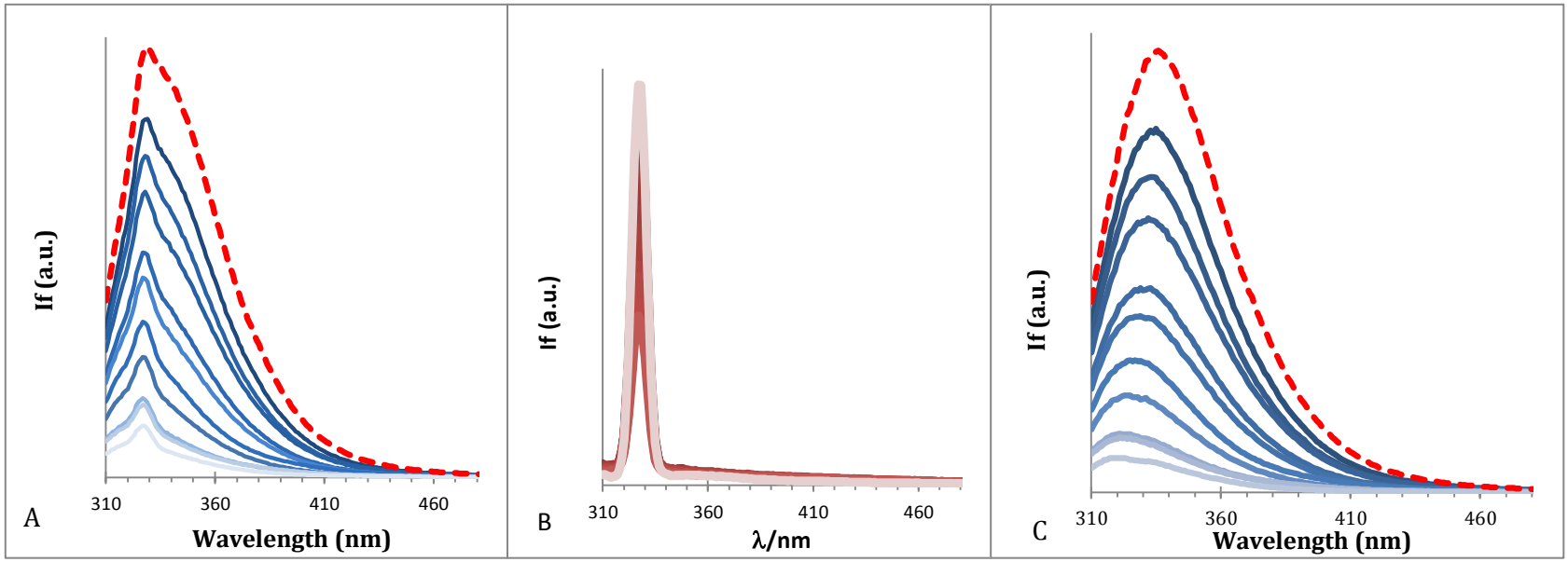

GG